



**Data Analysis on the
Roseville Rail Yard Air Monitoring Project**

YEAR ONE INTERIM REPORT

Prepared for

Placer County Air Pollution Control District
11464 B Avenue
Auburn, CA 95603

Prepared by

David E. Campbell and Eric M Fujita
Desert Research Institute
Division of Atmospheric Sciences
2215 Raggio Parkway
Reno, NV 89512

JUNE 5, 2006

TABLE OF CONTENTS

1. INTRODUCTION	1-1
1.1 Overview of RRAMP	1-1
1.2 Objectives of RRAMP Data Analysis	1-2
2. EVALUATION AND VALIDATION OF RRAMP DATA	2-1
2.1 Measurement Methods	2-1
2.1.1 Aethalometer	2-1
2.1.2 Beta Attenuation Monitors	2-2
2.1.3 Nitric oxide (NO) and nitrogen oxides (NO _x)	2-2
2.1.4 Thermal Optical Carbon Measurements	2-3
2.2 Determination of Measurement Precision and Bias Using Collocation Data	2-5
2.2.1 Aethalometers	2-5
2.2.2 BAMs	2-6
2.3 Comparison of Time-Averaged Continuous Monitor Data with Time-Integrated Gravimetric Mass and Elemental Carbon	2-7
2.3.1 Gravimetric mass vs. 24-hour averaged BAM PM concentrations	2-7
2.3.2 Elemental carbon vs. averaged Aethalometer black carbon concentrations	2-7
2.4 Time-Series and Correlation Analysis of Summer 2005 Data	2-7
2.4.1 5-minute Aethalometer Data	2-7
2.4.2 Review of Time-Series of Hourly Data	2-8
2.4.3 Correlations of Parameters	2-9
3. RESULTS	3-1
3.1 Comparisons of Diurnal Variations in Pollutant Concentrations at Downwind and Upwind Monitoring Sites	3-1
3.2 Upwind/Downwind Differences	3-1
3.3 Correlations of BC and NO with PM _{2.5}	3-2
4. CONCLUSIONS AND RECCOMENDATIONS	4-1
4.1 Data Evaluation and Validation	4-1
4.2 Data Analysis	4-2
5. REFERENCES	5-1

Appendix A: Manufacturer's Notes for the Aethalometer

LIST OF TABLES

Table 2–1. Summary of RRAMP Measurements During Summer 2005* 2-4

Table 2–2. Regression statistics for collocated aethalometer data with different averaging periods.
..... 2-10

Table 2–3. Error statistics for collocated aethalometer data with different averaging periods. 2-10

Table 2–4. Collocated aethalometer comparisons. Results from an EPA study are included for
comparison. 2-10

Table 2–5. Regression statistics for collocated BAM data with different averaging periods.... 2-11

Table 2–6. Error statistics for collocated BAM data with different averaging periods. 2-11

Table 3–1. Means and standard deviations for 1-hour and 7-hour mean BC, PM2.5, NO and
NOx concentrations from 2200 to 0500 at the four RRAMP sites and standard errors
of the means. The differences in mean concentrations between the two pairs of
downwind and upwind sites (Denio-Pool and Church-Vernon) and pooled standard
error of the differences and root mean squares of the measurement errors are also
shown. 3-15

LIST OF FIGURES

Figure 1–1. Map showing locations of the two upwind (Pool and Vernon) and two downwind (Denio and Church) sampling locations. The upwind/downwind directions between the Vernon/Church and Pool/Denio pairs are 137 and 162 degrees, respectively. ...1-3

Figure 2–1. Correlation of hourly BC (ng/m³) averaged data from collocated aethalometers 6/27.-7/11. Instrument A330 was later used at the Denio site, and A339 at Pool. .2-12

Figure 2–2. Correlation of hourly averaged BC (ng/m³) data from collocated aethalometers 10/28–11/13.2-12

Figure 2–3. Plot of relative difference between collocated aethalometers during periods 6/27.-7/11 (upper) and 10/28–11/13 (lower). A330 was later used at Denio site and A339 at Pool site. Data are hourly averages of channel 2 BC.2-13

Figure 2–4. Correlation of hourly averaged data from collocated aethalometers 8/24 -9/5. 623 was later used at Church and 625 at Vernon.2-14

Figure 2–5. Correlation of hourly averaged data from collocated aethalometers 10/28 – 11/13.2-14

Figure 2–6. Correlation of hourly averaged data from collocated aethalometers 8/24 -9/5. X-axis values are the median of 4 collocated instruments.2-15

Figure 2–7. Plot of relative difference between collocated aethalometers during periods 8/24 -9/5 (upper) and 10/28 – 11/13 (lower). 623 was used at Church site and 625 at Vernon site. Data are hourly averages of channel 2 BC.....2-16

Figure 2–8. Regression of collocated aethalometer data for 1-hour, 6-hour, and 24-hour averages.2-17

Figure 2–9. Correlation of hourly averaged PM_{2.5} (ug/m³) data from collocated BAMs 7/28-9/7. Outlier in lower right corner is excluded from regression. BAM 4515 was later used at Church site and BAM 4514 at Vernon.2-18

Figure 2–10. Correlation of hourly averaged PM_{2.5} (ug/m³) data from collocated BAMs 10/18-11/19. Outlier in upper right corner is excluded from regression.....2-18

Figure 2–11. Correlation of hourly averaged PM_{2.5} (ug/m³) data from collocated BAMs 6/24-7/8, with and without extreme from one event. EBAM 2238 was later used at Denio and EBAM 2238 at Pool.....2-19

Figure 2–12. Correlation of hourly averaged PM_{2.5} (ug/m³) data from collocated BAMs 10/21-11/14. Outlier on right is excluded from regression.2-19

Figure 2–13. Difference between collocated BAMs as a function of PM concentration. Data is hourly.....2-20

Figure 2–14. Relative error between collocated BAMs as a function of PM concentration.2-20

Figure 2–15. Regression of collocated BAM data for 1-hour, 6-hour, and 24-hour averages. ...2-21

Figure 2–16. Time-series plot of aethalometer data from Denio and Pool sites showing measurement noise in the data from Pool on August 6. The number after the site name indicates the wavelength channel (1=880 nm, 2=370 nm).2-22

Figure 2–17. Time-series plot for Oct.14 showing data gaps resulting from automatic tape advance.	2-22
Figure 2–18. Hourly wind speed during first 30 days of summer intensive.....	2-23
Figure 2–19. Hourly wind speed during middle 30 days of summer intensive.....	2-24
Figure 2–20. Hourly wind speed during last 30 days of summer intensive.....	2-25
Figure 2–21. Hourly wind direction during the first 30 days of summer intensive.....	2-26
Figure 2–22. Hourly wind direction during middle 30 days of summer intensive.....	2-27
Figure 2–23. Hourly wind direction during last 30 days of summer intensive.....	2-28
Figure 2–24. Hourly NO data during first 30 days of summer intensive.	2-29
Figure 2–25. Hourly NO data during middle 30 days of summer intensive.....	2-30
Figure 2–26. Hourly NO data during last 30 days of summer intensive.	2-31
Figure 2–27. Hourly NOx data during first 30 days of summer intensive.	2-32
Figure 2–28. Hourly NOx data during middle 30 days of summer intensive.....	2-33
Figure 2–29. Hourly NOx data during last 30 days of summer intensive.	2-34
Figure 2–30. Hourly black carbon data during first 30 days of summer intensive.....	2-35
Figure 2–31. Hourly black carbon data during middle 30 days of summer intensive.	2-36
Figure 2–32. Hourly black carbon data during last 30 days of summer intensive.....	2-37
Figure 2–33. Hourly PM2.5 data during first 30 days of summer intensive.	2-38
Figure 2–34. Hourly PM2.5 data during middle 30 days of summer intensive.....	2-39
Figure 2–35. Hourly PM2.5 data during last 30 days of summer intensive.	2-40
Figure 2–36. Scatter plot of hourly average vector wind speeds at the 4 sites vs. Roseville met tower. Hours when wind speed measured at the met tower was less than 1 m/s are not included.	2-41
Figure 2–37. Plots of black carbon/PM2.5 ratios at the four monitoring sites. Data are daily averages of data meeting the criteria for inclusion in the upwind/downwind analysis.	2-42
Figure 2–38. Plots of NO/NOx ratios at the four monitoring sites. Data are daily averages of data meeting the criteria for inclusion in the upwind/downwind analysis.....	2-43
Figure 2–39. Correlation of gravimetric mass from FRM filter samplers to 24-hour averaged PM2.5 from continuous mass monitors (BAMS and EBAMS). The outlier at Pool site is not included in the regression.....	2-44
Figure 2–40. Correlation of elemental carbon concentration measured from FRM samplers to 24-hr averaged black carbon concentration from Aethalometers at two different wavelengths.	2-45
Figure 3–1. Box and whiskers plots showing diurnal distribution of data at the Denio site.	3-4
Figure 3–2. Box and whiskers plots showing diurnal distribution of data at the Pool site.....	3-5

Figure 3–3. Box and whiskers plots showing diurnal distribution of data at the Church site	3-6
Figure 3–4. Box and whiskers plots showing diurnal distribution of data at the Vernon site	3-7
Figure 3–5. Box and whiskers plots showing distribution of data by day-of-week at the Denio site	3-8
Figure 3–6. Box and whiskers plots showing distribution of data by day-of-week at the Pool site.....	3-9
Figure 3–7. Box and whiskers plots showing distribution of data by day-of-week at the Church site.....	3-10
Figure 3–8. Box and whiskers plots showing distribution of data by day-of-week at the Vernon site	3-11
Figure 3–9. Frequency of wind direction (%) and average downwind minus upwind NO, BC and PM2.5 concentrations at the downwind sites in 10 degree wind sectors when wind speed > 1 m/s for all hours of the day.....	3-12
Figure 3–10. Frequency of wind direction (%) and average downwind minus upwind NO, BC and PM2.5 concentrations at the downwind sites in 10 degree wind sectors when wind speed > 1 m/s and time period between 10 PM and 5 AM.....	3-13
Figure 3–11. Frequency of wind direction (%) and average downwind minus upwind NO, BC and PM2.5 concentrations at the downwind sites in 10 degree wind sectors when wind speed > 1 m/s and time period between 6 AM and 9 PM.....	3-14
Figure 3–12. Means BC, PM2.5, NO and NOx concentrations at the four RRAMP monitoring sites and standard errors of the means. Differences of the two pairs of downwind and upwind sites (Denio-Pool and Church-Vernon) are also shown. Differences between the two downwind and two upwind sites are also shown for comparison.....	3-16
Figure 3–13. Distributions of hourly average BC concentrations (ug/m3) at Denio and the log transform of the data between 2200 and 0500 that meet selection criteria. Note that distribution of concentrations is approximately normal because measurements occurred during comparable atmospheric conditions.	3-17
Figure 3–14. Correlations of BC and NO with PM _{2.5} . Values are the difference in daily 7-hour (2200 to 0500) means between the downwind Denio site and the corresponding upwind values at Pool.....	3-18

1. INTRODUCTION

The characterization of a community's exposure to air pollutants is essential in assessing cumulative impacts to public health. An important part of such assessments is the identification and quantification of disproportionate impacts that may be experienced by certain communities due to their proximity to sources of hazardous air pollutants. At the request of the Placer County Air Pollution Control District (PCAPCD), the California Air Resources Board (ARB) initiated a risk assessment study in 2000 of diesel emissions from the Union Pacific Railroad's J.R. Davis Rail Yard, located in Roseville, CA. The results of this study, released in October 2004 (ARB, 2004), concluded excess cancer risk levels between 100 and 500 in a million in the neighborhood immediately downwind of the rail yard and risk levels between 10 and 100 in a million for up to 155,000 people that reside in a larger urbanized area downwind of the facility. Based upon these findings and community concerns, the PCAPCD initiated the Roseville Rail Yard Air Monitoring Project (RRAMP) in 2005. The purpose of this three-year monitoring study is to measure the air quality impacts of emissions, primarily diesel, from the rail yard facility and effects of mitigation measures that are implemented at the facility during this three-year period.

1.1 Overview of RRAMP

RRAMP is being funded by the Placer County APCD (PCAPCD), Sacramento Metro AQMD, Union Pacific Railroad (UPRR), and U.S. Environmental Protection Agency with in-kind support from the South Coast AQMD and California Air Resources Board. The main objectives of the RRAMP measurement program is to determine the localized air pollutant impacts from the emissions at the UPRR facility and to determine if any trends can be detected as a result of emissions mitigations which UPRR has agreed to implement over the three-year period of RRAMP. The air quality monitoring segment of the study commenced in summer 2005 and consists of intensive monitoring in each of the summers in 2005-2007 (mid-July to end of September).

Monitoring for the RRAMP consists of two upwind/downwind pairs of monitoring sites aligned as optimally as possible to wind direction that most persistently is perpendicular to the rail yard tracks. The prevailing winds during the late night through early morning hours in the summer months coincide with the conditions that are most favorable for achieving the monitoring objectives for the study. The map in Figure 1-1 shows the locations of the two upwind (Pool and Vernon) and two downwind (Denio and Church) sampling sites. The upwind/downwind wind directions between the Vernon/Church and Pool/Denio pairs are 137 and 162 degrees, respectively.

Selection of the two downwind monitoring locations were supported by a screening survey conducted by DRI (Campbell and Fujita, 2005) of the spatial variations in black carbon, PM_{2.5} and NO_x concentrations around the UPRR's J.R. Davis rail yard. The survey data showed that the impacts of the rail yard emissions were most significant to those residences closest to the NW boundary fence line, and occurred mainly during the early morning hours. The greatest concentrations of idling locomotives were located at the maintenance shop near the northeast end of Circuit Drive and adjacent to the Denio's livestock auction yard near the southwest end of Circuit Drive. Concentrations of NO and BC dropped sharply away from the rail yard and approached background levels within 300 to 500 m from the fence line. No evidence was found

for fumigation of locomotive diesel emissions from aloft that would result in higher concentrations in downwind location. No indication of significant impacts from other sources was observed during the study. Based on these observations, the optimal locations for monitoring were found to be in or near the vacant lot between Ivy, Oakland, Hickory, and Church Streets. However, the locations of highest exposures varied depending upon specific wind direction and where and how many locomotives were idling.

Meeting RRAMP objectives depend upon factors that may contribute to the overall uncertainty in downwind/upwind differences in pollutant concentrations over a three year period. These factors include precision and accuracy of measurements, diurnal, daily, seasonal, and annual variations in meteorological conditions that affect transport and dispersions of emissions, spatial and temporal variations in activity patterns that can affect the concentrations measured at downwind locations under the same meteorological conditions, and the expected changes in emission levels due to the mitigation measures that will be implemented by UPRR during the 3-year study relative to overall measurement uncertainty.

1.2 Objectives of RRAMP Data Analysis

This report is the first of three annual reports that provide descriptive and statistical analyses of the RRAMP data. Data analysis effort for the first two annual reports consists of the following six tasks.

1. Provide additional review of the RRAMP monitoring data to identify possible outliers and other data inconsistencies.
2. Provide general descriptive statistics for each measured parameter.
3. Compare the RRAMP black carbon (aethalometer) and PM_{2.5} (BAM) measurements with Federal Reference Method (FRM) particulate data and determine degree of correlation among methods.
4. Examine the temporal variations in specific ratios of pollutants and characterize variations in contributions of aged versus fresh emissions and elemental carbon versus total carbonaceous particulate matter.
5. Perform statistical analyses to determine upwind/downwind differences in concentrations of black carbon and PM_{2.5}.
6. Using BC and/or EC as surrogates to estimate the mass concentrations and associated uncertainties of diesel particulate matter (DPM) levels at the downwind monitoring sites.

The final report at the end of the three-year monitoring program will include the following additional task.

7. Examine trends in black carbon and PM_{2.5} concentrations over the three-year duration of the RRAMP and determine their statistical significance.

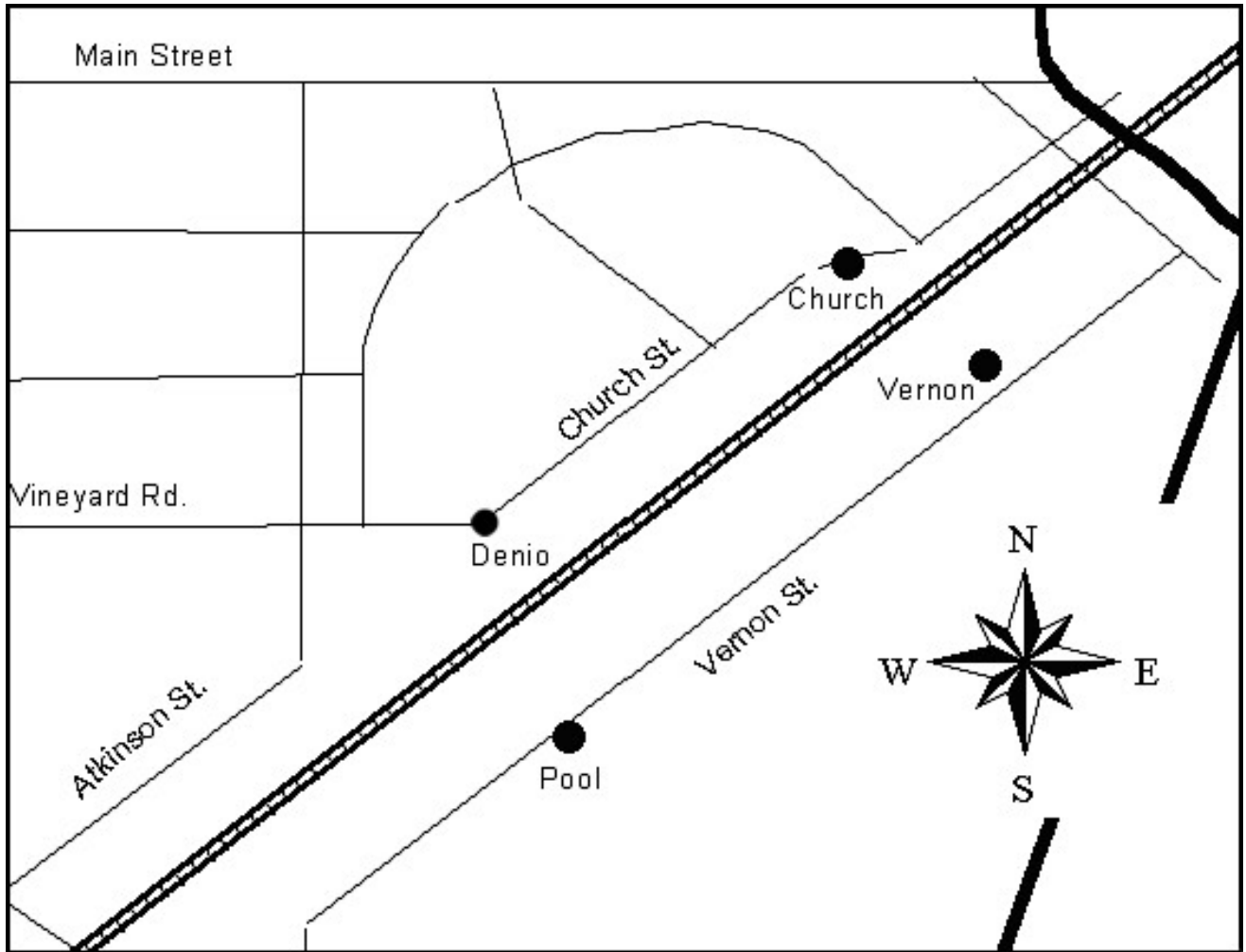


Figure 1-1. Map showing locations of the two upwind (Pool and Vernon) and two downwind (Denio and Church) sampling locations. The upwind/downwind directions between the Vernon/Church and Pool/Denio pairs are 137 and 162 degrees, respectively.

2. EVALUATION AND VALIDATION OF RRAMP DATA

The quantification of differences in the measured parameters between the upwind and downwind sites requires an understanding of the strengths and weaknesses of the data. A substantial portion of this report deals with methods for evaluating the data in terms of relative precision between the paired samplers and determining the existence of biases. In addition, exceptional events and characteristics of the data that may affect our ability to observe differences between paired measurements have been investigated and are described. Quantification of relative precision and bias are evaluated largely by examining the collocated sampler data collected before and after the summer sampling period, and accuracy is assessed by comparing time-averaged continuous sampler data with results from time-integrated filter methods. This section describes the methods that were used during the summer 2005 measurement program and estimates of measurement precision and bias.

2.1 Measurement Methods

Measurements at each of the four RRAMP sites during summer 2005 consisted of continuous (hourly average) wind speed and wind direction, aethalometer for black carbon, Beta Attenuation Monitors (BAM) for PM_{2.5} mass, chemiluminescent NO/NO_x analyzers, and 24-hour integrated FRM PM_{2.5} gravimetric mass (every 9th day) and PM_{2.5} organic and elemental carbon (every 3rd day except 9th day sample which were used for mass). The four aethalometers and four BAMs were co-located to assess measurement precision during a 2-4 week period prior to and after each intensive period (5-minute averages). Table 2-1 provides an inventory of the data collected during summer 2005. The data sets were compiled and quality assured by PCAPCD staff.

2.1.1 Aethalometer.

The aethalometer instrument continuously passes ambient air through a quartz-fiber filter tape. Light absorbing particles such as black carbon (BC) cause attenuation of a light beam incident on the tape. By assuming that all light-absorbing material is black carbon, and that the absorption coefficient of the black carbon is known and constant, the net attenuation signals can be converted into black carbon mass concentrations. The time resolution of the aethalometer is on the order of a fraction of a minute depending on ambient black carbon concentration. Detection limit for the aethalometer is ~ 0.1 µg/m³ black carbon for a one minute average.

Two models manufactured by Magee Scientific were used in this study: the rack-mounted AE-20 model at Denio and Pool sites, and the 'portable' model AE-42 at Church and Vernon. Both models measure attenuation at two wavelengths (880 nm and 370 nm) and have identical sample collection, detection, and software systems. Flow rates were set to 5 lpm for all units, and data was recorded at the default 5-minute time intervals. Data were collected at both wavelengths, but all black carbon data in the following analyses is from the 370nm wavelength of the aethalometer (channel 2) unless otherwise specified. This wavelength was recommended by the TAC, and is also sensitive to organic species emitted by diesel vehicles in addition to "elemental carbon". Since the shorter wavelength also responds to some aromatic compounds such as PAHs the resulting data is sometimes termed "UVPM", however in this document we have used the term BC since we expect the majority of the optical attenuation to be due to carbon

soot. A more detailed discussion of the ramifications of using the UV wavelength data can be found in the Aethalometer handbook distributed by the manufacturer (See Appendix A).

There are several operational features of the aethalometer that can affect comparability of data from multiple instruments. Baseline measurements are made after each tape advance resulting in a 15 minute gap in the data. These tape advances can be set at fixed intervals or initiated automatically at set threshold opacity. The instruments were operated during RRAMP in the latter mode resulting in 15-minute gaps that occur at interval of two or more hours. Operating the aethalometers with synchronized, fixed time intervals between each filter tape advance will yield precision data that can differ from operating them with unsynchronized, fixed filter opacity as the trigger for tape advances. Aethalometer data is also known to be strongly affected by electronic noise spikes that create exaggerated increases or decreases in individual measurements of light attenuation. These issues are discussed further in Section 3.1 Another factor that contributes measurement uncertainty is the effect of filter loading on light absorption measurements. The aethalometer has been shown to over predict BC concentrations on a fresh filter and under predict BC concentrations on a loaded filter (Arnott et al., 2005). Arnott et al. found that the aethalometer BC measurements correlate well with photoacoustic BC and thermal optical elemental carbon if the data are averaged over the full range of filter loading. All of the effects mentioned above can be minimized by averaging the data over longer intervals.

2.1.2 Beta Attenuation Monitors

Beta rays (electrons with energies in the 0.01 to 0.1 MeV range) are attenuated according to an approximate exponential (Beer's Law) function of particulate mass, when they pass through deposits on a filter tape. Automated Beta Attenuation Monitor (BAM) samplers utilize a continuous filter tape, first measuring the attenuation through the unexposed segment of tape to correct for blank attenuation. The tape is then exposed to ambient sample flow, accumulating a deposit. The beta attenuation measurement is repeated. The blank-corrected attenuation readings are converted to mass concentrations, with averaging times as short as 30 minutes. Detection limit is $\sim 5 \mu\text{g}/\text{m}^3$ for a one-hour average.

Met One E-BAMs were used at the Denio and Pool sites. Manufacturer's specifications cite an accuracy of 2.5 ug for a 24 hour average, and a $\pm 3\%$ accuracy in the volumetric flow rate. The BAM 1020 model, which has a specified accuracy of $\pm 8\%$ for 1-hour measurements and $\pm 2\%$ for 24-hour averages, was used at Church and Vernon. Cyclones with a 2.5um cut point were used on all units.

2.1.3 Nitric oxide (NO) and nitrogen oxides (NOx).

NO is continuously measured by the chemiluminescence nitric oxide-ozone method (OCM). This method is based on the gas-phase chemical reaction of NO with ozone. In this method ambient air is mixed with a high concentration of ozone so that any NO in the air sample will react and thereby produce light. The light intensity is measured with a photomultiplier and converted into an electronic signal that is proportional to the NO concentration. To measure NOx concentrations, the sum of NO and NO₂ (nitrogen dioxide), the air sample is first reduced to NO by a heated catalyst (molybdenum or gold in the presence of CO) adding to the NO already present in the sample, then passes into the reaction chamber for measurement as

described above. The NO₂ concentration is derived by subtracting the NO concentration measurement from the NO_x concentration measurements. Four Horiba NO_x instruments were used in the study. This instrument has a zero stability of 10 ppb in 24 hours and span drift of less than 1 percent.

2.1.4 Thermal Optical Carbon Measurements

Elemental carbon (EC) and organic carbon (OC) were measured by thermal optical reflectance (TOR) method using the IMPROVE (Interagency Monitoring of Protected Visual Environments) temperature/oxygen cycle (IMPROVE TOR). Samples were collected on quartz filters. A section of the filter sample is placed in the carbon analyzer oven such that the optical reflectance or transmittance of He-Ne laser light (632.8 nm) can be monitored during the analysis process. The filter is first heated under oxygen-free helium purge gas. The volatilized or pyrolyzed carbonaceous gases are carried by the purge gas to the oxidizer catalyst where all carbon compounds are converted to carbon dioxide. The CO₂ is then reduced to methane, which is quantified by a flame ionization detector (FID). The carbon evolved during the oxygen-free heating stage is defined as “organic carbon”. The sample is then heated in the presence of helium gas containing 2 percent of oxygen and the carbon evolved during this stage is defined as “elemental carbon”. Some organic compounds pyrolyze when heated during the oxygen-free stage of the analysis and produce additional EC, which is defined as pyrolyzed carbon (PC). The formation of PC is monitored during the analysis by the sample reflectance or transmittance. EC and OC are thus distinguished based upon the refractory properties of EC using a thermal evolution carbon analyzer with optical (reflectance or transmittance) correction to compensate for the pyrolysis (charring) of OC. Carbon fractions in the IMPROVE method correspond to temperature steps of 120°C (OC1), 250°C (OC2), 450°C (OC3), and 550°C (OC4) in a nonoxidizing helium atmosphere, and at 550°C (EC1), 700°C (EC2), and 850°C (EC3) in an oxidizing atmosphere. The IMPROVE method uses variable hold times of 150-580 seconds so that carbon responses return to baseline values.

Because EC and OC are operationally defined by the method, the specific instrument used, details of its operation, and choice of thermal evolution protocol can influence the split between EC and OC. Visual examination of filter darkening at different temperature stages have shown that substantial charring takes place within the filter, possibly due to adsorbed organic gases or diffusion of vaporized particles. The filter transmittance is more influenced by within-filter charring, whereas the filter reflectance is dominated by charring of the near-surface deposit. TOR and TOT corrections converge in the case of only a shallow surface deposit of EC or only a uniformly distributed pyrolyzed organic carbon (POC) through the filter and diverge when EC and POC exist concurrently at the surface and are distributed throughout the filter, respectively, especially when the surface EC evolves prior to the POC. The difference between TOR and TOT partly depends on the POC/EC ratio in the sample. Thus, highly loaded source samples would yield similar EC values for TOR and TOT corrections, while lightly loaded source and ambient samples would typically yield different EC values. While EC values for TOR may tend toward higher EC due to underestimation of the POC correction, higher absorption efficiency of POC within the filter may tend toward lower EC values for TOT.

Table 2-1. Summary of RRAMP Measurements During Summer 2005*.

	Denio Site					
	Wind Spd	Wind Dir	NO	NOx	Aeth	EBAM
monitoring period	7/15 - 10/15	7/15 - 10/15	7/21 - 10/15	7/21 - 10/15	7/15 - 10/15	7/15 - 10/15
total hours	2232	2232	2087	2087	2232	2232
count	2228	2228	1978	1978	2225	2226
%	99.8%	99.8%	94.8%	94.8%	99.7%	99.7%
avg.			76.87	112.38	1.80	13.14

	Pool Site					
	Wind Spd	Wind Dir	NO	NOx	Aeth	EBAM
monitoring period	7/15 - 10/15	7/15 - 10/15	7/24 - 10/15	7/24 - 10/15	7/15 - 10/15	7/15 - 10/15
total hours	2232	2232	2015	2015	2232	2232
count	2232	2232	1930	1930	2105	2232
%	100%	100%	95.8%	95.8%	94.3%	100%
avg.			9.48	26.62	0.76	9.95

	Church St. Site					
	Wind Spd	Wind Dir	NO	NOx	Aeth	BAM
monitoring period	9/7 - 10/15	9/7 - 10/15	8/9 - 10/15	8/9 - 10/15	9/9 - 10/15	9/7 - 10/15
total hours	925	925	1621	1621	875	925
count	780	780	1573	1573	875	780
%	84.3%	84.3%	97.0%	97.0%	100%	84.3%
avg.			70.68	102.87	1.86	16.74

	Vernon St. Site					
	Wind Spd	Wind Dir	NO	NOx	Aeth	BAM
monitoring period	9/7 - 10/15	9/7 - 10/15	9/13 - 10/15	9/13 - 10/15	9/9 - 10/15	9/7 - 10/15
total hours	925	925	781	781	875	925
count	925	925	781	781	839	925
%	100%	100%	100%	100%	95.9%	100%
avg.			18.99	36.70	1.06	11.69

* Units for NO and NOx are ppb; units for Aethalometer black carbon and EBAM/BAM PM2.5 mass are $\mu\text{g}/\text{m}^3$.

2.2 Determination of Measurement Precision and Bias Using Collocation Data

The instruments used at the four sites were collocated and operated for approximately two weeks prior to and following the summer upwind/downwind monitoring period. Data from those collocation tests were studied in detail and the following observations were made. Due to the additional complexity inherent in the aethalometer black carbon measurement method, both the original 5-minute discrete measurements as well as time-averaged versions of that data were analyzed. PM data from the beta attenuation monitors (BAMs) was examined on an hourly basis only. No collocation data was collected for the NO/NO_x instruments since they can be calibrated at regular intervals using standards of known concentration.

2.2.1 Aethalometers

Good agreement was observed between the aethalometers used at Denio and Pool sites during pre-study collocation tests, as shown in Figure 2–1. The dashed lines show the range of residuals relative to the regression line, +50% and -30%. Results are similar for this pair of instruments during the post-study collocation, as shown in Figure 2–2. Figure 2–3 shows the distribution of relative differences between the two instruments for both collocation periods. The distribution is somewhat skewed to the positive at lower concentrations, but in both charts the differences appear to stabilize at about +/- 40% for concentrations above 3000 ng/m³. Note that the errors appear to be proportional to the measured concentration, rather than a consistent absolute variability.

Agreement between the pair of instruments later used at the Church/Vernon pair of sites was not very good during the pre-study collocation, as shown in Figure 2–4, which has a slope of 0.87 despite the strong correlation ($r^2 = 0.95$). Figure 2–6 indicates that the aethalometer used at Vernon (625) showed a 5-10% negative bias relative to the other units collocated with it. Data from the two other units collocated at Denio site during this period are not shown in the chart, because they were not significantly different from unit 623 overall. The data from the unit used at Church (623) contained several serious outliers at both high and low BC concentrations.

Collocated data collected after the summer intensive (Figure 2–5) shows much better agreement between the two units used at Church and Vernon, but there is substantial scatter. The dashed lines show the range of residuals relative the regression line, +/- 35% and Figure 2–7 shows the convergence to a +/- 40% difference above 3000 ng/m³ in the post-study data, which is consistent with the collocation data for the other pair of instruments.

Aethalometer data is known to be strongly affected by electronic noise spikes that create exaggerated increases or decreases in individual measurements of light attenuation. Since the instruments estimate black carbon concentrations based on the slope of the change in attenuation, a single spike will produce two periods of inaccurate measurement. However, time-averaging those two periods together will negate the effect of the spike and give the correct value. Problems can occur when the time-averaged values do not contain a sufficient number of individual measurements to effectively cancel out the noise (this issue is discussed in the 2005 version of the aethalometer documentation provided by Magee Scientific). In this study the instruments were operated with the default 5-minute time constant, so each hourly average contains a maximum of 12 discrete measurements. Therefore, the probability of the two halves of a noise-related “bounce” in the signal being split between two hourly averages is 1:6. Averaging

over a 6-hour period reduces the probability to 1:36, as well as reducing the effect of the inaccurate measurement by approximately a factor of 6.

Figure 2–8 shows graphically the effect of increasing the time-averaging period on the correlation of the collocated sampler data. Scatter is dramatically reduced by averaging over a 6-hour period, rather than hourly, but no further improvement is evident for 24 hour averaged data. This visual observation is confirmed by the regression statistics presented in Table 2–2. The apparent decrease in correlation for the 24-hour averaged data may be due to the decreased range of values and small number of data points that result. Table 2–3 compares the error statistics for the three averaging periods. The mean error values are the average of the differences in BC concentration between a pair of collocated instruments, and the standard deviation of those differences is also included. The values labeled Propagated Error are calculated using the standard deviation of the 5-minute data differences propagated as the RMS for the longer averages. Note that this value is similar to the standard deviation of the errors for the 6-hour averages, suggesting that the errors are indeed random.

A comparison of the regression statistics for the sampler pairs to those from independent verification testing reported by the manufacturer is shown in Table 2–4. Although the precision from this study is generally not as good as would be expected from the EPA study if one examines the hourly data, the 24-hour averaged data yielded very similar precision to that in the EPA study. This again suggests that the poor precision in the 1-hour averaged data may be due to electronic noise.

Although the regressions indicate some statistically significant deviation from a 1:1 slope, and small but non-zero intercepts, these deviations are much smaller than the standard errors of the means that were calculated for the upwind/downwind pair measurements so we have decided not to attempt to adjust for the possible minor biases that they suggest. The slope observed for unit 625 during the first collocation period is more significant. The problem was apparently eliminated before or during the summer monitoring period at an unknown time and that unit was later used at the Vernon site for only about 1 month. This potential bias of up to 10% relative to the upwind site is quite small, however, in comparison to the observed upwind/downwind differences in BC.

2.2.2 BAMs

Data from the collocated continuous PM samplers (BAMs and EBAMs) shows good agreement for the pair later used at the Church and Vernon sites (Figure 2–9 and Figure 2–10), but a bias of about 15% for the other pair (Figure 2–11 and Figure 2–12). Scatter is substantial for both pairs and uniform in all cases indicating measurement precision of approximately +/- 10 ug/m³.

In contrast to the proportional error observed for the aethalometers, the BAMs exhibit a random error with a relatively fixed absolute range (i.e., the range of error does not vary with measured concentration) as shown by Figure 2–13 and Figure 2–14.

Despite the different nature of the random error, the magnitude can again be reduced to manageable size by time-averaging the data over periods longer than one hour, as shown in Figure 2–15 and Table 2–5. As with the aethalometer data, there is a dramatic improvement when a 6-hour period is used but relatively little when increasing to 24-hours. Table 2–6 again compares the error statistics for the three averaging periods. In this case the propagated error

value is similar to the standard deviation of the errors for the 6-hour and 24-hour averages, strongly suggesting that the errors are random.

2.3 Comparison of Time-Averaged Continuous Monitor Data with Time-Integrated Gravimetric Mass and Elemental Carbon

2.3.1 Gravimetric mass vs. 24-hour averaged BAM PM concentrations

Data from the Denio site were poorly correlated ($r^2=0.42$) due to the narrow range of measured PM_{2.5} concentrations. Gravimetric mass concentrations were between 13-16 $\mu\text{g}/\text{m}^3$ for all but one day. Poor correlation ($r^2=0.50$) at Pool is due to one outlier, otherwise there is good overall agreement ($r^2=0.90$, slope=1.00). The Aug, 17 gravimetric mass is suspect because it is the only case where Pool>Denio, is inconsistent with BAM data, and is significantly larger than other concentrations measured at Pool site.

There is insufficient data (3 samples at each) for evaluation for Church and Vernon. However, combining all data for the 4 sites, except the outlier at Pool, gives good correlation ($r^2=0.87$) and excellent agreement (slope=0.99) indicating that errors are random and no systematic bias exists. See Figure 2–39. Analysis of the absolute errors (grav mass – avg BAM) shows a slight bias (mean = 0.13 $\mu\text{g}/\text{m}^3$), and a 2-sigma range of $\pm 2.7 \mu\text{g}/\text{m}^3$. This suggests that errors in the individual hourly measurements that were averaged could be on the order of 10-15 $\mu\text{g}/\text{m}^3$, which is consistent with the results of the collocation testing. This is a substantially higher error estimate than that provided by the manufacturer (2.5 $\mu\text{g}/\text{m}^3$); but that specification does not take into account the relatively low PM concentrations during this study or the use of a size-selective inlet.

2.3.2 Elemental carbon vs. averaged Aethalometer black carbon concentrations

Good correlations were observed for each of the 4 sites, but there is significant scatter for highest concentrations at Denio site. All sites show a 20-30% bias of EC relative to the average BC. The relationship $0.74 \cdot \text{BC} = \text{EC}$ appears to hold for all data, as shown in Figure 2–40. The correlation was not significantly different for the other wavelength channel (880 nm) suggesting that there is little influence from organic species on the black carbon measurement. The consistent bias in EC relative to BC may be indicative of greater specificity to inorganic carbon in the aethalometer method than in the TOR method. Since EC is an operationally defined parameter it may not be appropriate to correct the BC data to match it unless compatibility with other data sets is desired.

2.4 Time-Series and Correlation Analysis of Summer 2005 Data

2.4.1 5-minute Aethalometer Data

Due to the inherent peculiarities of the aethalometer discussed earlier, the data from these instruments was given additional attention. The original 5-minute time-integrated measurements were obtained and examined day by day in time-series plots to look for indications of systematic conditions or exceptional events that would adversely affect the data. The following observations were made:

Unit A339 at Pool site experienced severe electronic noise on several days (7/22, 7/24, 8/6) during which the recorded 5-minute BC concentration would “bounce” from large positive to large negative values (<-5 ug/m³ in some cases) over periods ranging from 10 minutes to an hour. Since these excursions did not correspond to peaks at the downwind site (no data is available from the other upwind site), or in the data from the other wavelength channel in some cases, we conclude that they are due to an instrument malfunction. The problem was much worse for Channel 1 data. See Figure 2–16. Although these noise spikes are not expected to have a substantial impact on the daily average values, they can seriously affect hourly values so data for the identified periods was excluded from the upwind/downwind analysis. Data from an additional aethalometer (A476) that was collocated at the Pool site was substituted during the period 8/1 12:00 – 8/7 04:00.

At Church and Vernon sites the negative noise spikes were never larger than -1.5 ug/m³, and at Denio never larger than -1.0 ug/m³. Periods of excessive noise resulting in significantly negative values occurred at Church on 10/15, Vernon on 9/21 and at both sites between 9/26-9/27. At Denio on 8/29 there was a very large, sudden spike followed by a 2-hour period of negative readings. Similar behavior occurred on 8/2 and 8/3. These days were excluded from analysis.

The very large single-point spike at Vernon on 9/25 at 10:30 is not consistent with other sites and was removed. Excluding this point changes the hourly average from 6.3 to 0.6 ng/m³.

Automatic tape advance resulted in loss of 15 minutes of data at irregular intervals. These data gaps appear to occur more frequently when BC concentrations are higher, as shown in Figure 2–17 and may bias the averaged data. Removing data for those hours during which a tape advance occurred (criteria=less than 11 measurements) should improve the comparison between sites on an hourly basis, but may bias the overall results even further somewhat by reducing the relative number of hours during high concentration periods. As with the large signal noise effects, this problem can be circumvented by examining the data over longer time periods. We recommend synchronizing the tape changes for all instruments during future monitoring, even if it results in more gaps in the data.

2.4.2 Review of Time-Series of Hourly Data

The hourly data for each parameter was plotted as a time series for the duration of the summer intensive to look for indications of systematic conditions or exceptional events that would adversely affect the data. The following observations were made:

Wind Data

Comparison of the wind speed and direction time-series shows similar patterns at all sites. Peak wind speeds were generally lower at the upwind sites, but showed the same diurnal pattern as downwind sites and the met tower at the Roseville AQMD station. See Figure 2–18, Figure 2–19, and Figure 2–20. Higher peak wind speeds at the downwind sites may be due to the greater “fetch” provided by the open rail yard when winds are in the prevailing southeasterly direction

NO/NO_x

All major peaks have corresponding peaks in data from at least one of the other sites. Range of data is comparable for all three one month periods. See Figure 2–24 to Figure 2–29.

There were a few brief periods where both NO and NO_x were negative, which were removed from the data. Hours where NO was slightly negative (>-3 ppb) were not removed to prevent biasing the averages since these occurred at both Denio and Pool during periods of low NO_x concentration. NO/NO_x data from the sampler at the Pool site was adjusted by a factor of 1.2 to account for the results of an ARB field audit.

Black carbon

Diurnal patterns and relative magnitudes are consistent with the expected upwind/downwind pattern. See Figure 2–30, Figure 2–31, and Figure 2–32

PM_{2.5}

BAM data were negative 3%, 6%, 0%, and 2% of hours for which there are data at Denio, Pool, Church, and Vernon, respectively. Negative values ranged from -1 to -5 µg/m³ and appear occur intermittently suggesting a problem with baseline drift. See Figure 2–33, Figure 2–34, and Figure 2–35.

2.4.3 Correlations of Parameters

Wind vectors

Since wind data contains both magnitude and direction components it is difficult to evaluate fully in a temporal plot. In order to better assess the similarity of wind patterns at the 4 sites we have prepared scatter plots comparing the X (easterly) and Y (northerly) wind vectors measured at the 4 monitoring locations with the corresponding data from the met tower at the Roseville district air quality station. As shown in Figure 2–36, the patterns are similar for all sites, and show particularly good agreement for the Y direction.

PM vs. BC

It is instructive to examine the correlation of the hourly black carbon to particulate mass for each site, in order to look for instances where the ratio of BC to PM is unrealistic. Even in aerosols that are composed purely of fresh diesel engine exhaust we expect the ratio to be no greater than 0.50 – 0.75, based on direct measurements of vehicle emissions. As Figure 2–37 shows, the ratio is consistently well below the 1. Higher BC/PM ratios are observed at the downwind sites than at the upwind sites, which is consistent with diesel exhaust impact.

NO vs. NO_x

Figure 2–38 shows time series of NO/NO_x ratios at the four monitoring sites. Data are daily averages of data meeting the criteria for inclusion in the upwind/downwind analysis. Note that the ratios at the downwind sites are consistently higher than at the two upwind sites. This reflects the impact of fresh NO_x emissions from the rail yard at the downwind sites. Ratios are not shown when daily average NO_x concentrations were too low (<20 ppb) to allow calculation of a meaningful ratio.

Table 2–2. Regression statistics for collocated aethalometer data with different averaging periods.

	1-hour	6-hour	24-hour
slope	0.92 ± 0.02	0.94 ± 0.03	0.89 ± 0.12
intercept (µg/m³)	0.26 ± 0.07	0.19 ± 0.12	0.38 ± 0.37
r²	0.90	0.95	0.87

Table 2–3. Error statistics for collocated aethalometer data with different averaging periods.

	1-hour	6-hour	24-hour
mean error (µg/m³)	-0.02	-0.01	-0.08
stdev of error	0.78	0.44	0.39
propagated error	n/a	0.32	0.16
CV of error	27%	16%	14%

Table 2–4. Collocated aethalometer comparisons. Results from an EPA study are included for comparison.

Instruments	A330/A339	A330/A339	623/625	623/625	Pittsburgh	Fresno
Test Period	6/27/05-7/11/06	10/28/05-11/13/05	8/24/05-9/5/05	10/28/05-11/13/05	8/1/00-9/1/00	12/18/00-1/17/01
data averaging	1 hour	1 hour	1 hour	1 hour	5 minute	5 minute
mean BC (ug/m3)	2.2	2.8	2.3	2.7	1.3	6.1
<u>regression</u>						
r ²	0.86	0.90	0.95	0.92	0.93	0.95
slope	0.96	0.98	0.87	0.99	0.91	1.00
intercept	0.19	0.04	0.05	0.03	0.05	0.06
CV	21%	27%	18%	21%	18%	12%
<u>relative difference</u>						
mean	5.4%	-0.8%	-10.6%	0.2%		
stdev	22%	25%	12%	21%		
skew	0.94	0.88	0.72	0.09		
data averaging	24 hour	24 hour	24 hour	24 hour	24 hour	24 hour
<u>regression</u>						
r ²	0.99	0.93	0.96	0.99	0.98	1.00
slope	0.95	1.06	0.88	0.98	0.96	1.00
intercept	0.15	-0.10	0.05	0.04	0.00	-0.05
CV	2.8%	14.1%	5.1%	3.5%	4.2%	2.7%

Table 2–5. Regression statistics for collocated BAM data with different averaging periods.

	1-hour	6-hour	24-hour
slope	0.84 ± 0.03	1.06 ± 0.05	1.07 ± 0.07
Intercept (ug/m3)	3.85 ± 0.59	0.76 ± 0.75	0.76 ± 0.98
r2	0.65	0.90	0.96

Table 2–6. Error statistics for collocated BAM data with different averaging periods.

	1-hour	6-hour	24-hour
mean error (ug/m3)	-1.7	-1.6	-1.7
stdev of error	6.4	2.6	1.2
propagated error	n/a	2.6	1.3
CV of error	47%	19%	9%

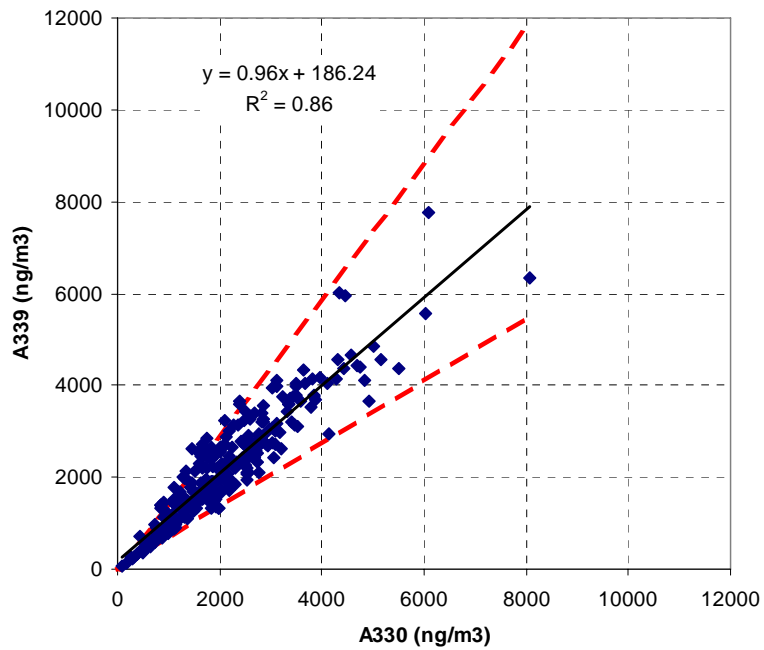


Figure 2–1. Correlation of hourly BC (ng/m³) averaged data from collocated aethalometers 6/27.-7/11. Instrument A330 was later used at the Denio site, and A339 at Pool.

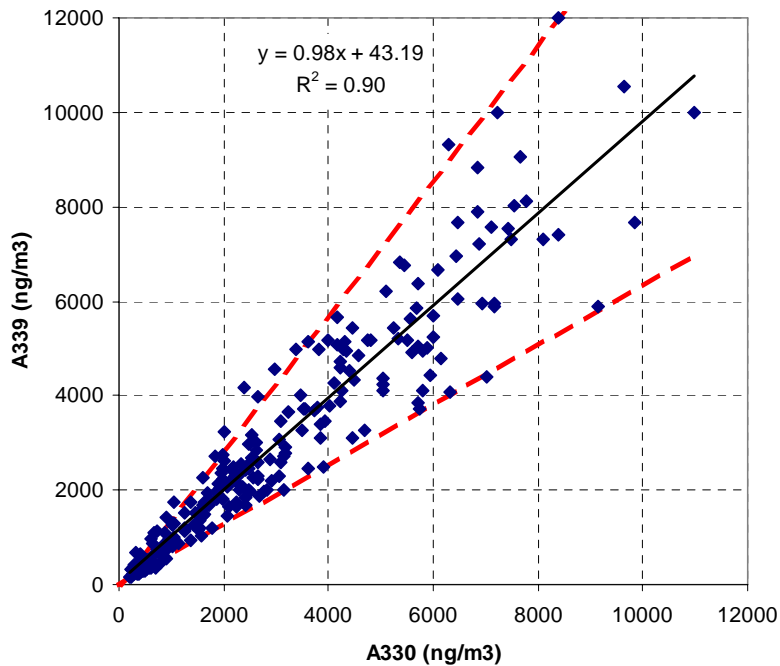


Figure 2–2. Correlation of hourly averaged BC (ng/m³) data from collocated aethalometers 10/28–11/13.

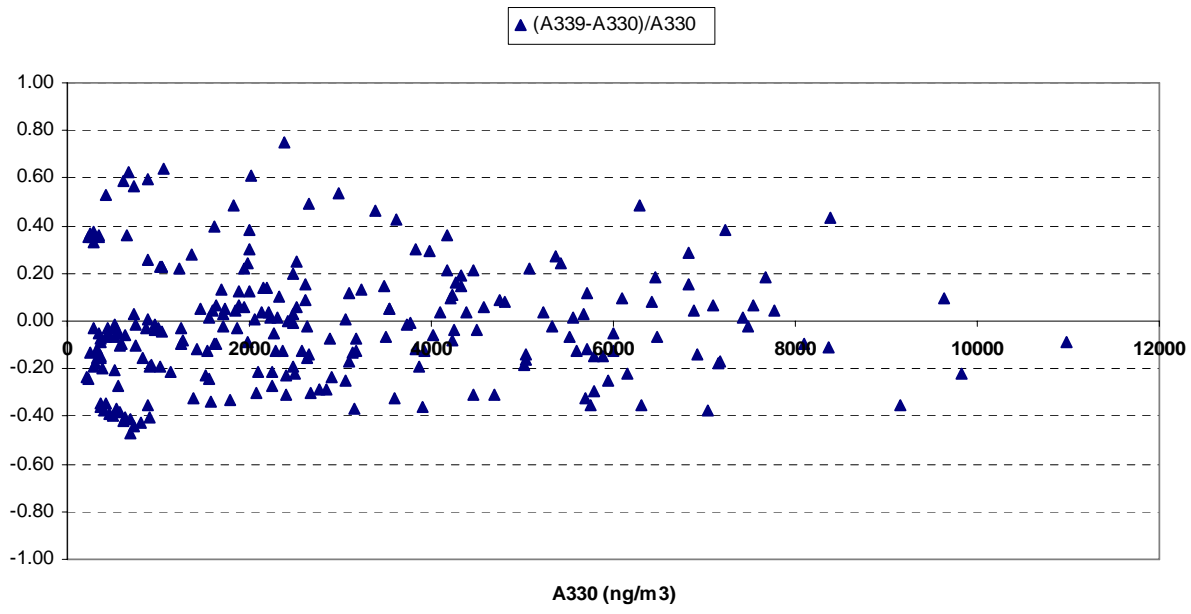
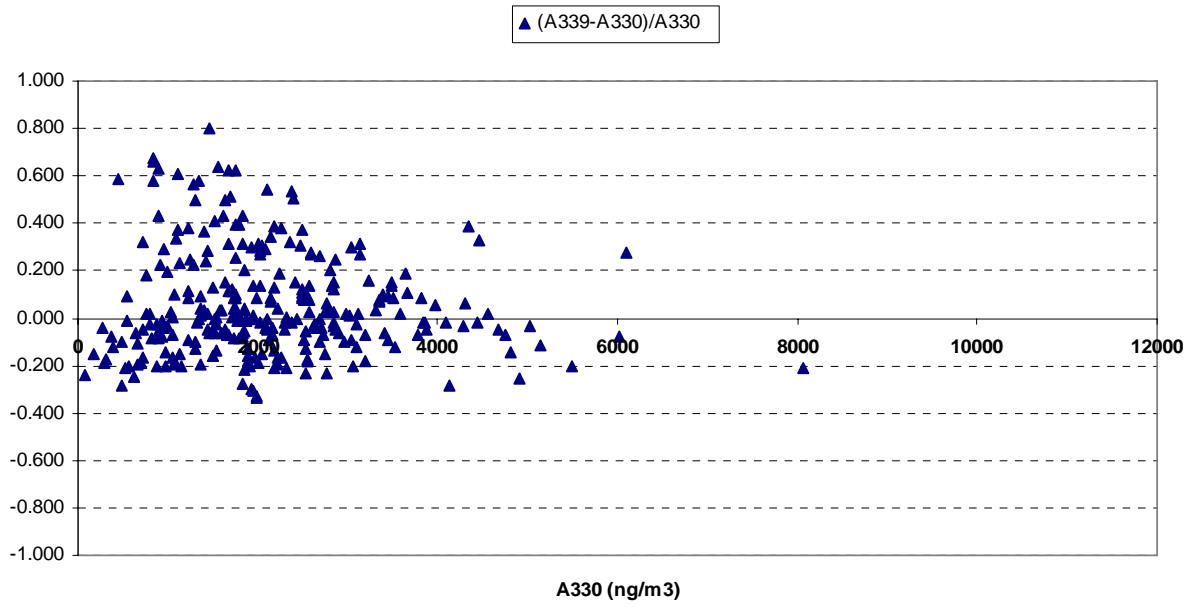


Figure 2-3. Plot of relative difference between collocated aethalometers during periods 6/27.-7/11 (upper) and 10/28-11/13 (lower). A330 was later used at Denio site and A339 at Pool site. Data are hourly averages of channel 2 BC.

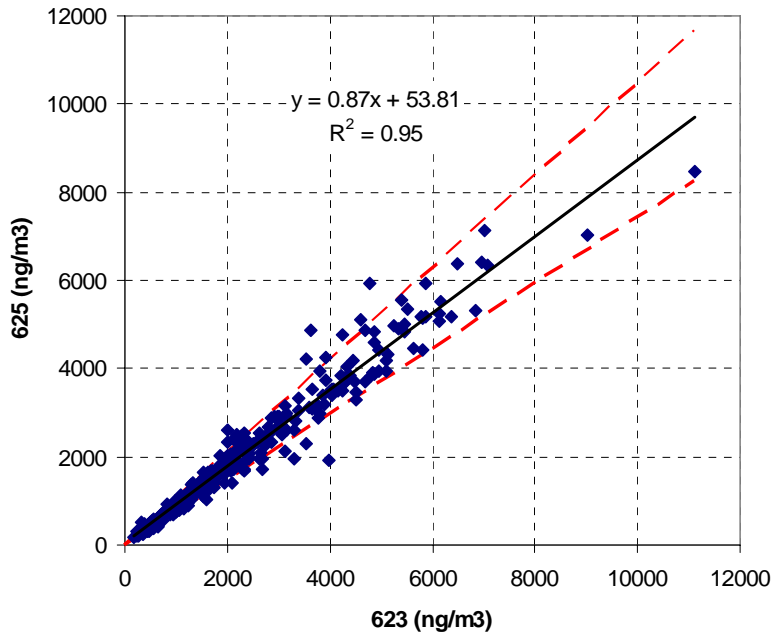


Figure 2–4. Correlation of hourly averaged data from collocated aethalometers 8/24 -9/5. 623 was later used at Church and 625 at Vernon.

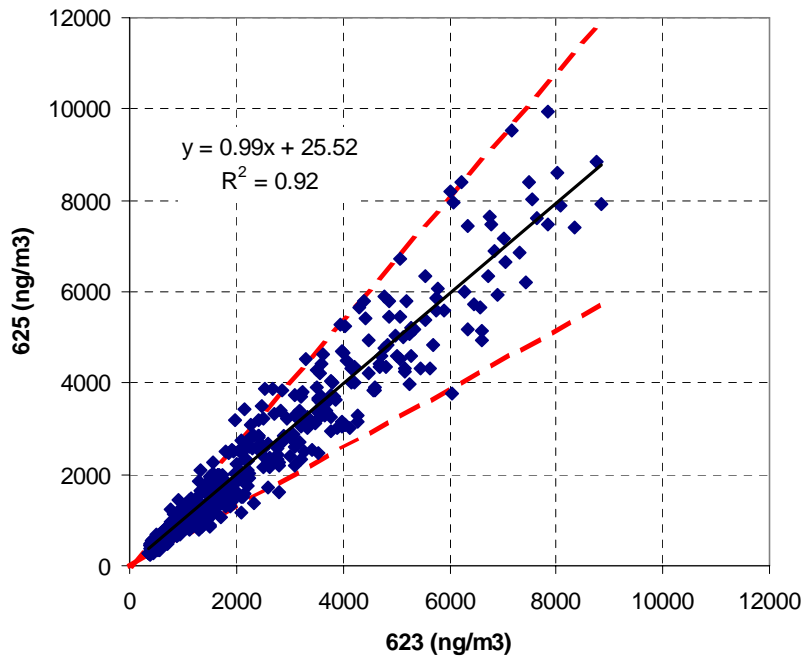


Figure 2–5. Correlation of hourly averaged data from collocated aethalometers 10/28 – 11/13.

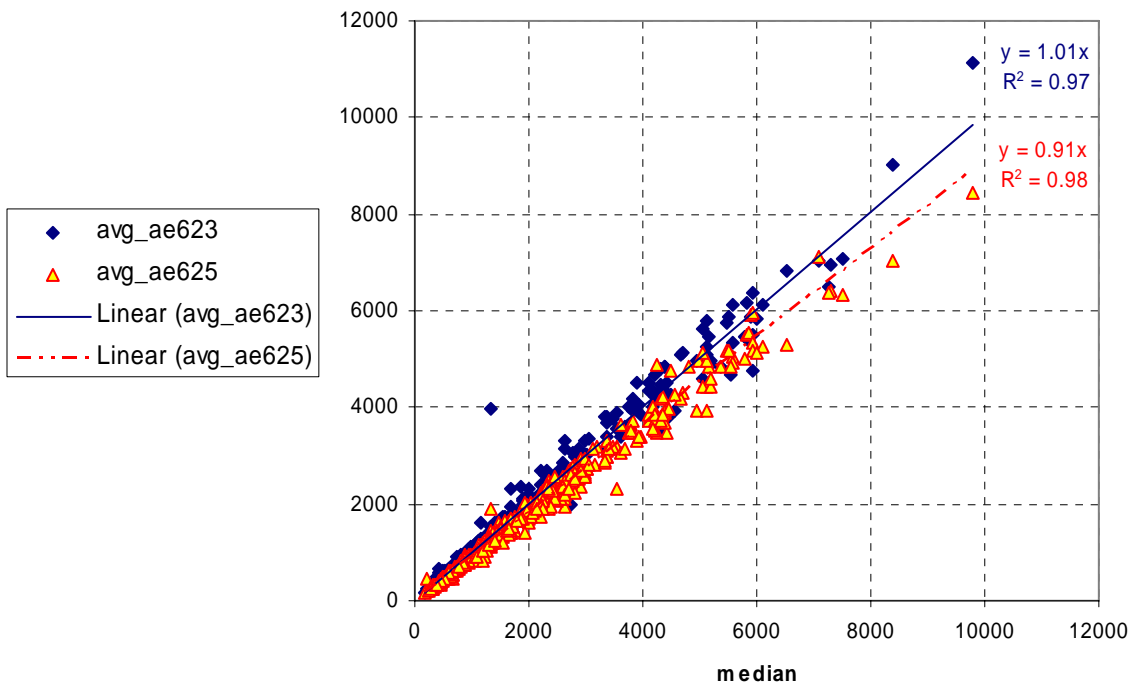


Figure 2–6. Correlation of hourly averaged data from collocated aethalometers 8/24 -9/5. X-axis values are the median of 4 collocated instruments.

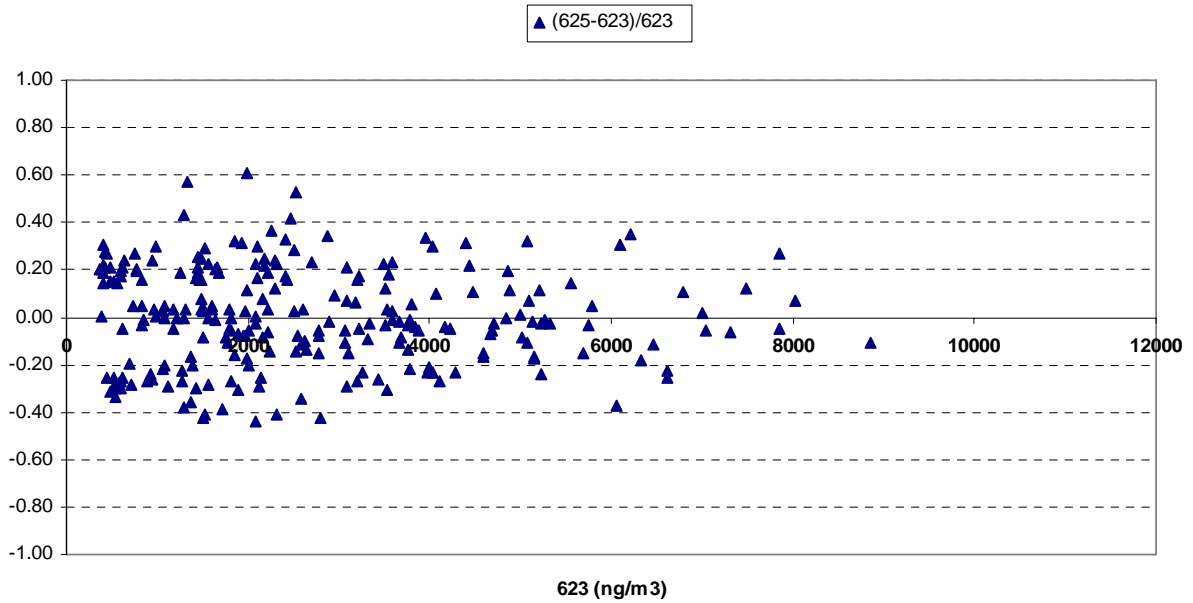
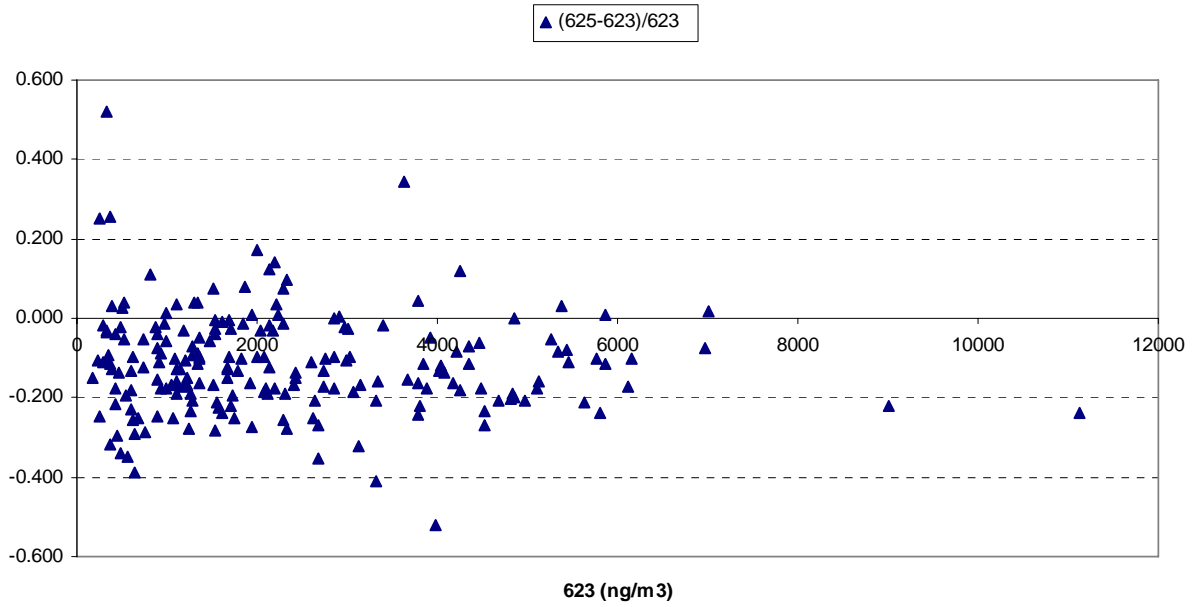


Figure 2-7. Plot of relative difference between collocated aethalometers during periods 8/24 -9/5 (upper) and 10/28 – 11/13 (lower). 623 was used at Church site and 625 at Vernon site. Data are hourly averages of channel 2 BC.

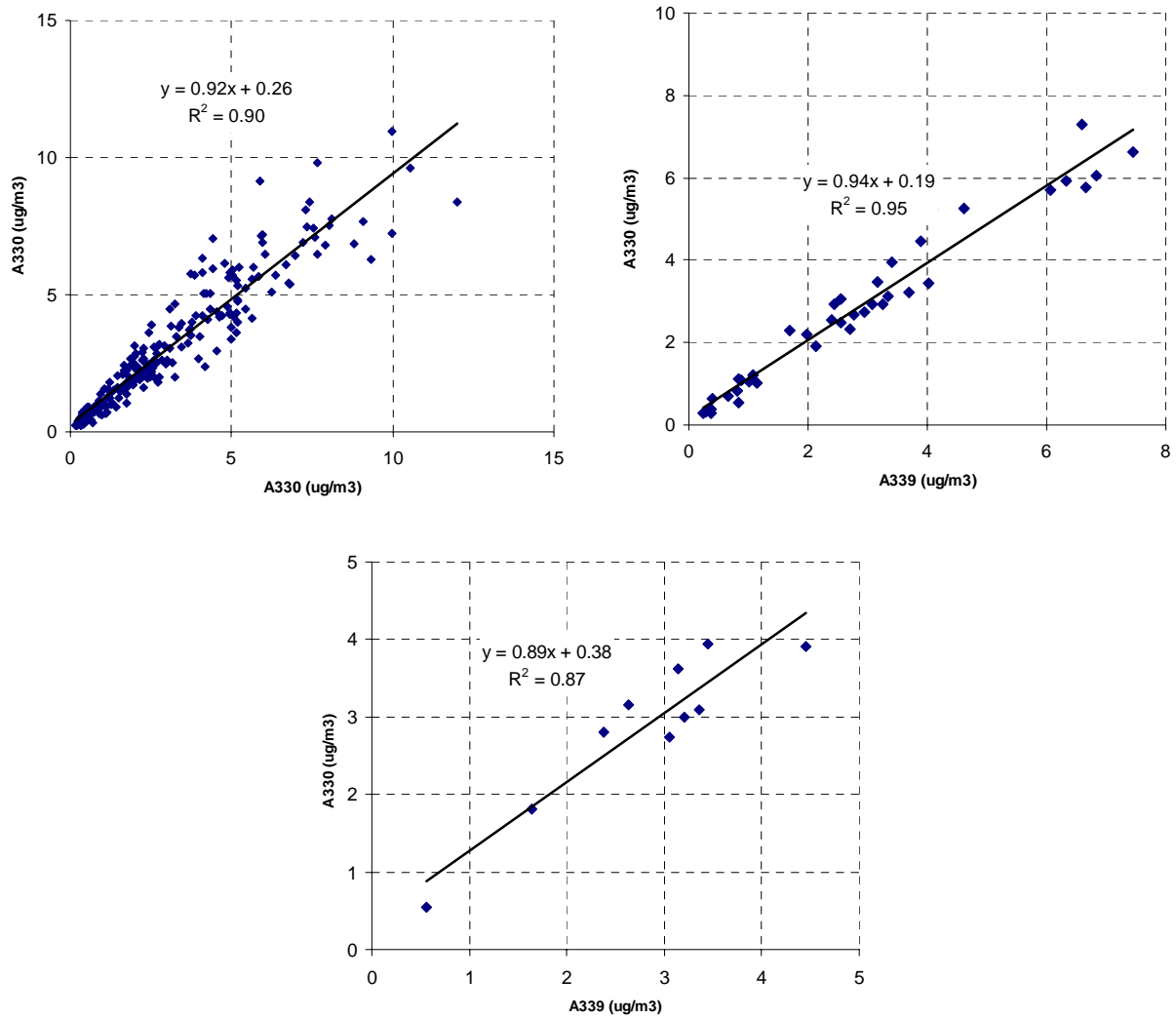


Figure 2–8. Regression of collocated aethalometer data for 1-hour, 6-hour, and 24-hour averages.

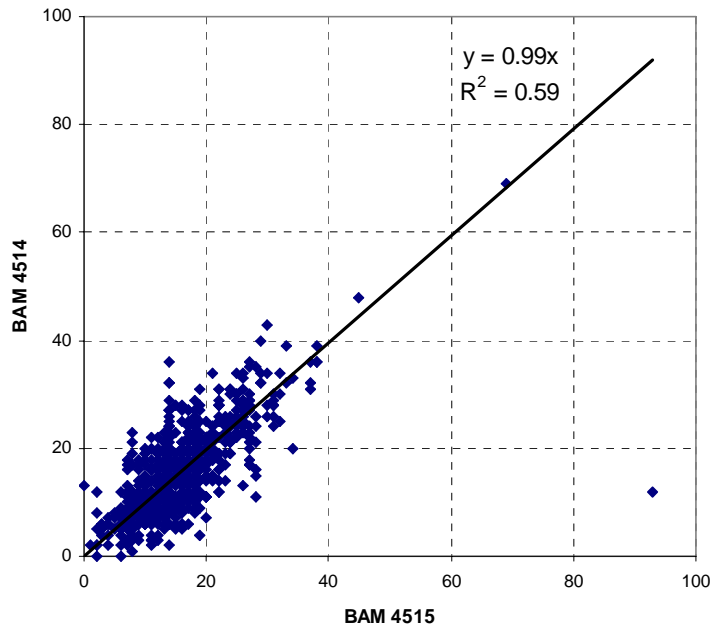


Figure 2–9. Correlation of hourly averaged PM2.5 (ug/m3) data from collocated BAMs 7/28-9/7. Outlier in lower right corner is excluded from regression. BAM 4515 was later used at Church site and BAM 4514 at Vernon.

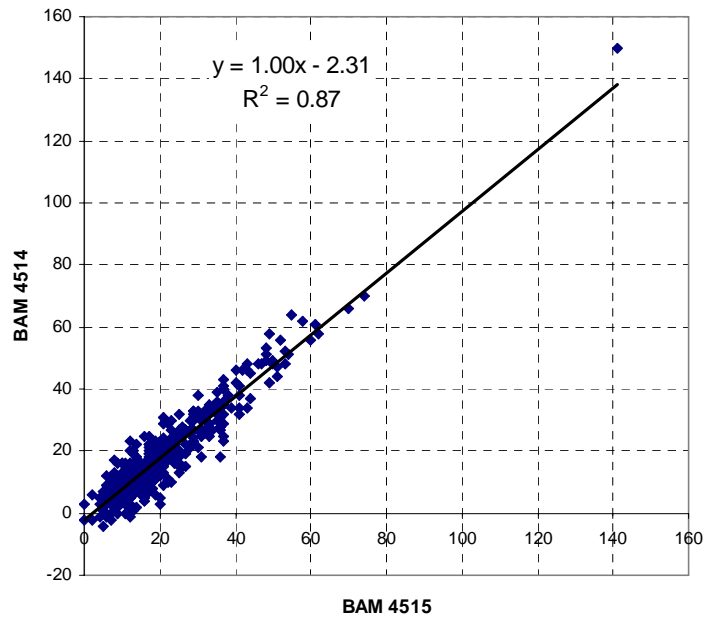


Figure 2–10. Correlation of hourly averaged PM2.5 (ug/m3) data from collocated BAMs 10/18-11/19. Outlier in upper right corner is excluded from regression.

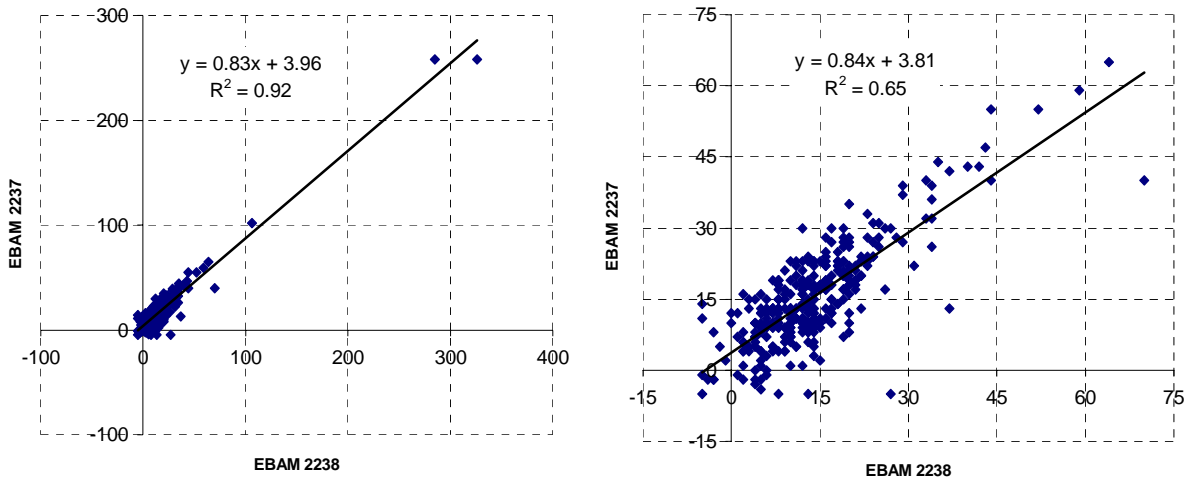


Figure 2–11. Correlation of hourly averaged PM_{2.5} (ug/m³) data from collocated BAMs 6/24-7/8, with and without extreme from one event. EBAM 2238 was later used at Denio and EBAM 2238 at Pool.

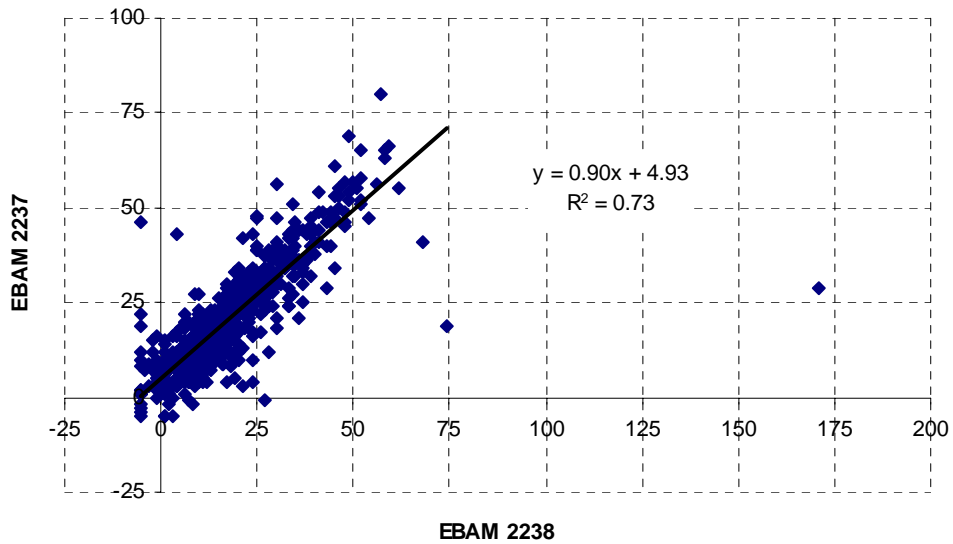


Figure 2–12. Correlation of hourly averaged PM_{2.5} (ug/m³) data from collocated BAMs 10/21-11/14. Outlier on right is excluded from regression.

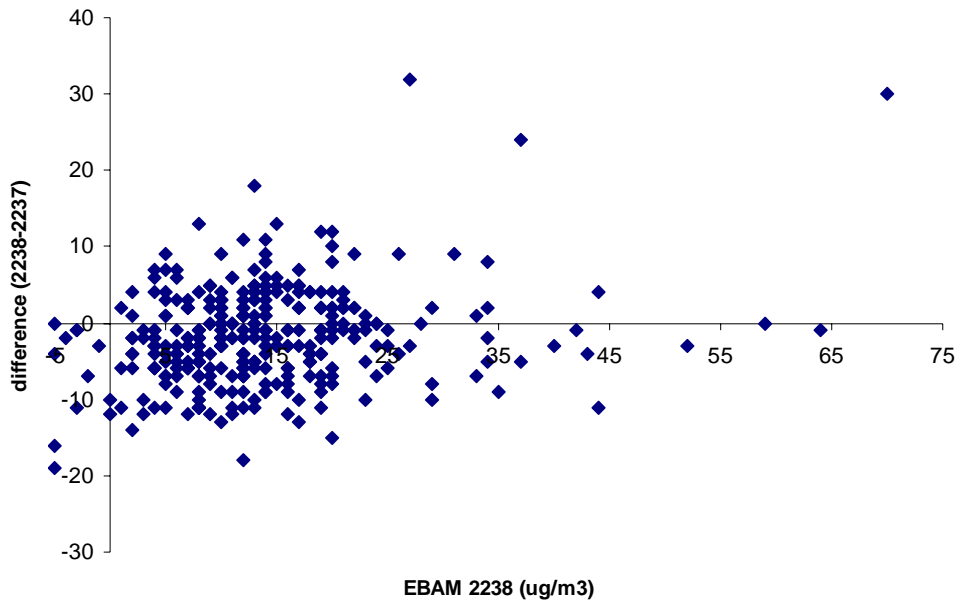


Figure 2–13. Difference between collocated BAMs as a function of PM concentration. Data is hourly.

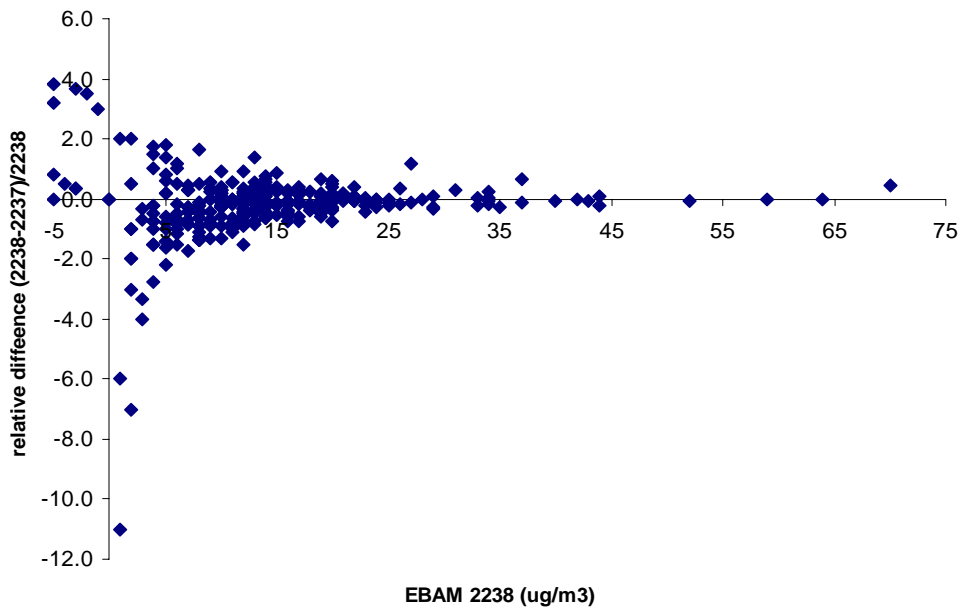


Figure 2–14. Relative error between collocated BAMs as a function of PM concentration.

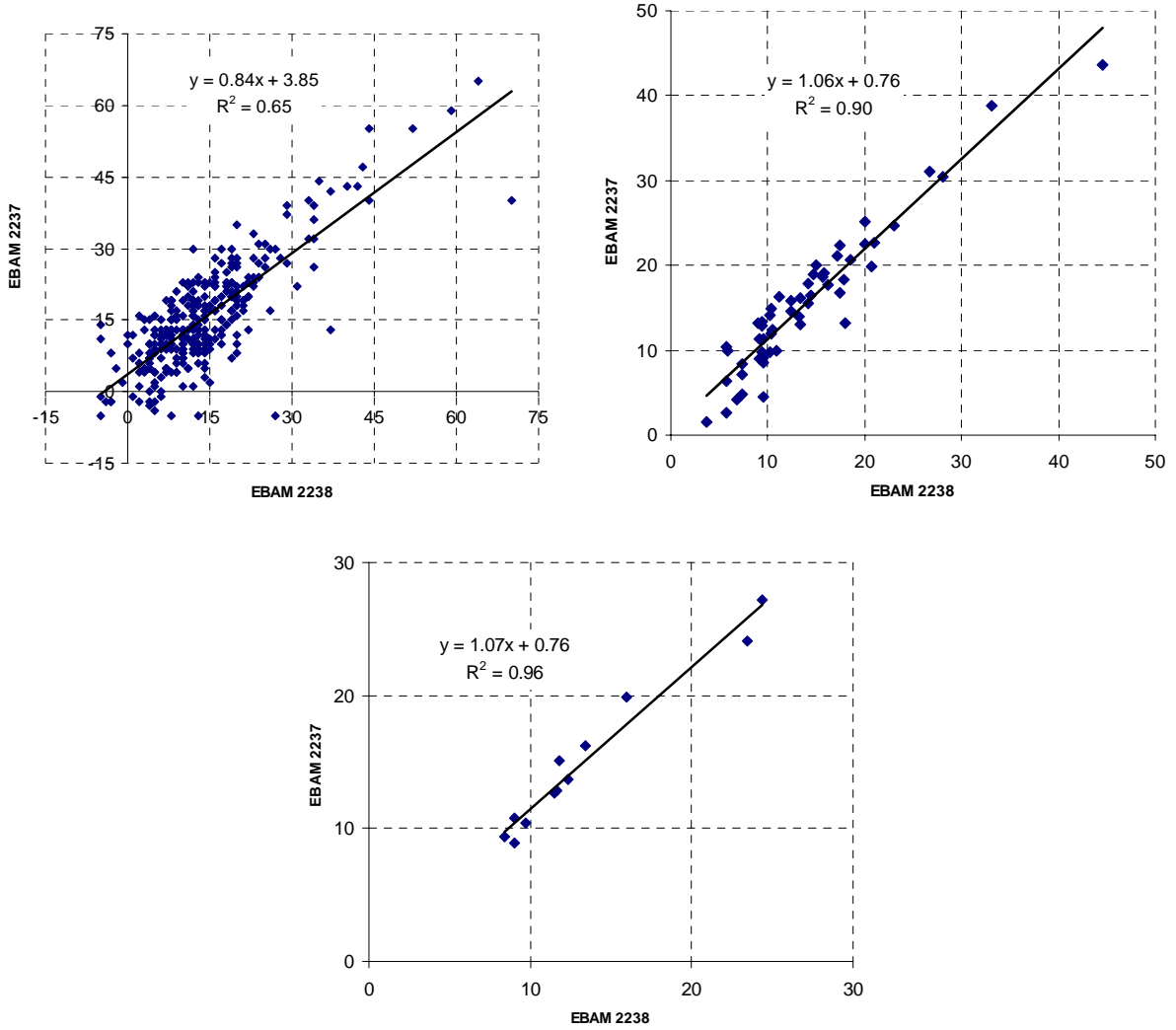


Figure 2–15. Regression of collocated BAM data for 1-hour, 6-hour, and 24-hour averages.

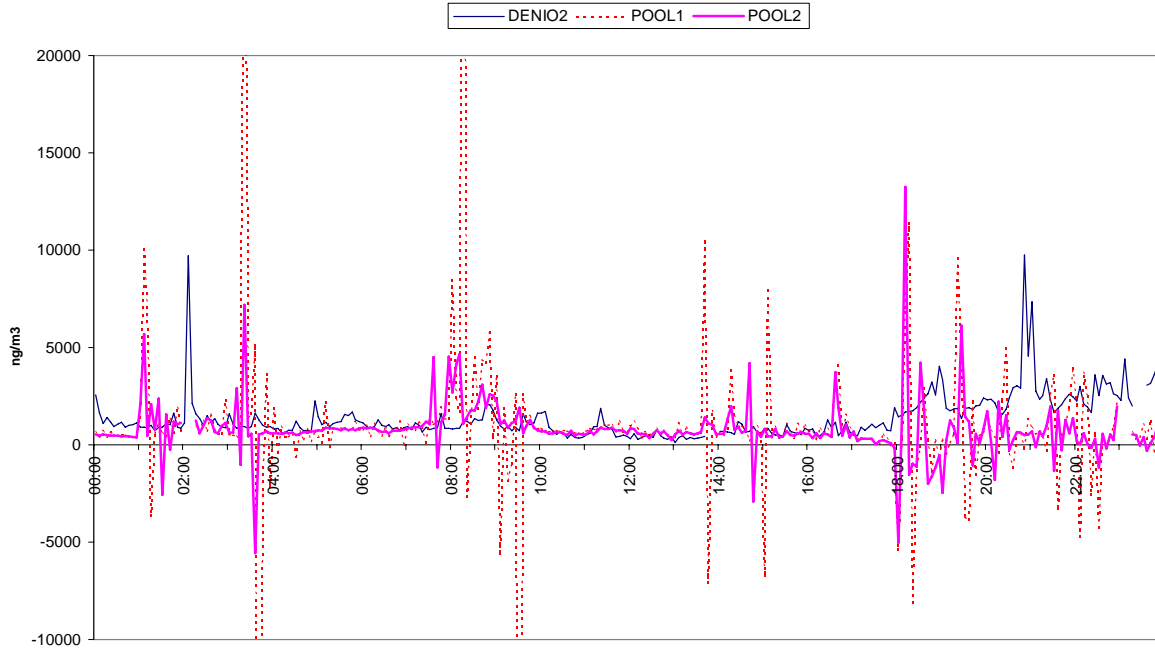


Figure 2–16. Time-series plot of aethalometer data from Denio and Pool sites showing measurement noise in the data from Pool on August 6. The number after the site name indicates the wavelength channel (1=880 nm, 2=370 nm).

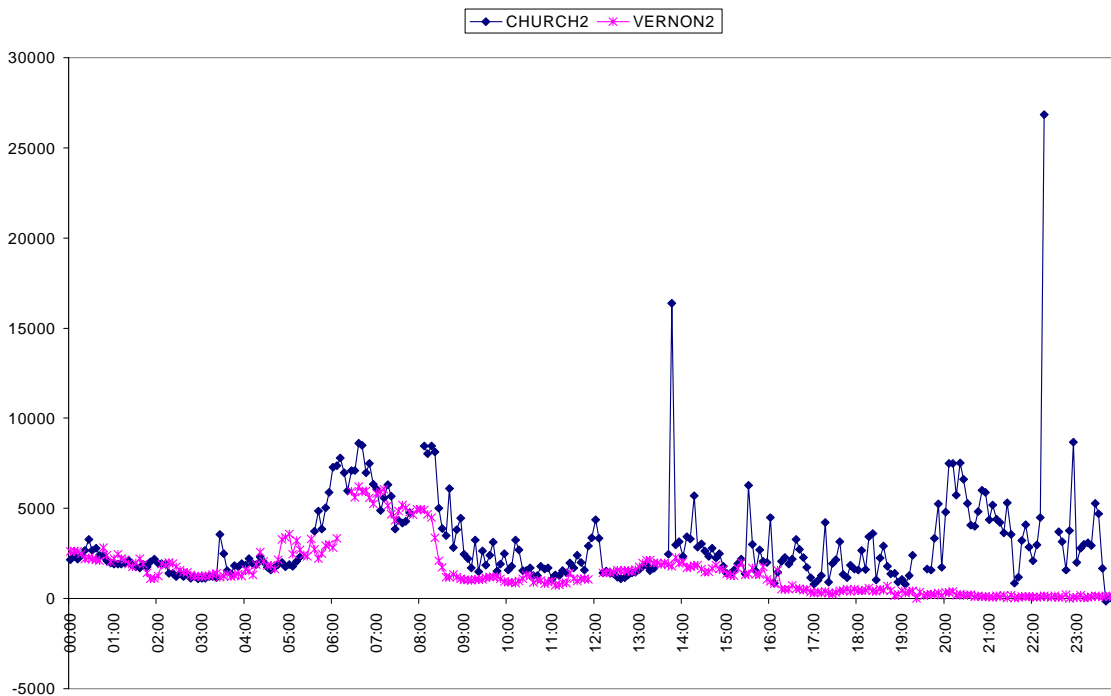


Figure 2–17. Time-series plot for Oct.14 showing data gaps resulting from automatic tape advance.

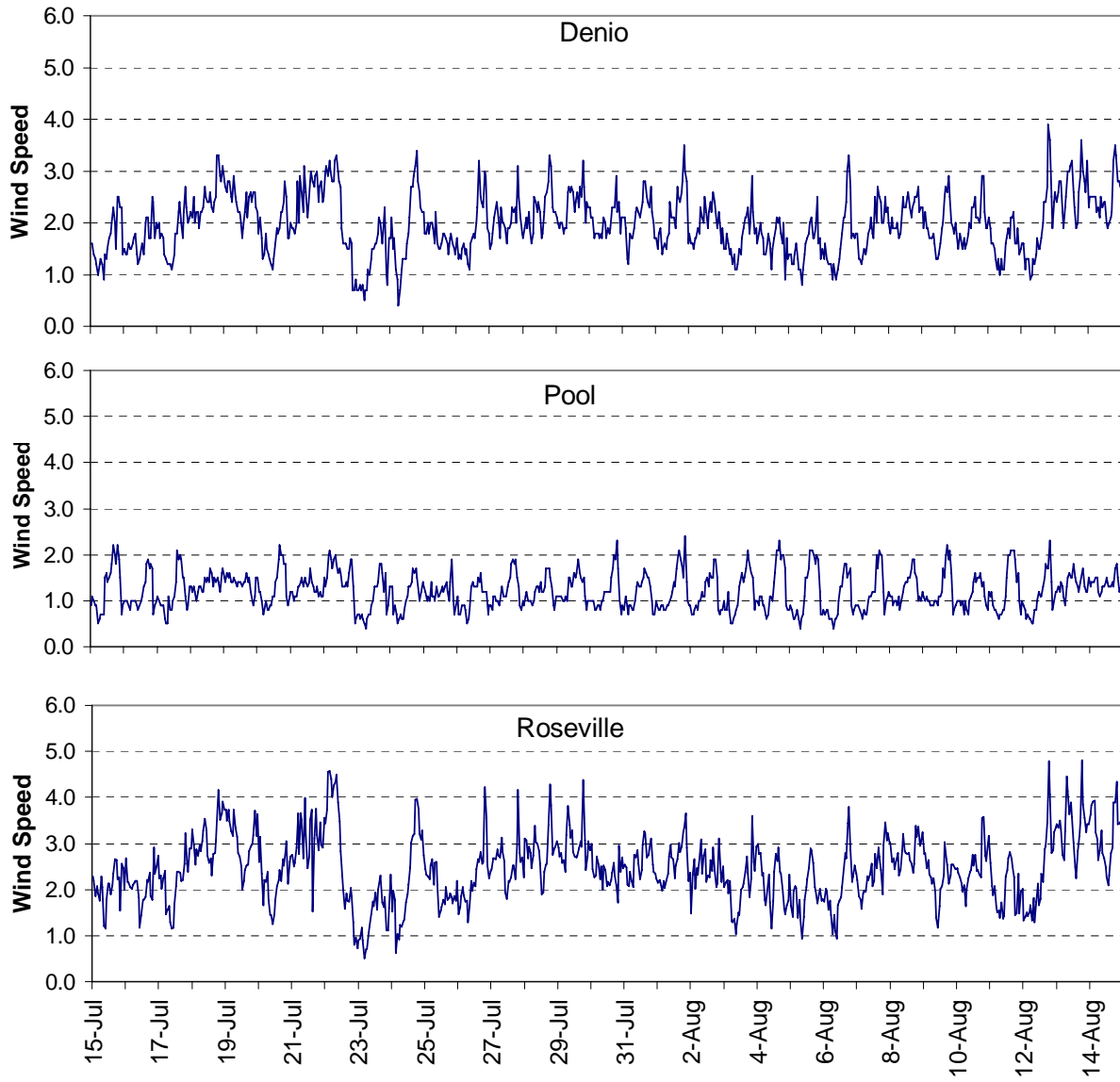


Figure 2–18. Hourly wind speed during first 30 days of summer intensive.

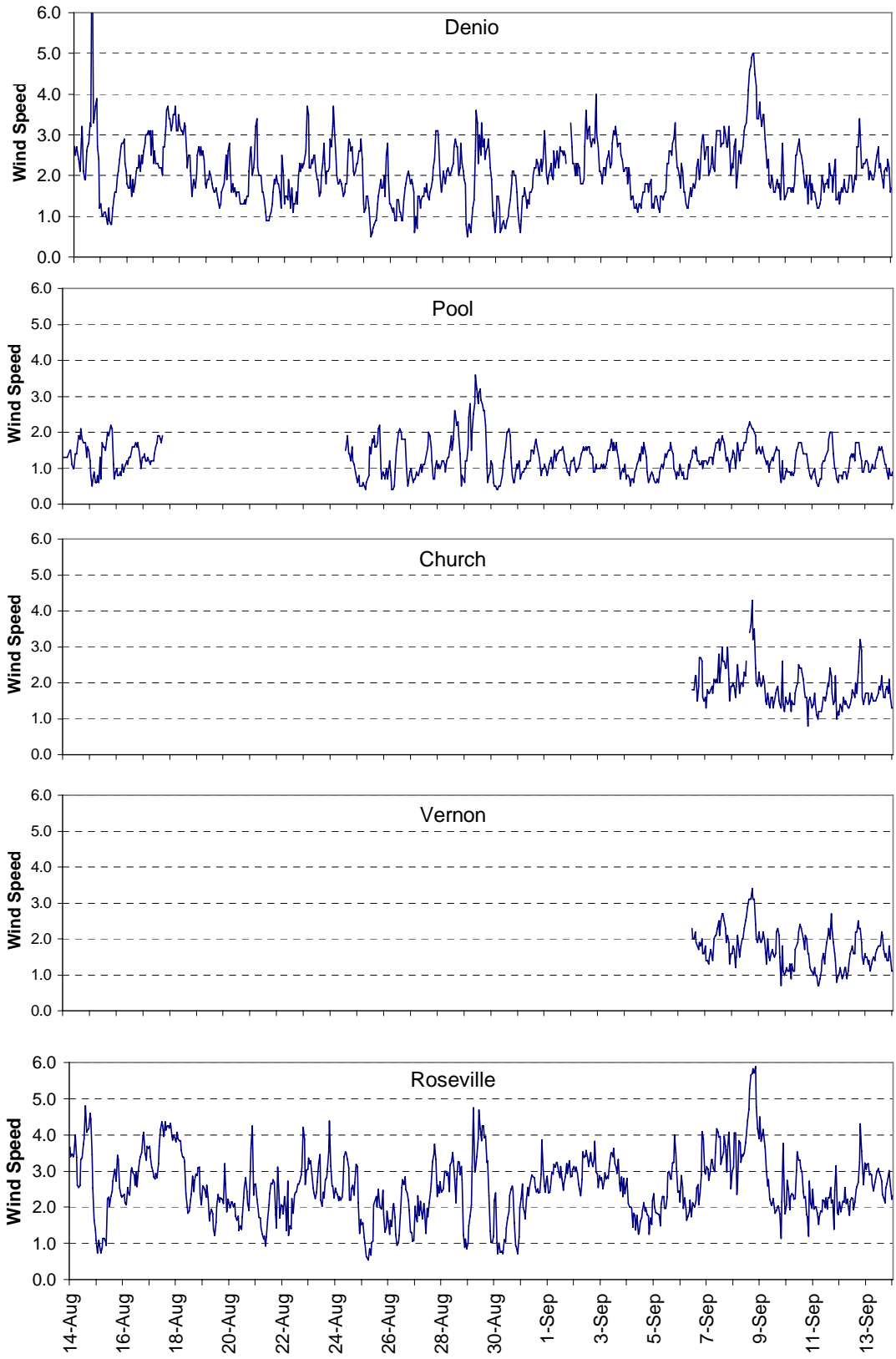


Figure 2–19. Hourly wind speed during middle 30 days of summer intensive.

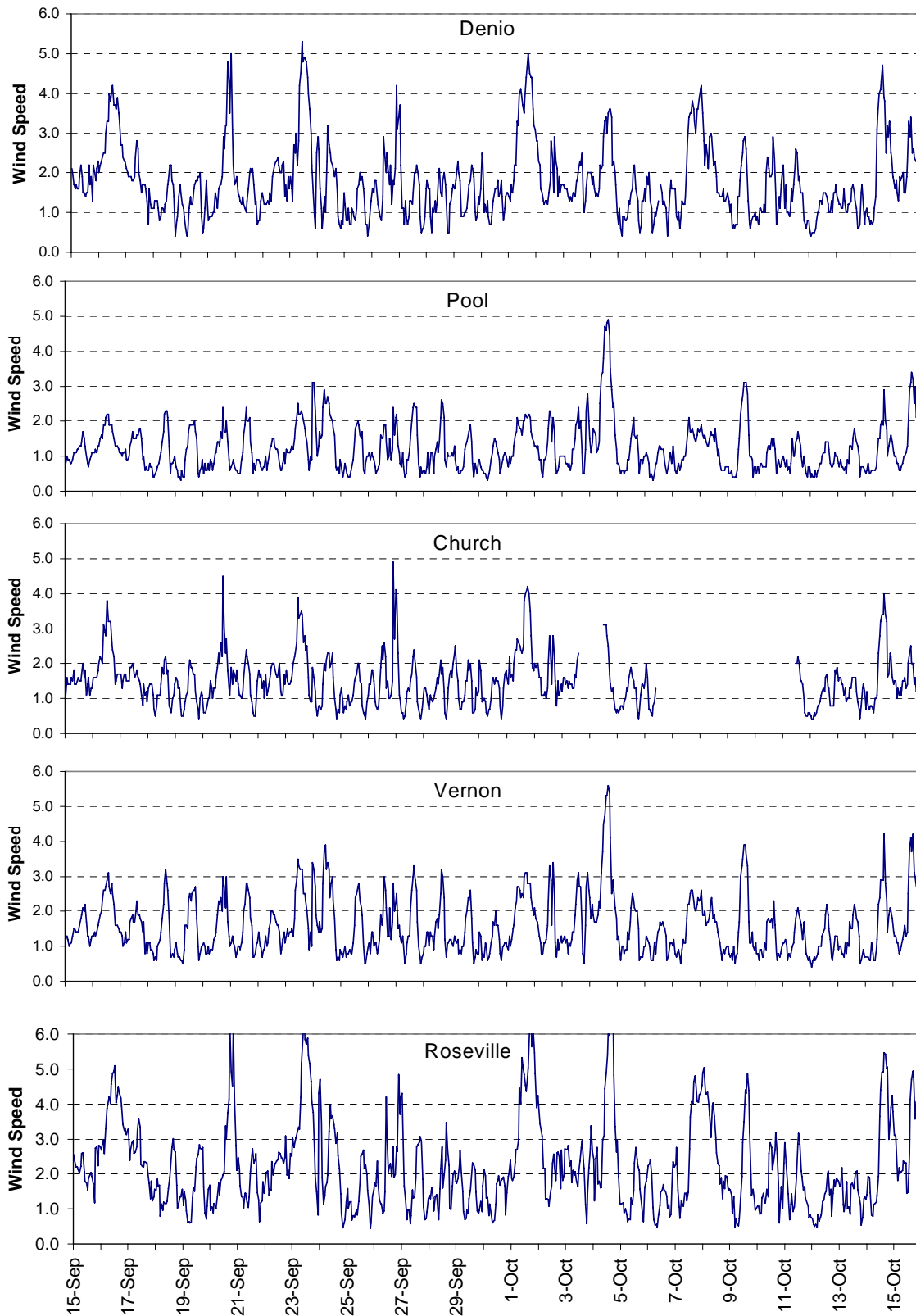


Figure 2–20. Hourly wind speed during last 30 days of summer intensive.

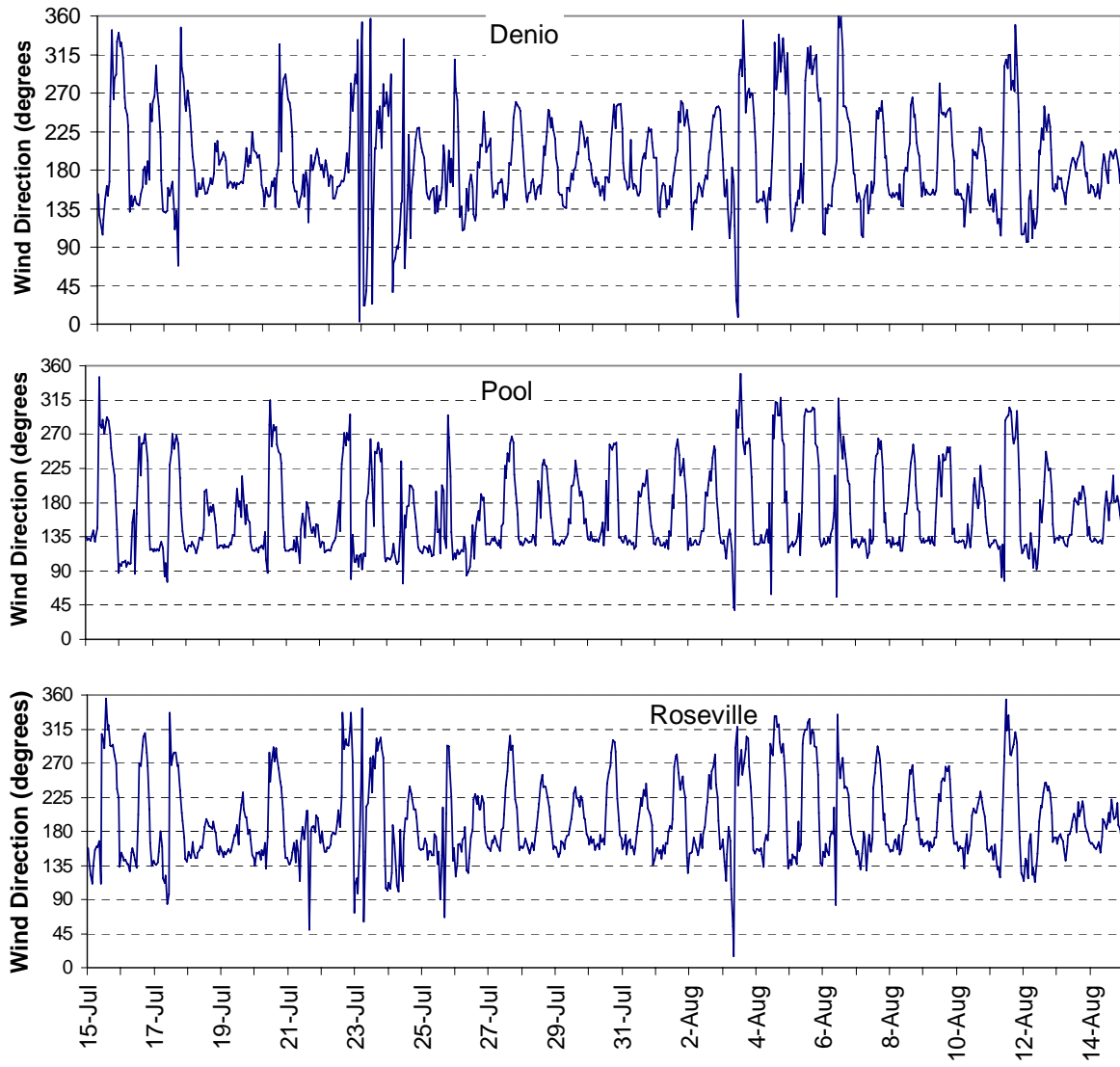


Figure 2–21. Hourly wind direction during the first 30 days of summer intensive.

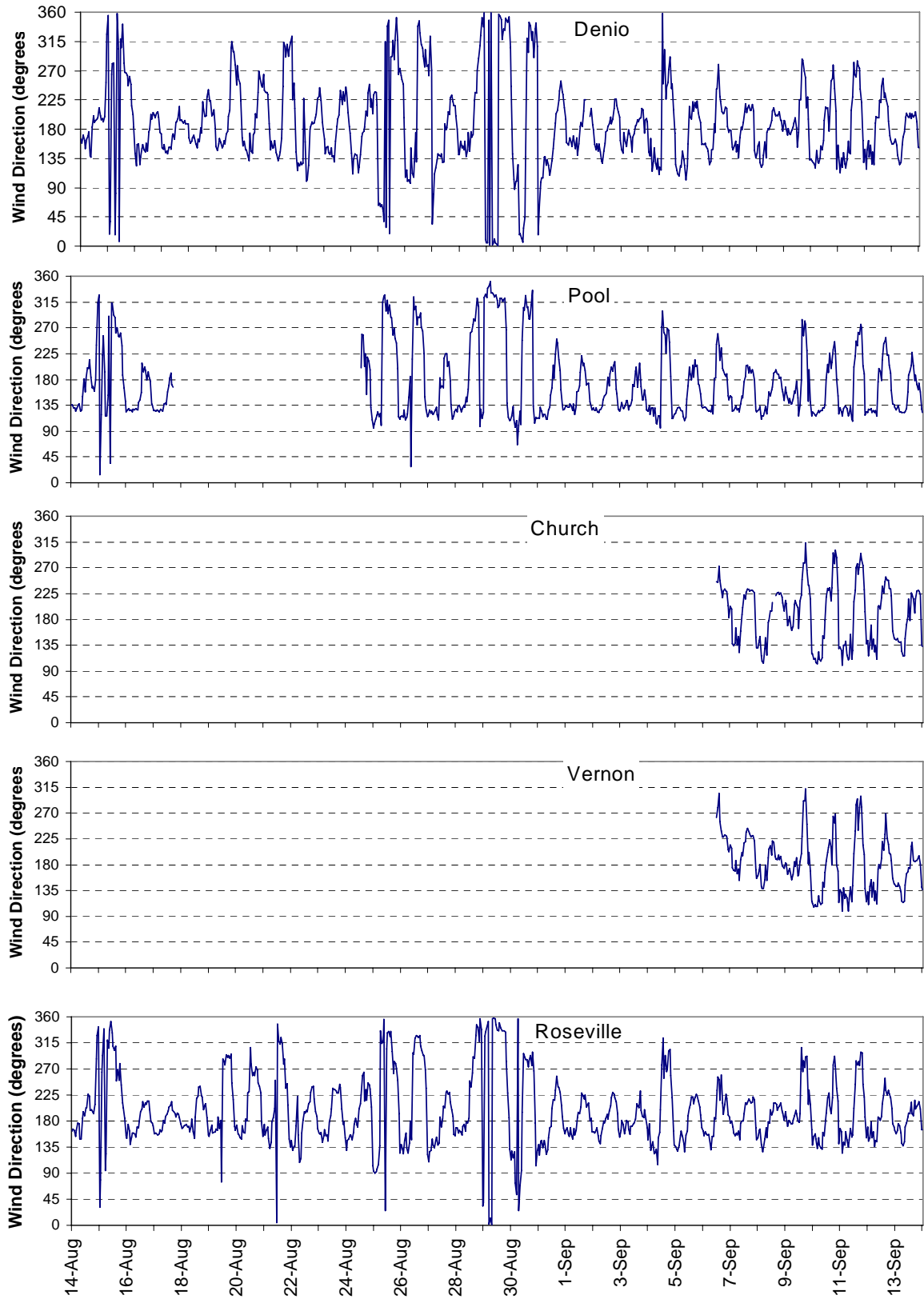


Figure 2–22. Hourly wind direction during middle 30 days of summer intensive.

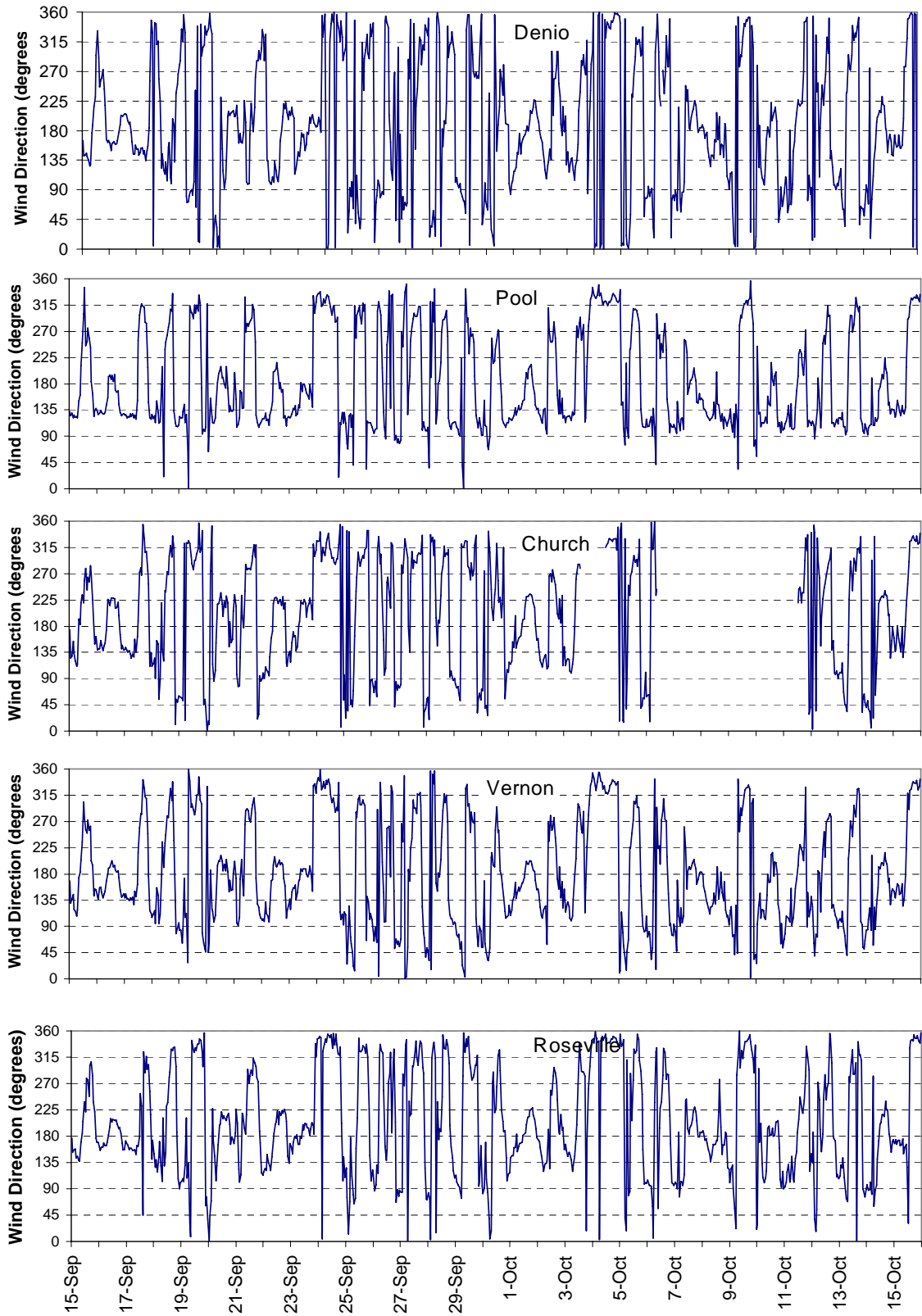


Figure 2–23. Hourly wind direction during last 30 days of summer intensive.

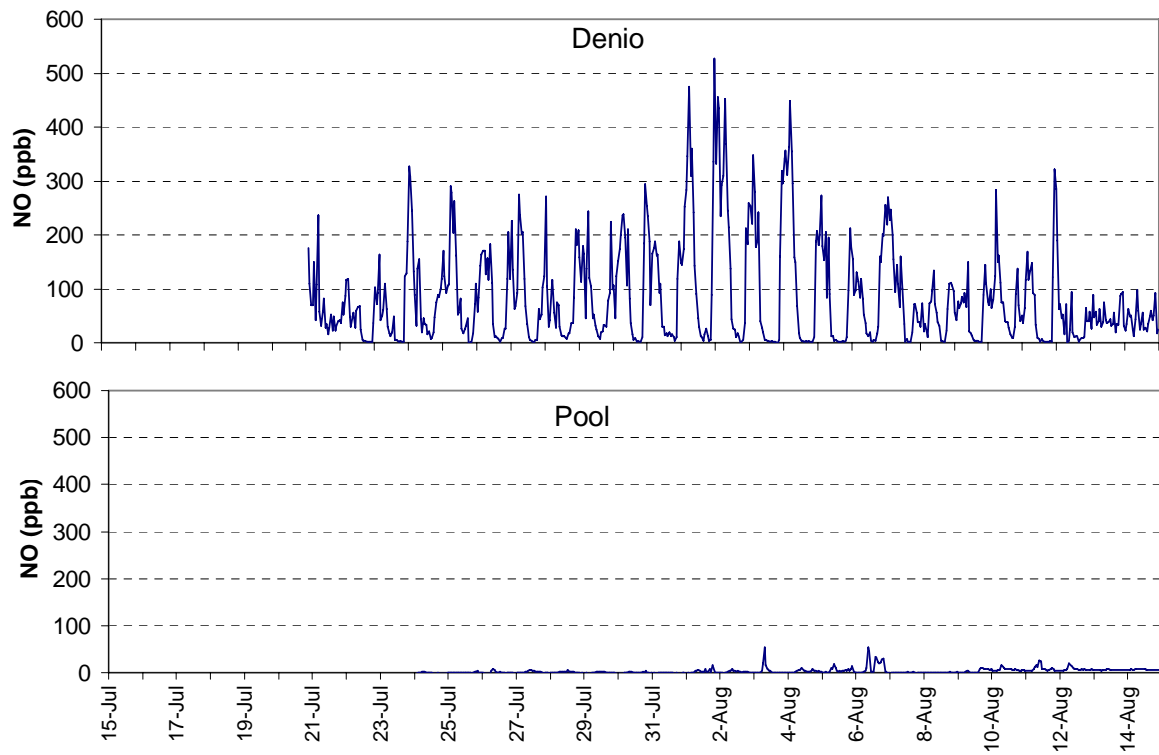


Figure 2–24. Hourly NO data during first 30 days of summer intensive.

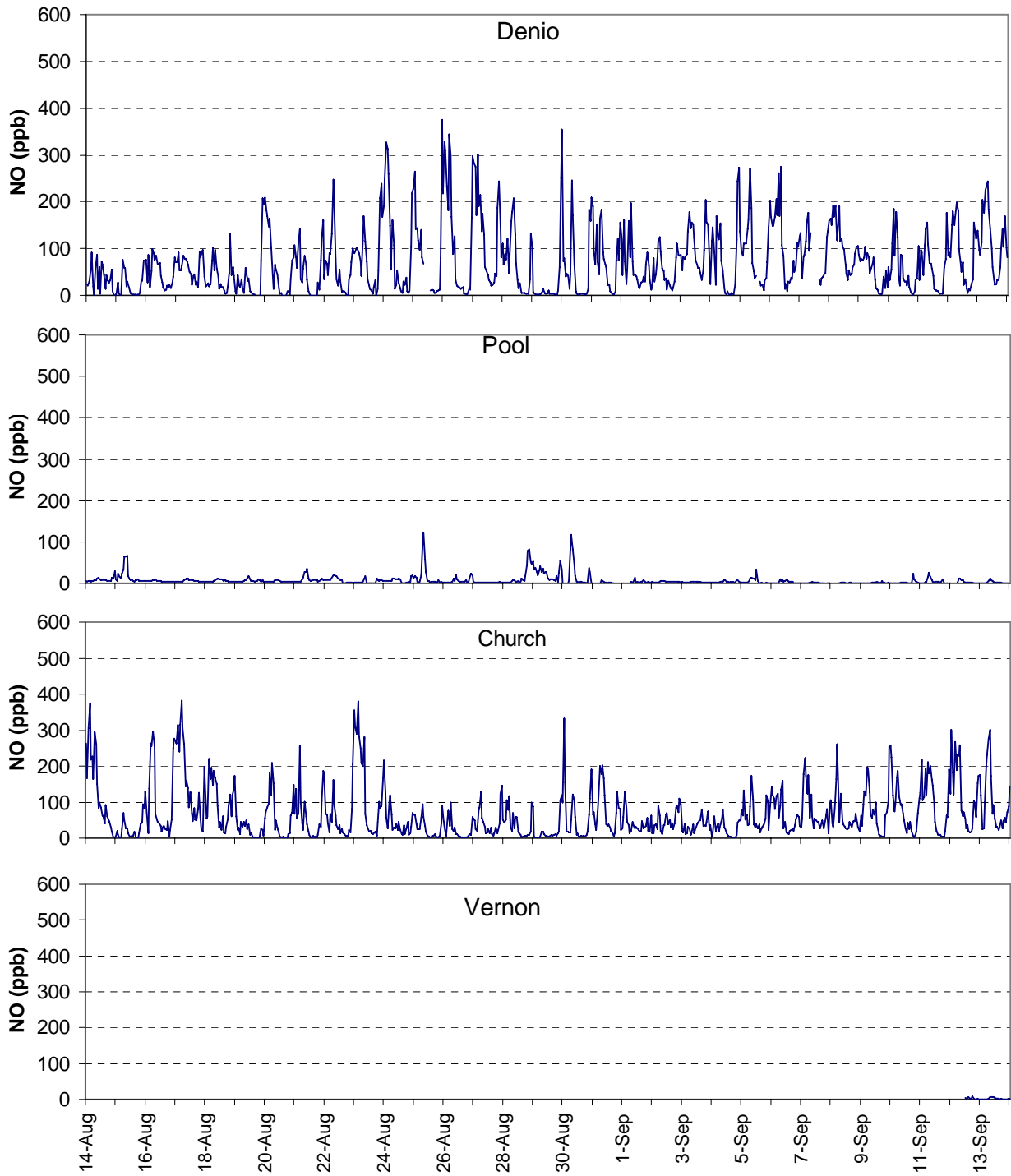


Figure 2–25. Hourly NO data during middle 30 days of summer intensive.

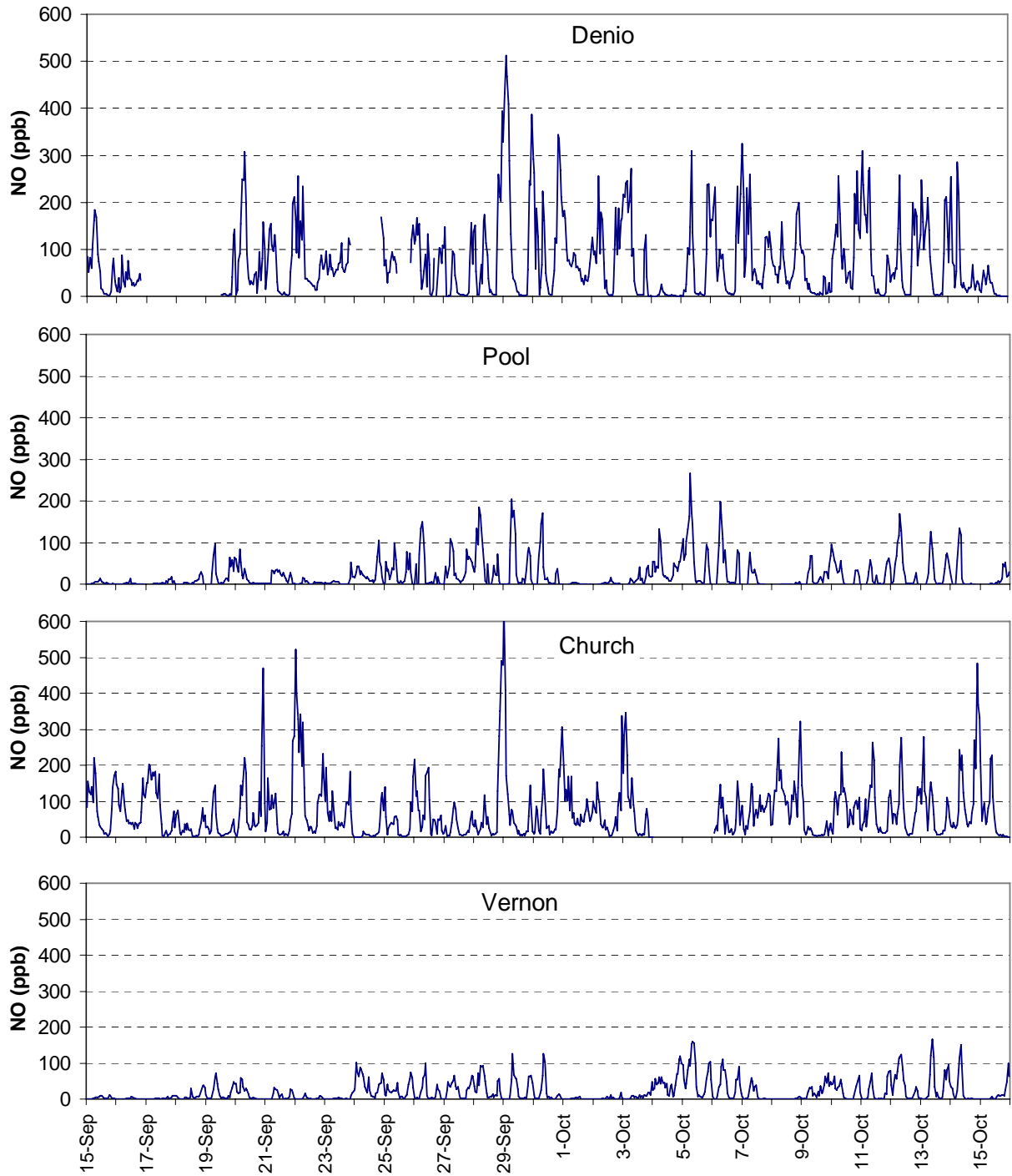


Figure 2–26. Hourly NO data during last 30 days of summer intensive.

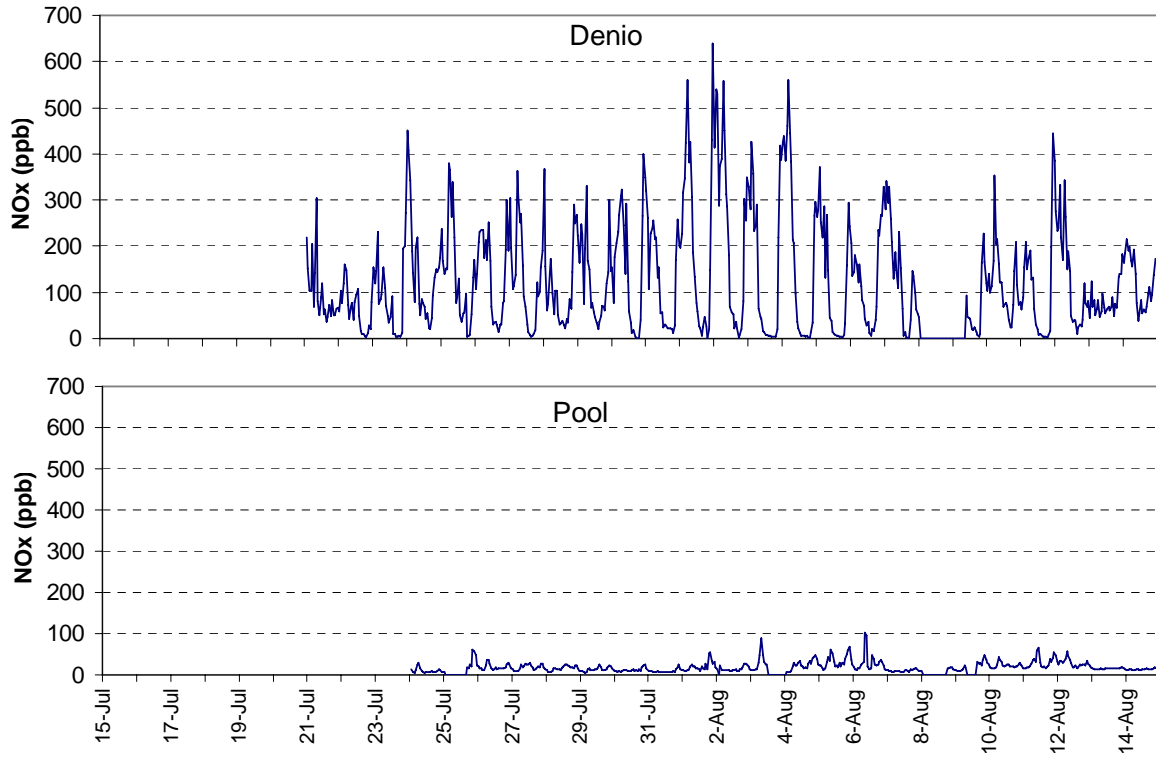


Figure 2–27. Hourly NOx data during first 30 days of summer intensive.

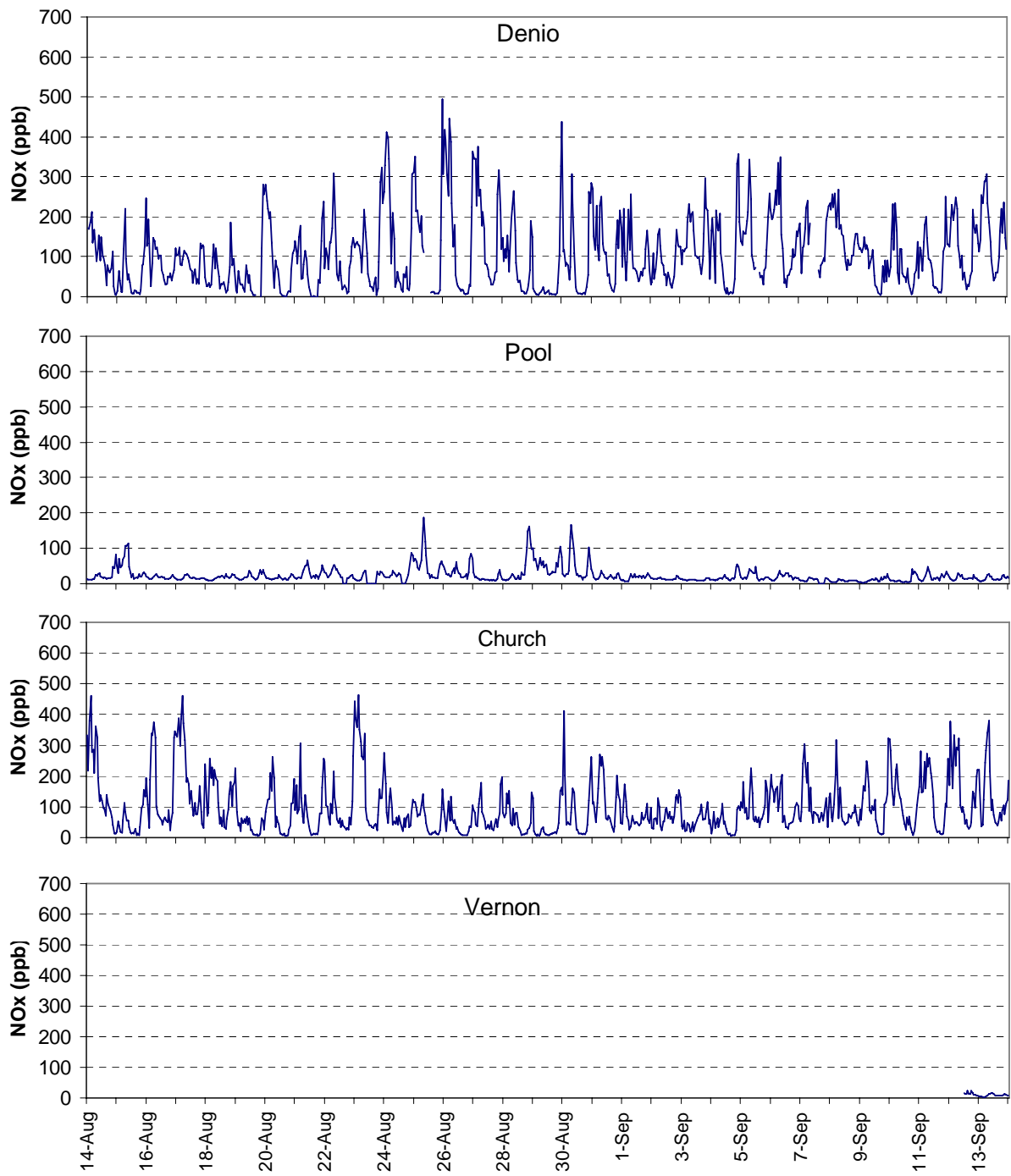


Figure 2–28. Hourly NOx data during middle 30 days of summer intensive.

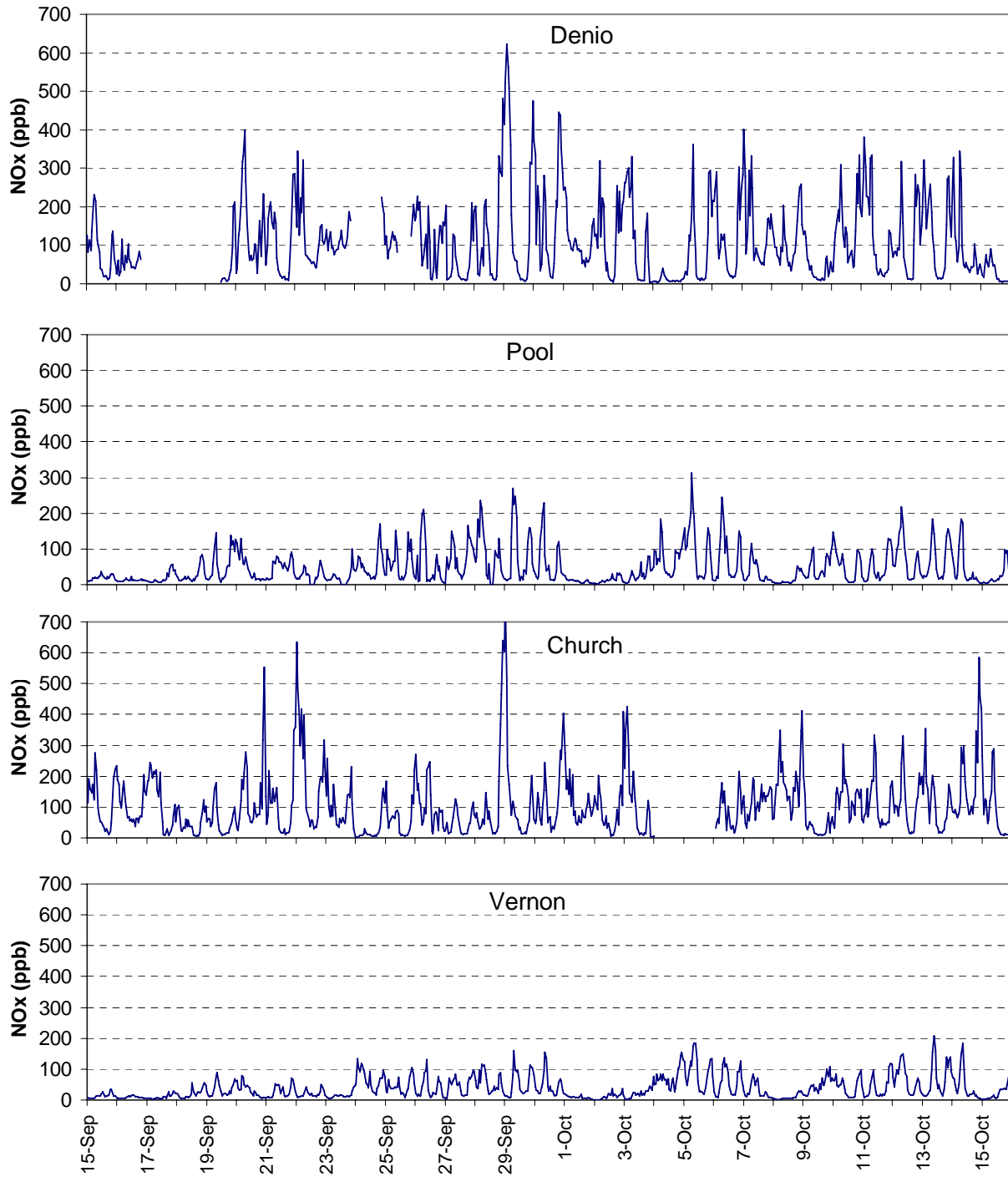


Figure 2–29. Hourly NOx data during last 30 days of summer intensive.

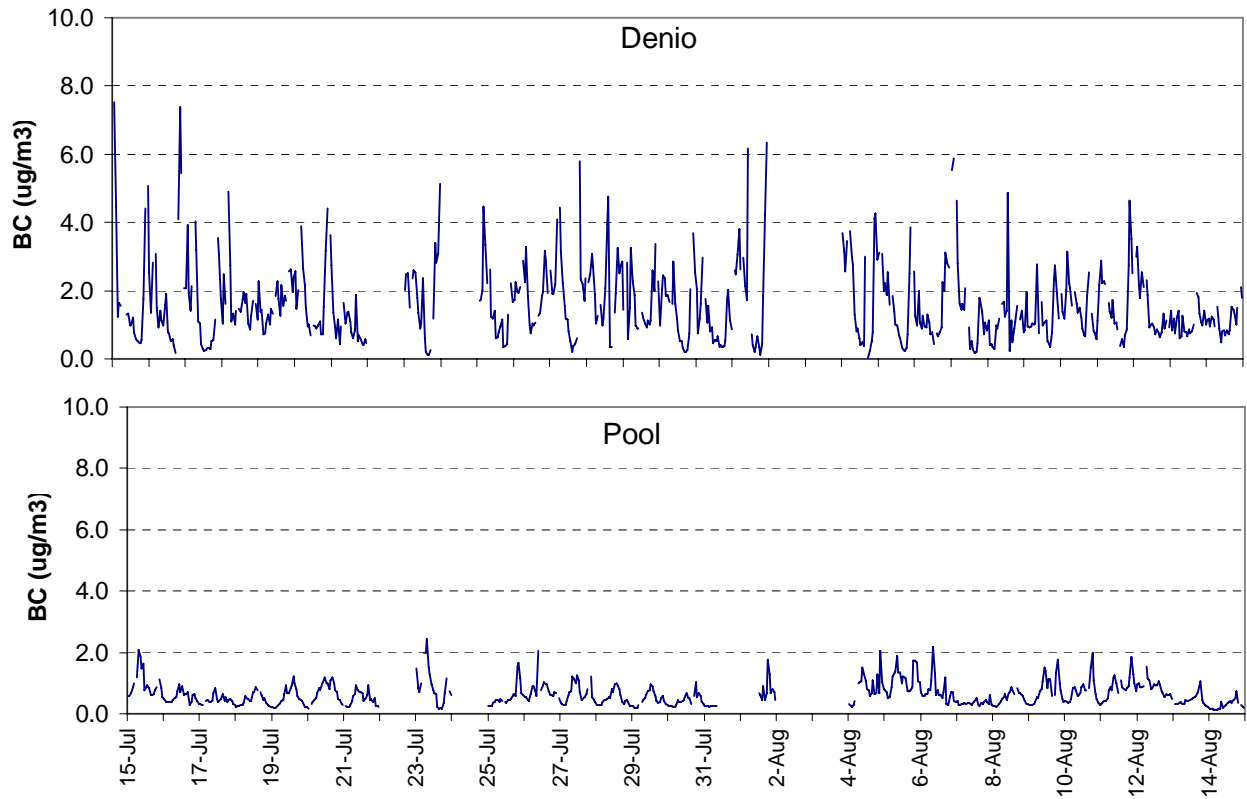


Figure 2–30. Hourly black carbon data during first 30 days of summer intensive.

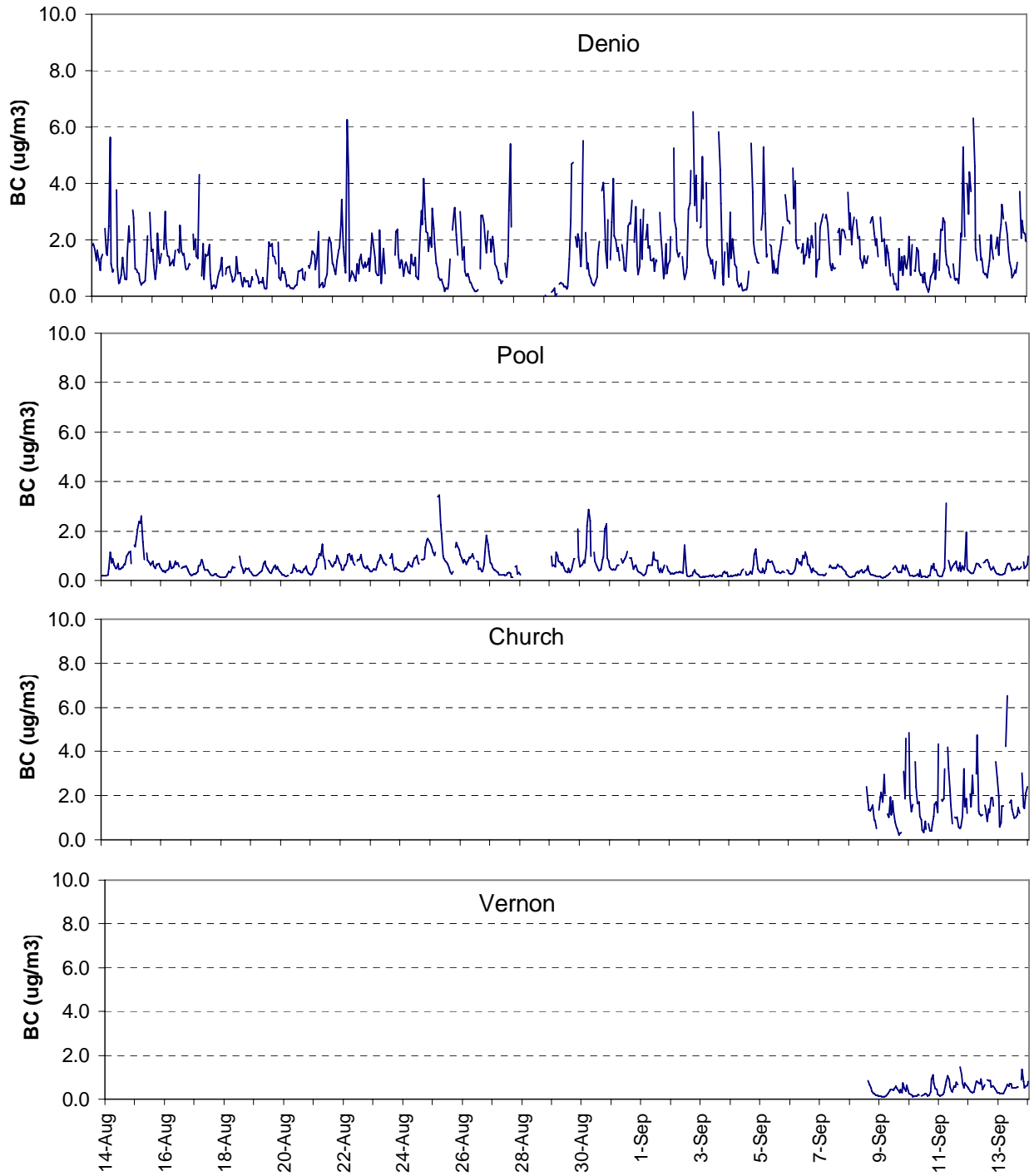


Figure 2–31. Hourly black carbon data during middle 30 days of summer intensive.

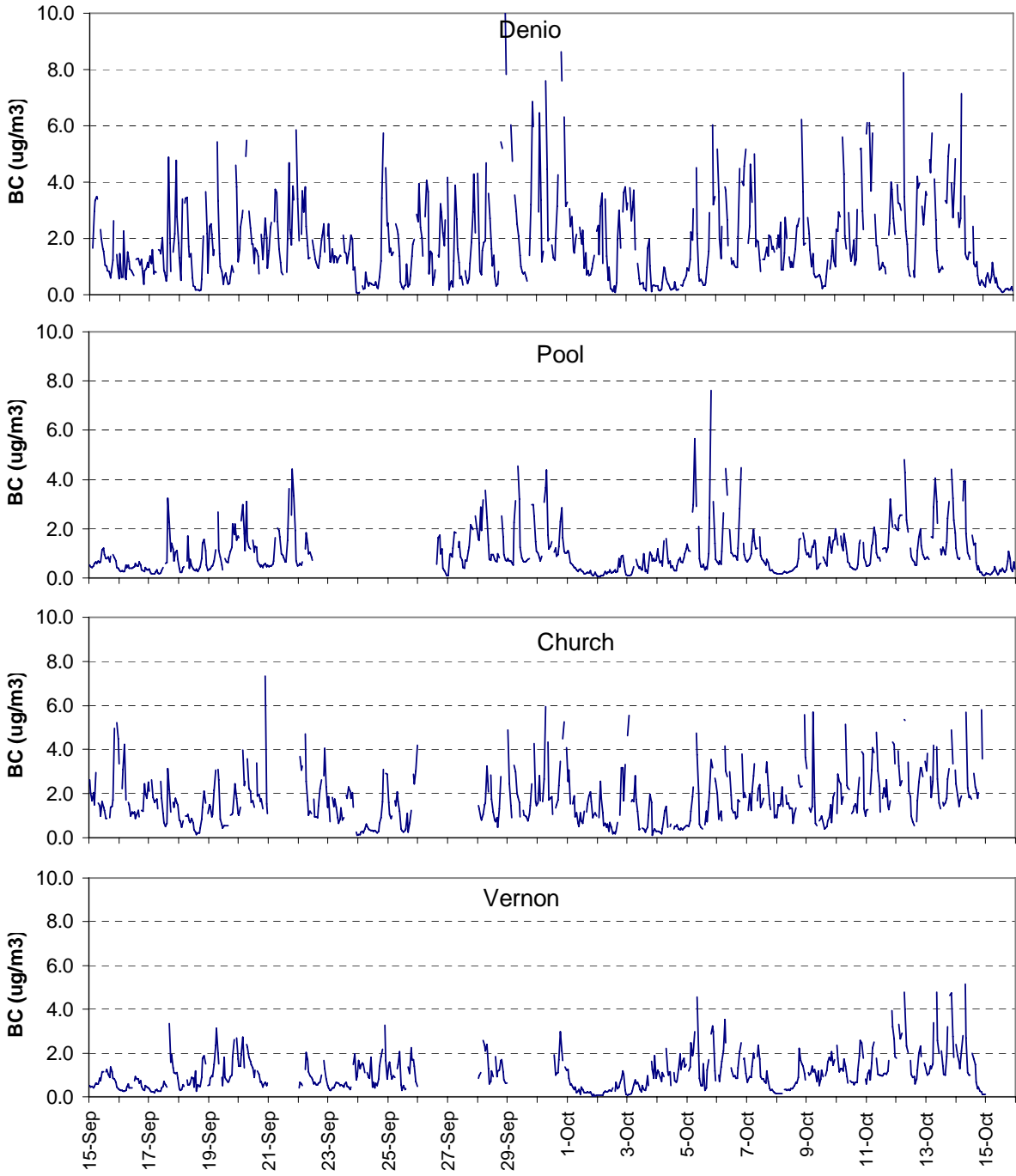


Figure 2–32. Hourly black carbon data during last 30 days of summer intensive.

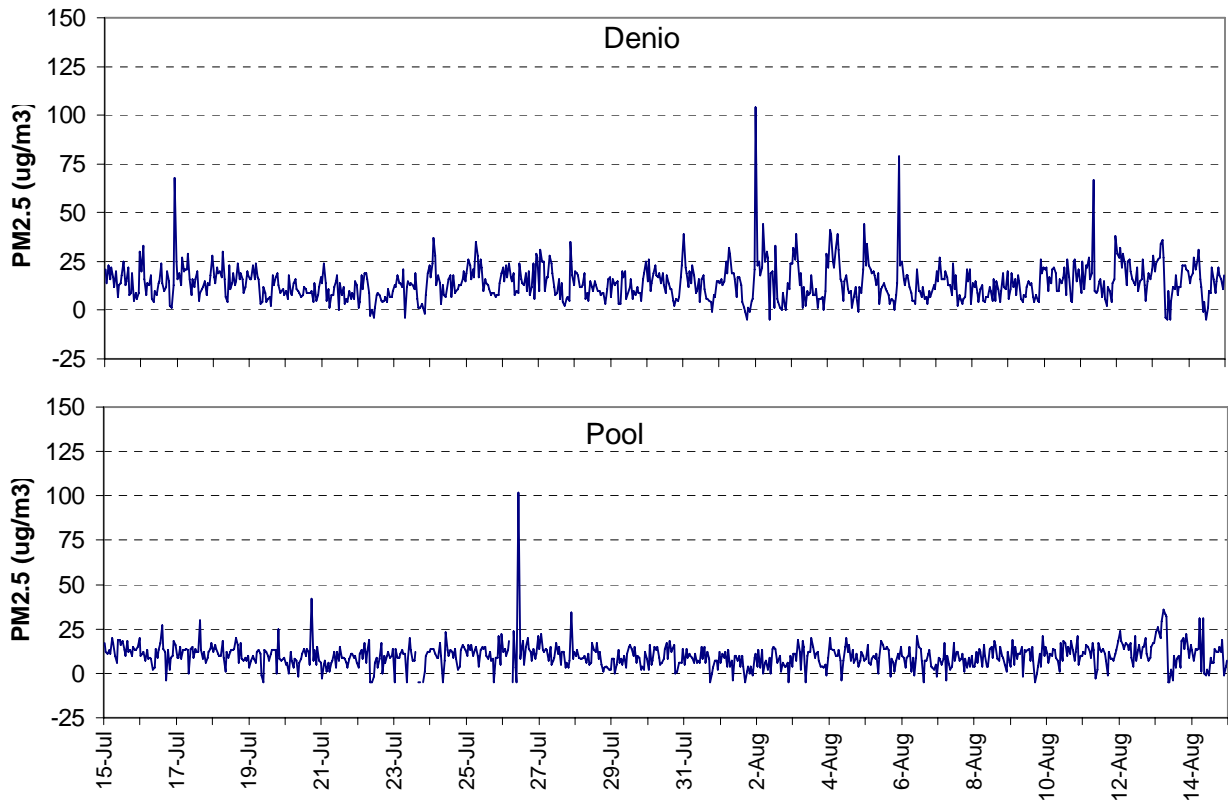


Figure 2–33. Hourly PM2.5 data during first 30 days of summer intensive.

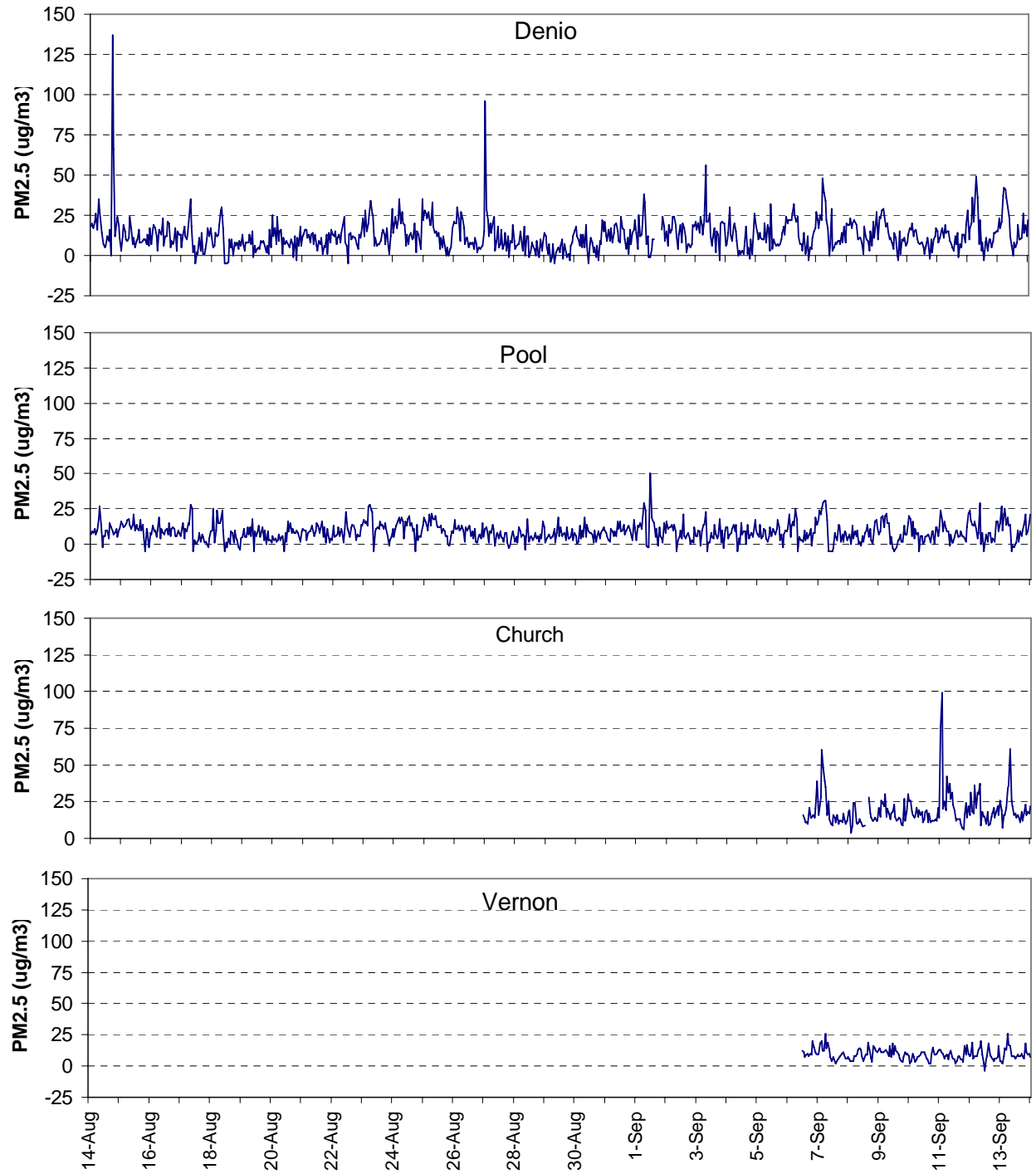


Figure 2–34. Hourly PM2.5 data during middle 30 days of summer intensive.

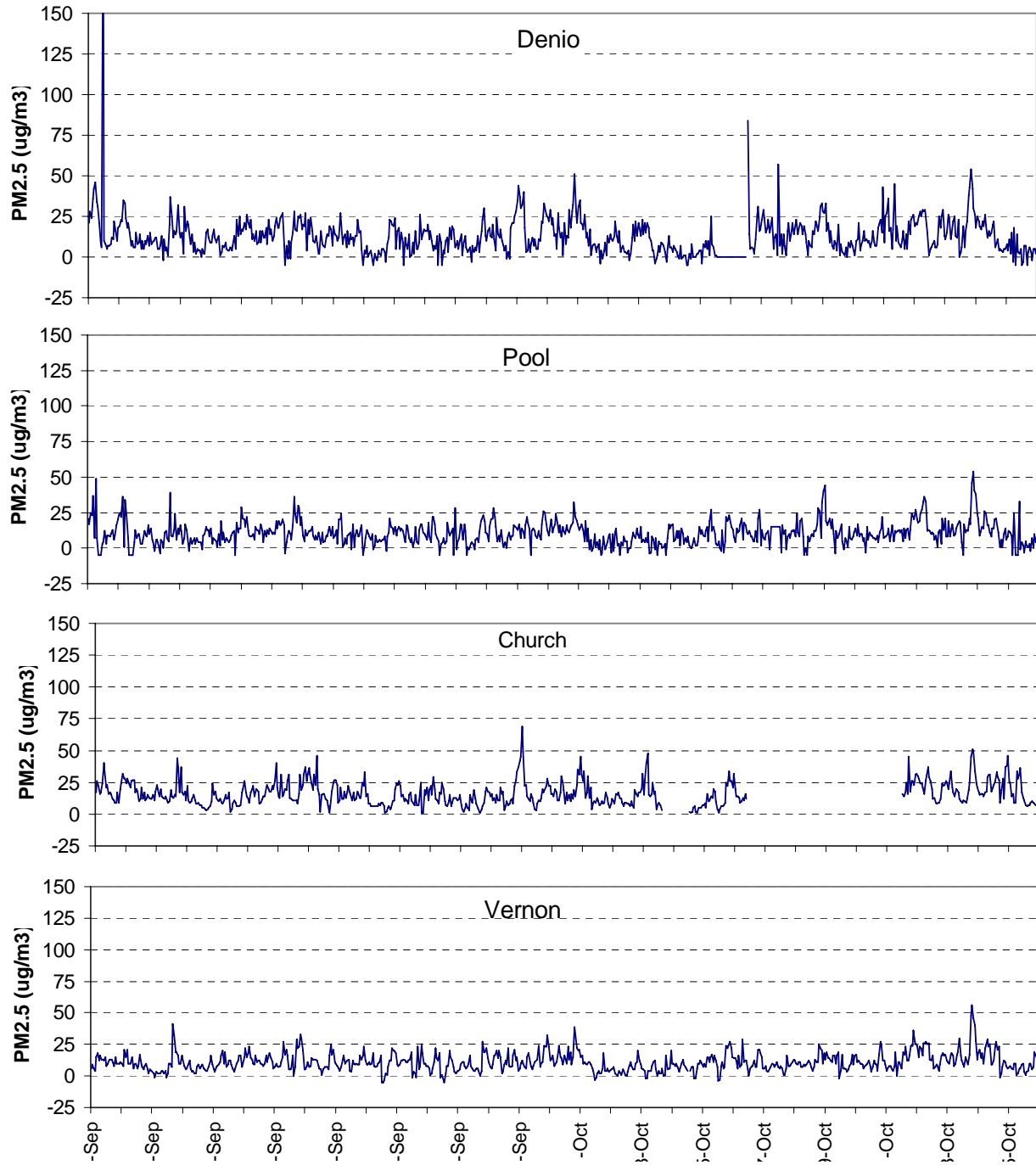


Figure 2–35. Hourly PM2.5 data during last 30 days of summer intensive.

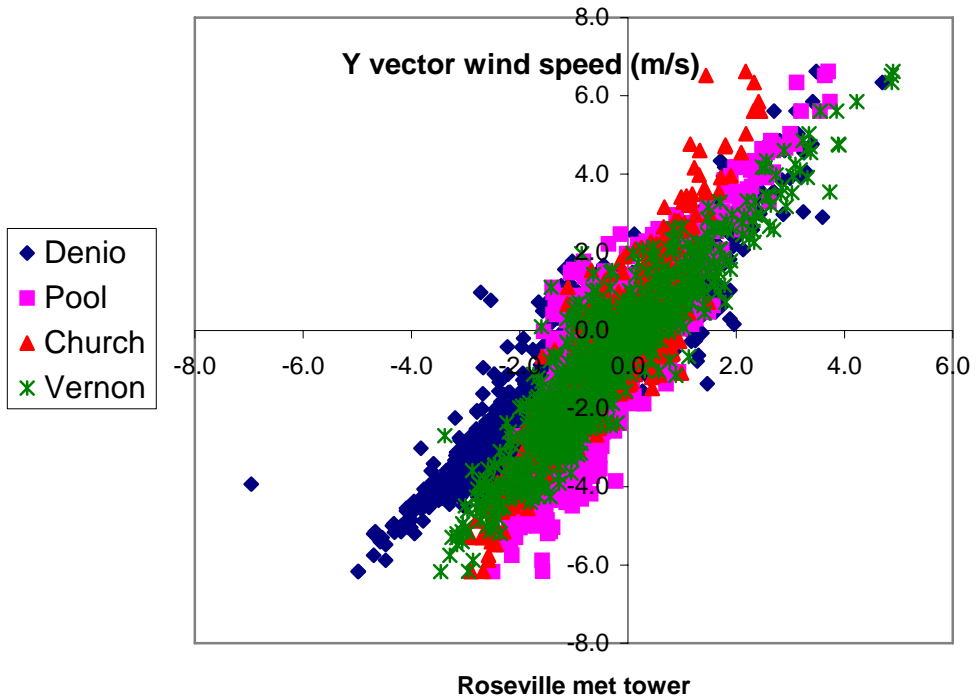
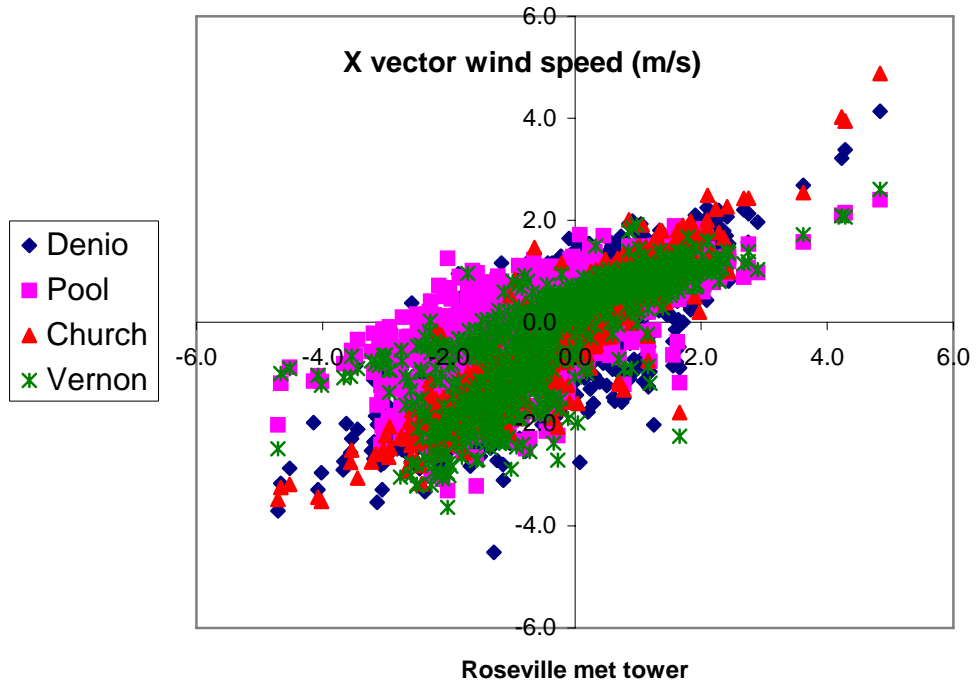


Figure 2–36. Scatter plot of hourly average vector wind speeds at the 4 sites vs. Roseville met tower. Hours when wind speed measured at the met tower was less than 1 m/s are not included.

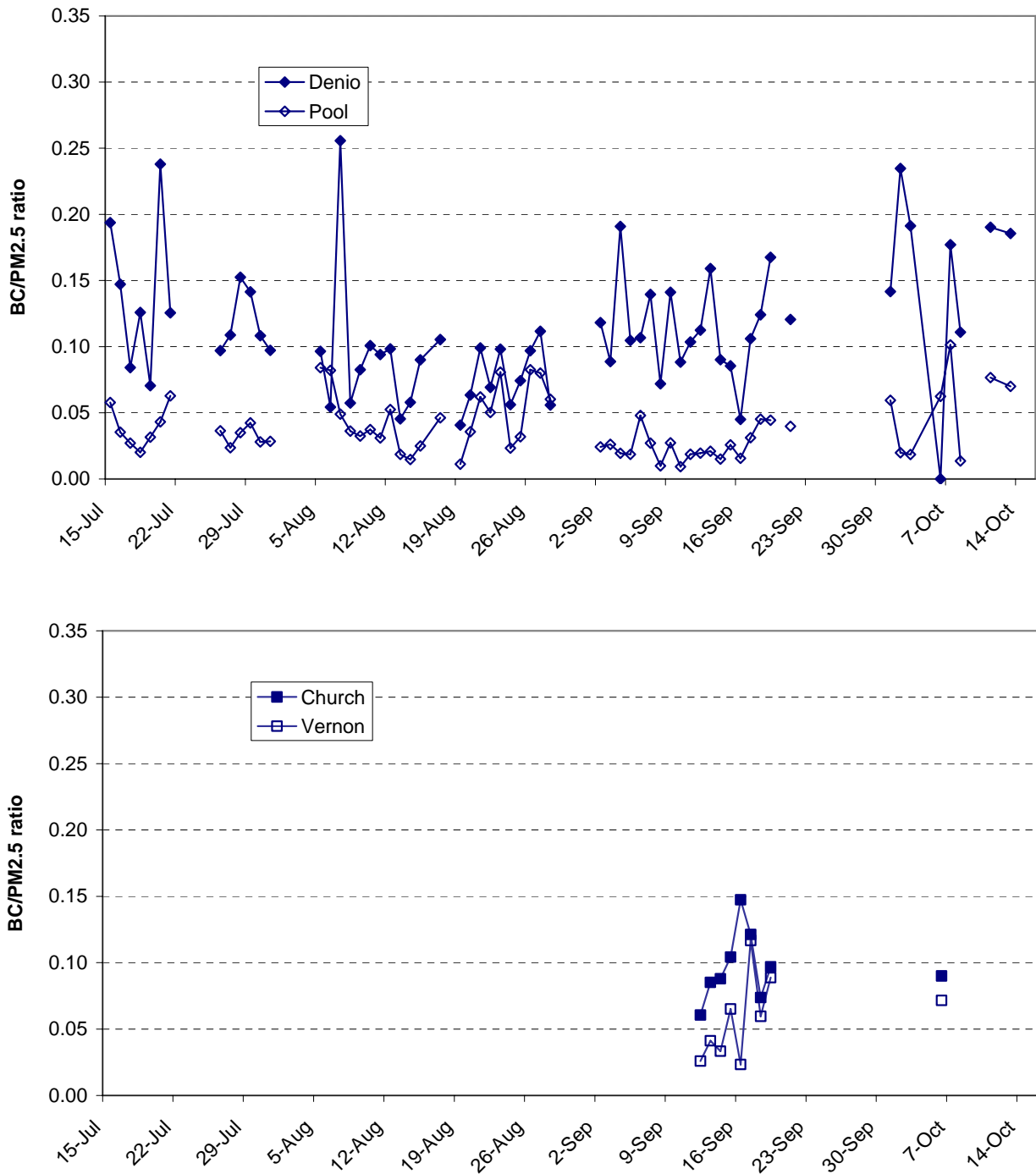


Figure 2–37. Plots of black carbon/PM2.5 ratios at the four monitoring sites. Data are daily averages of data meeting the criteria for inclusion in the upwind/downwind analysis.

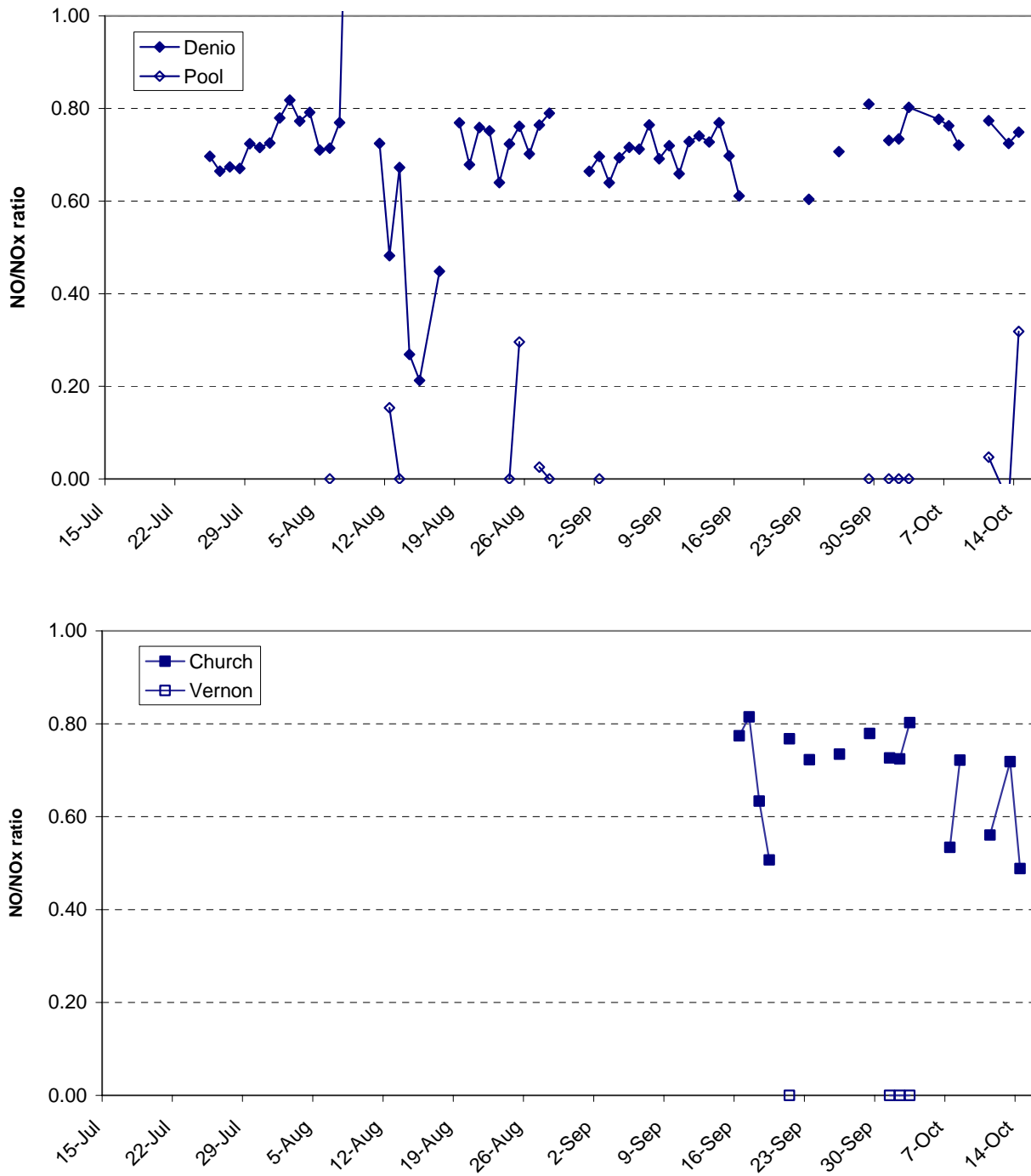
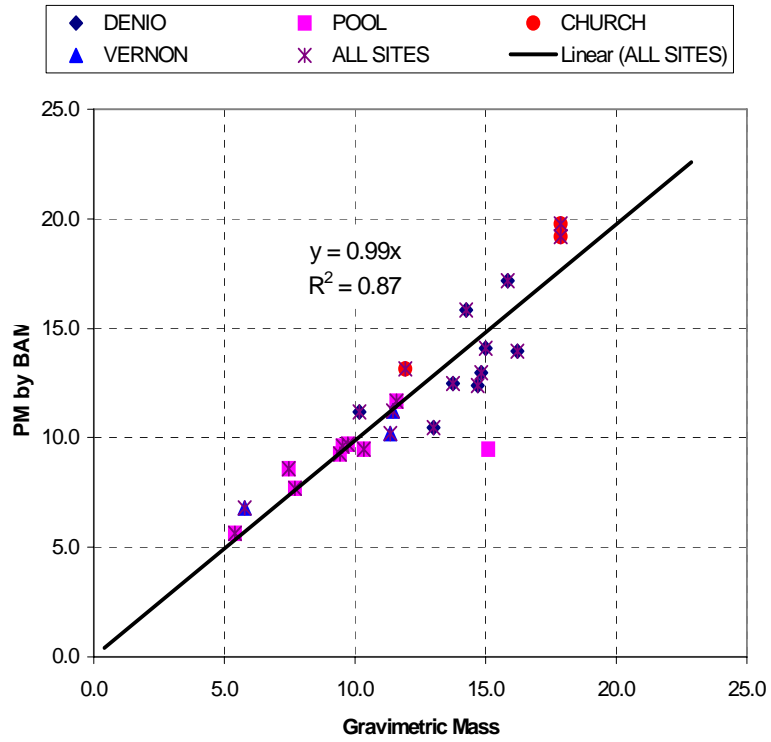


Figure 2-38. Plots of NO/NO_x ratios at the four monitoring sites. Data are daily averages of data meeting the criteria for inclusion in the upwind/downwind analysis.



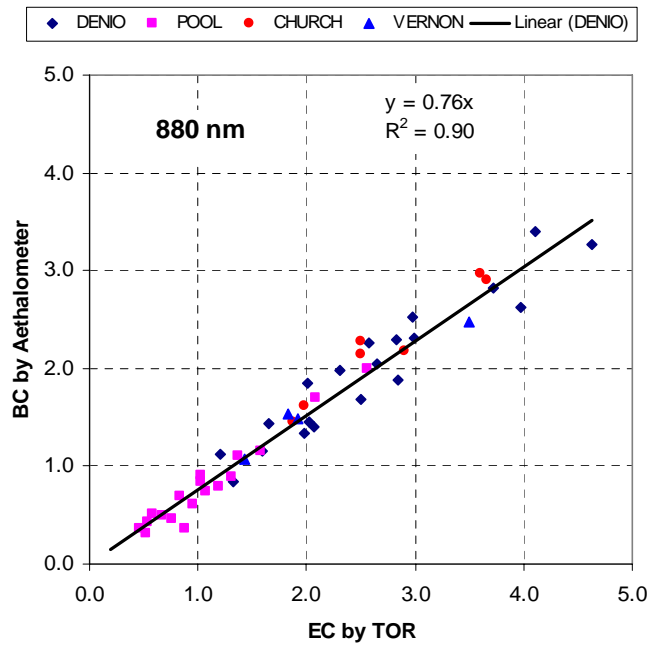
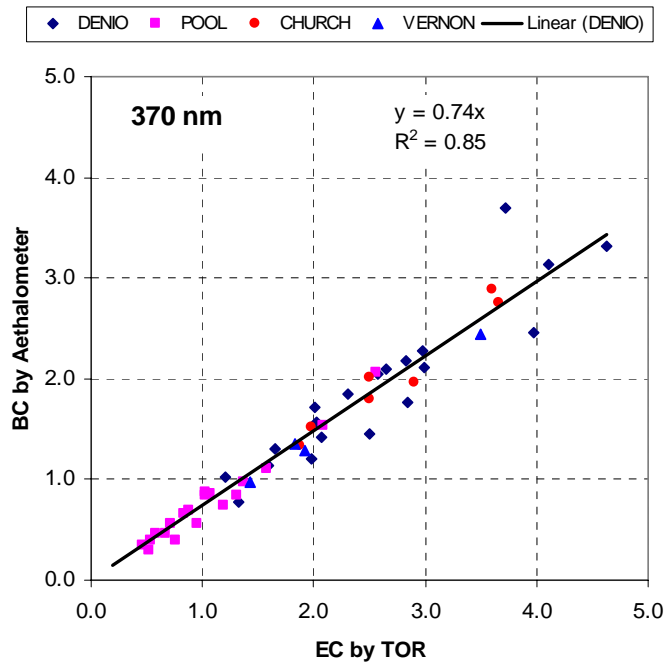


Figure 2–40. Correlation of elemental carbon concentration measured from FRM samplers to 24-hr averaged black carbon concentration from Aethalometers at two different wavelengths.

3. RESULTS

This section summarizes results of the analysis of RRAMP data to quantify the localized air pollutant impacts from the emissions at the UPRR facility. First we compared the mean diurnal variations in pollutant concentrations at the downwind and upwind monitoring sites. The purpose of these comparisons is to determine whether differences in diurnal patterns of rail yard emissions are detectable in the data. The mean pollutant concentrations were then determined for each monitoring site using the selection criteria for the downwind/upwind analysis. Differences in pollutant concentrations for the pairs of downwind and upwind sites were compared to the standard errors in the mean and propagated measurement uncertainties to address the hypothesis that differences in downwind and upwind pollutant concentrations are statistically significant. Finally, we examine correlations of BC and NO with $PM_{2.5}$ to determine the relationships of BC and NO with $PM_{2.5}$ and how much of the variations in $PM_{2.5}$ are explained by BC and NO.

3.1 Comparisons of Diurnal Variations in Pollutant Concentrations at Downwind and Upwind Monitoring Sites

The diurnal variations in hourly NO, NO_x, BC and $PM_{2.5}$ are shown for the four sites in Figure 3-1 to Figure 3-4. All diurnal patterns show the expected variations due to varying mixing heights during the day with minimum concentration during the afternoons. The upwind sites tend to show higher concentrations due to increased traffic during morning and afternoon commutes, especially for NO and NO_x. Similar, but smaller, increases are evident for BC. $PM_{2.5}$ show minimal diurnal variation at the upwind sites. In contrast, the two downwind sites show higher concentrations of NO/NO_x, BC and $PM_{2.5}$ throughout the nighttime hours with no increase in concentrations during the morning commute period. The effect of commute traffic should also be evident in the day of week variations in pollutant concentrations at the downwind and upwind sites. The distribution of pollutant concentrations by day of the week is shown in Figure 3-5 to Figure 3-8. Pollutant concentrations are generally lower on weekend at the two upwind sites. The Church site shows slightly lower pollutant concentrations during weekends and the Denio site shows no variations in pollutant concentrations by day of week. These results are consistent with impact of pollutant emissions from the rail yard at the downwind sites.

3.2 Upwind/Downwind Differences

We examined the downwind minus upwind concentrations of NO, BC and $PM_{2.5}$ for the two pairs of upwind/downwind sampling locations in order to develop a basis for selecting appropriate subsets of the data that would be use to establish the impact of emissions from the rail yard on downwind pollutant levels. The locations of the two upwind (Pool and Vernon) and two downwind (Denio and Church) sampling sites are shown in Figure 1-1. The frequency of wind direction (%) and the average downwind minus upwind NO, BC and PM concentrations at the two downwind sites are shown in 10 degree wind sectors for wind speed > 1 m/s for all hours of the day in Figure 3-9, for times between 10 PM to 5 AM in Figure 3-10 and times between 6 AM and 9 PM in Figure 3-11. The red and blue diamonds on the outer circumference of the wind and pollutant concentration roses denote the upwind/downwind wind directions between the Vernon/Church (137°) and Pool/Denio (162°) pairs, respectively.

The wind data show that the winds were consistent with upwind and downwind designations of the sampling sites. The winds were predominantly from the south between 110 to 225 degrees at all hours the day. Winds are mostly SE or perpendicular to the rail tracks during the overnight hours from 10 PM to 5 AM and shifts to SW for the period 6 AM to 9 PM. During the overnight period, the winds are mostly from the wind sector bounded by the red and blue diamonds. Although winds from the east were not frequent, pollutant concentrations were the highest from this direction during the overnight hours at both Denio and Church sites.

Based on these results, we suggested the following screening criteria for estimating the downwind minus upwind concentrations. These criteria were reviewed and approved by the RRAMP Technical Advisory Committee.

- Wind from a semi-circular arc between 45 and 225 degrees (i.e. arc midpoint is perpendicular to the railroad tracks).
- Winds from 1 to 5 m/s to avoid calm or windy conditions.
- Time period restricted to 10 PM to 5 AM to provide consistent mixing depths and atmospheric stability. The 2200-0500 average required a minimum of four valid hourly records.

Table 3–1 shows the means and standard deviations in the 1-hour and 7-hour average BC, PM_{2.5}, NO and NO_x concentrations during 2200 to 0500 at the four RRAMP sites and standard errors of the means. The differences in mean concentrations between the two pairs of downwind and upwind sites (Denio-Pool and Church-Vernon) and pooled standard error of the differences are also shown. Using a 2-sample unequal variance (heteroscedastic) Student's *t*-test, these differences are all significant at above the 99% confidence level. The graphical displays of the downwind-upwind differences are shown in Figure 3–12. Note that the ratios of pollutant concentrations at the upwind relative to downwind sites are lowest for NO and are larger in increasing order for NO₂, BC and PM. The increasing ratios from NO to PM are consistent with larger contributions of urban background to the measured PM and BC concentrations. Figure 3-12 also shows the differences between the two downwind and two upwind sites. These differences are small in comparison and are not statistically significant.

The statistical methods that were applied in the downwind-upwind analysis are applicable to data that are normally distributed. Although air quality data are typically log-normally distributed, our approach is appropriate because the selection criteria for the analysis limits the data to those collected under similar atmospheric conditions. Figure 3–13 shows distributions of hourly averaged BC concentrations at Denio between 2200 and 0500 that meet selection criteria and the log transform of the data. Note that distribution of concentrations is approximately normal

3.3 Correlations of BC and NO with PM_{2.5}

An objective of RRAMP includes estimating the mass concentrations and associated uncertainties of diesel particulate matter (DPM) levels at downwind monitoring sites. Because EC or BC as a fraction of TC is much higher in diesel emissions than other combustion sources,

they can potentially serve as surrogates for DPM. A scaling factor for the measured EC or BC based on the EC or BC to $PM_{2.5}$ ratio from dynamometer tests of diesel vehicles or ambient measurements in locations where ambient PM is due overwhelmingly to diesel exhaust may provide a reasonable estimate. We will explore this approach in the next annual report.

As an initial exploratory review of the data, we examined the correlations of BC and NO with $PM_{2.5}$ in Figure 3–14. All values in the correlations are the daily 7-hour (2200 to 0500) means at the downwind Denio site and are corrected for the corresponding upwind values at Pool. We have not studied these correlations in detail and provide only qualitative interpretations of these plots at this point. NO appears to be reasonably correlated with $PM_{2.5}$. The regression line goes through the origin, suggesting that most of the upwind corrected $PM_{2.5}$ is associated with diesel engine exhaust from the rail yard. The slope of the regression for the correlation of BC with $PM_{2.5}$ is 1.75 or BC/ $PM_{2.5}$ ratio of 0.57, which would not be unreasonable for diesel exhaust. However, there is more scatter for this correlation.

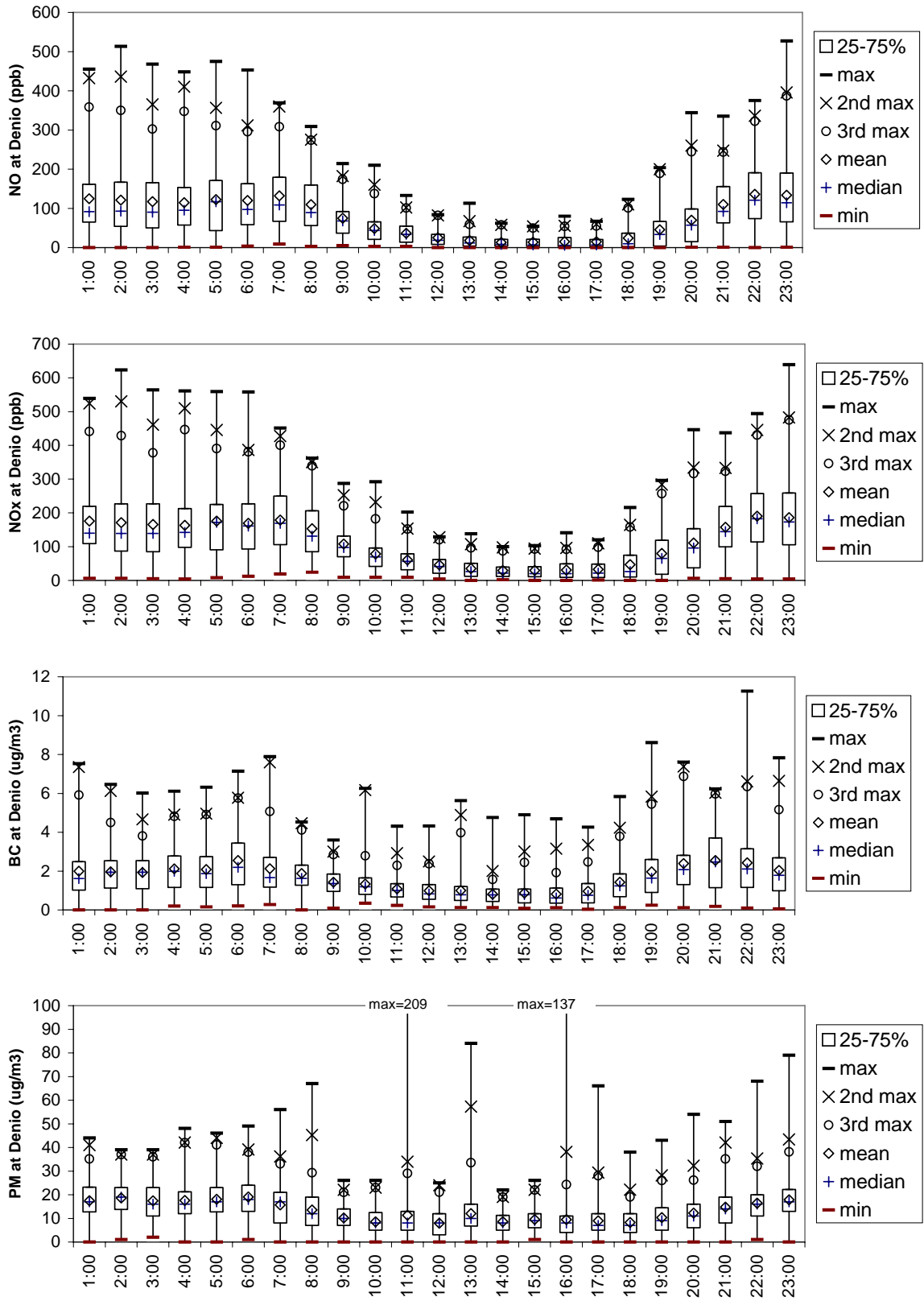


Figure 3–1. Box and whiskers plots showing diurnal distribution of data at the Denio site.

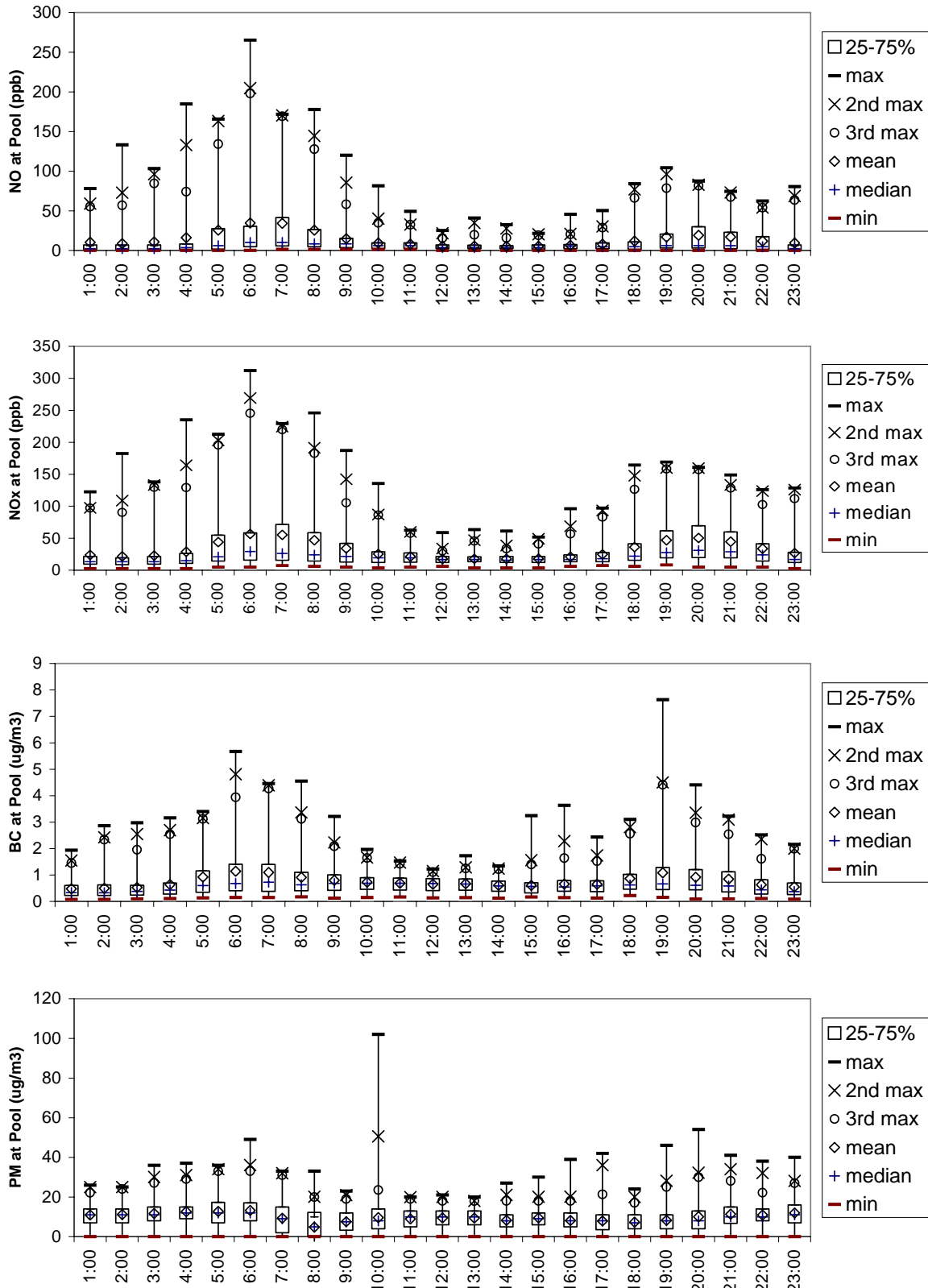


Figure 3–2. Box and whiskers plots showing diurnal distribution of data at the Pool site

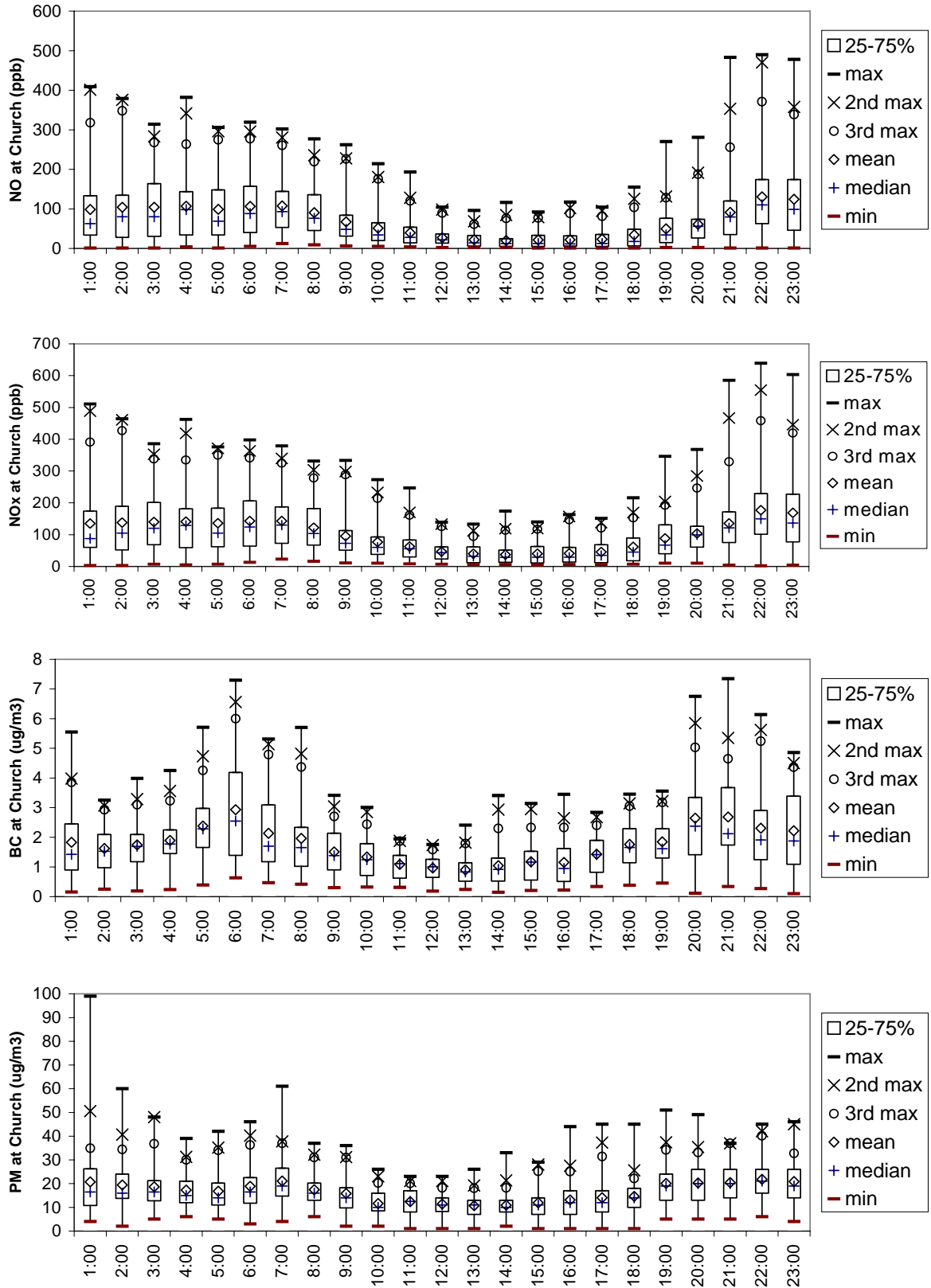


Figure 3–3. Box and whiskers plots showing diurnal distribution of data at the Church site

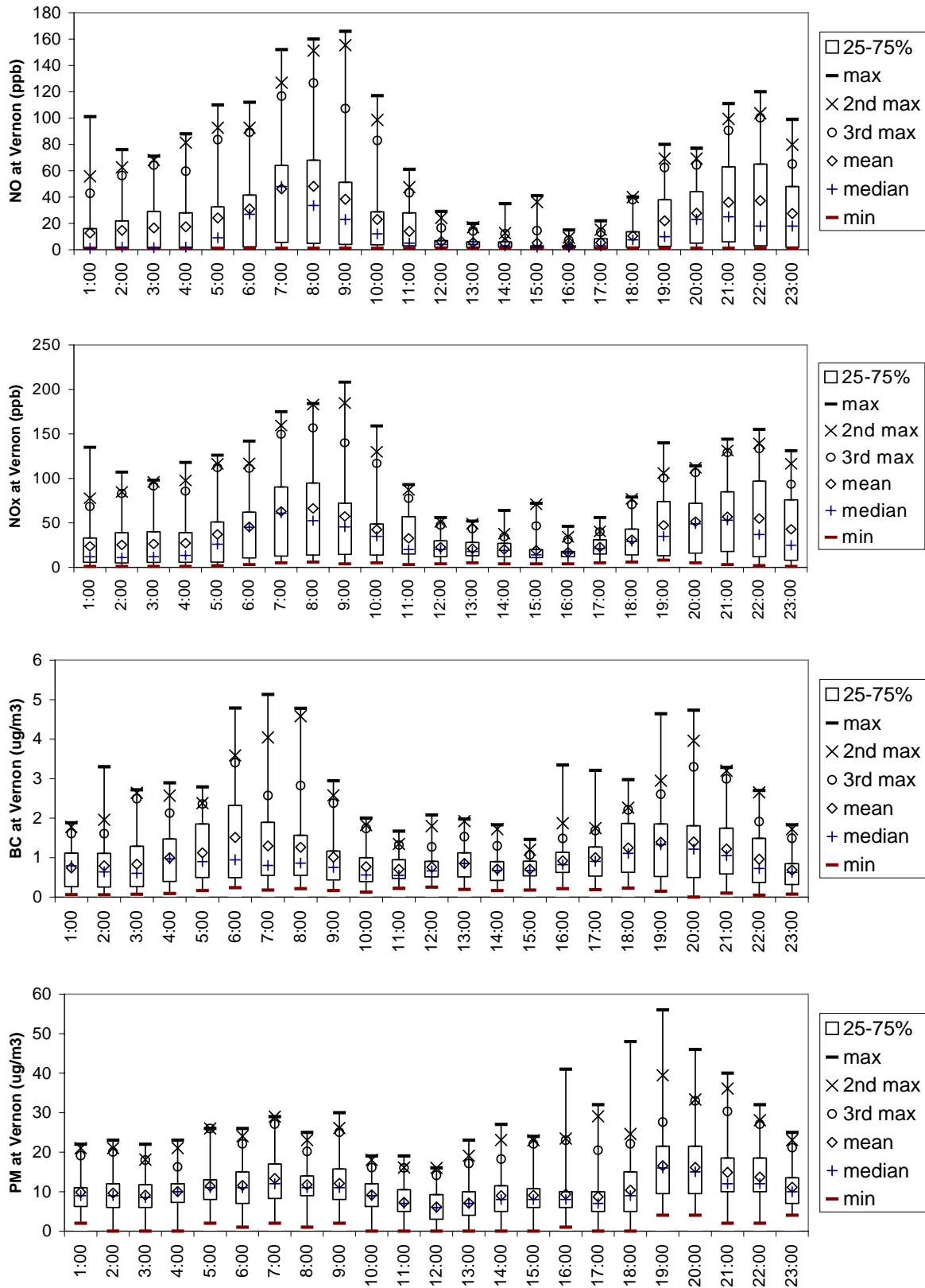


Figure 3-4. Box and whiskers plots showing diurnal distribution of data at the Vernon site

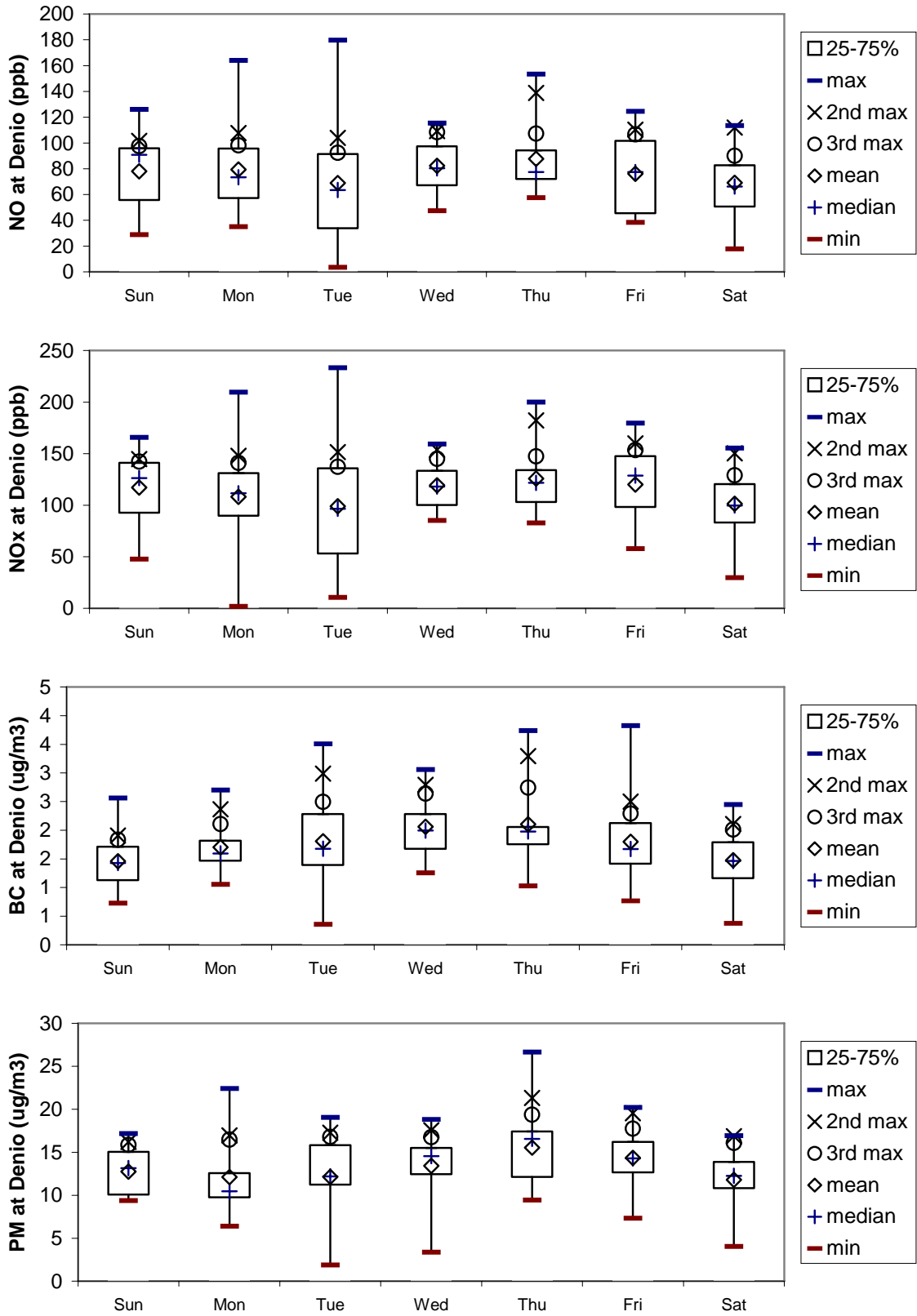


Figure 3–5. Box and whiskers plots showing distribution of data by day-of-week at the Denio site

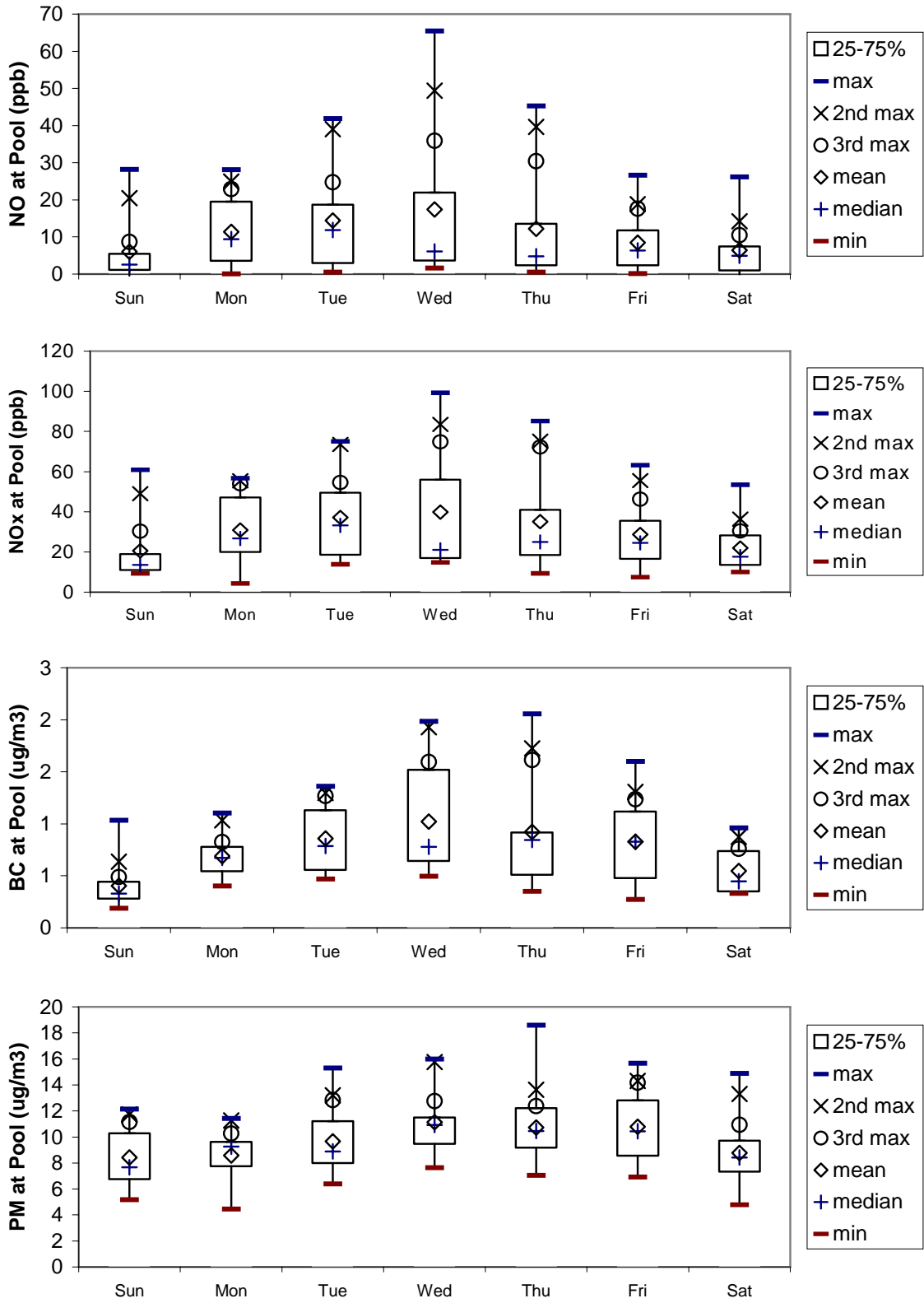


Figure 3–6. Box and whiskers plots showing distribution of data by day-of-week at the Pool site

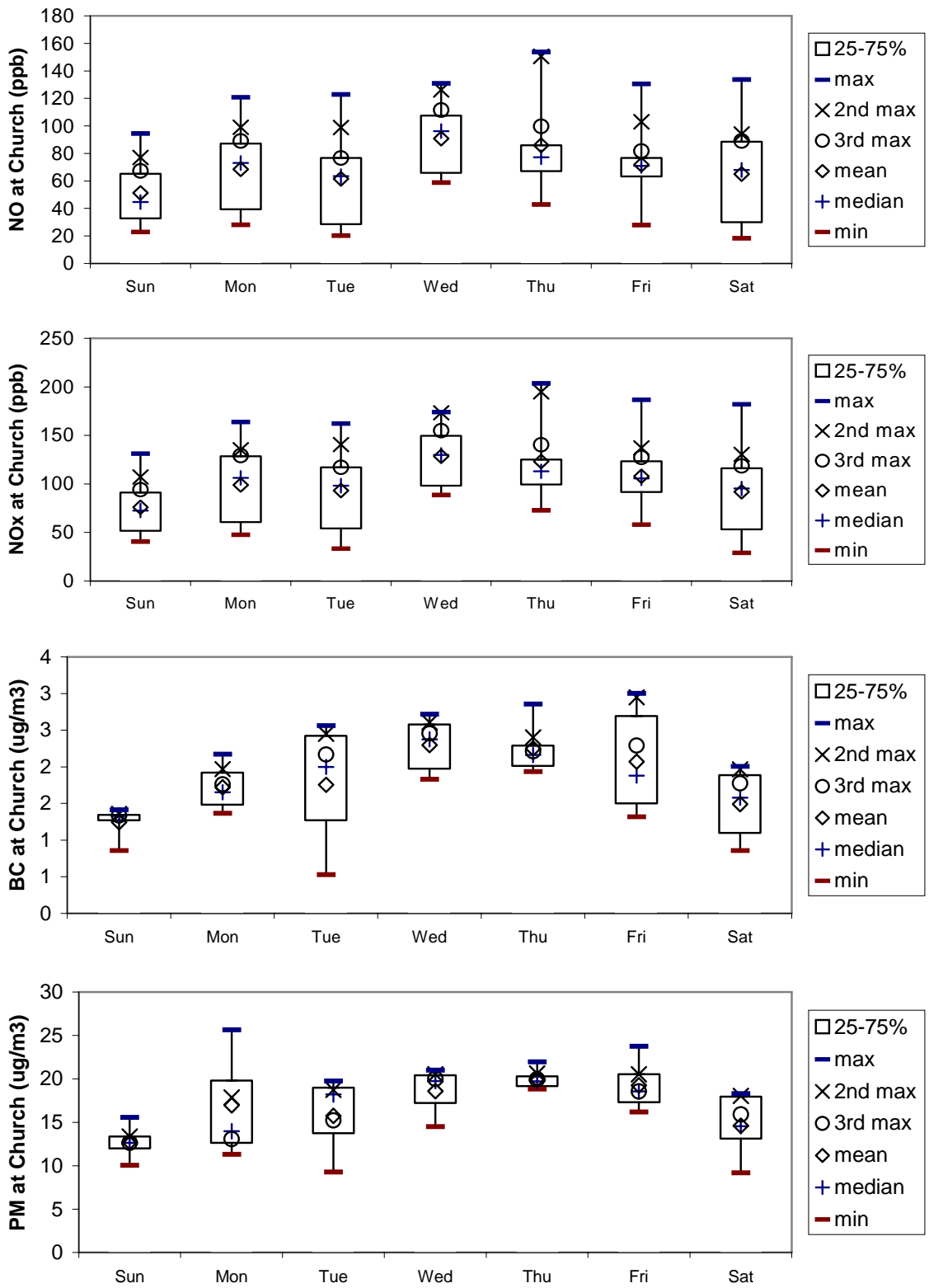


Figure 3-7. Box and whiskers plots showing distribution of data by day-of-week at the Church site

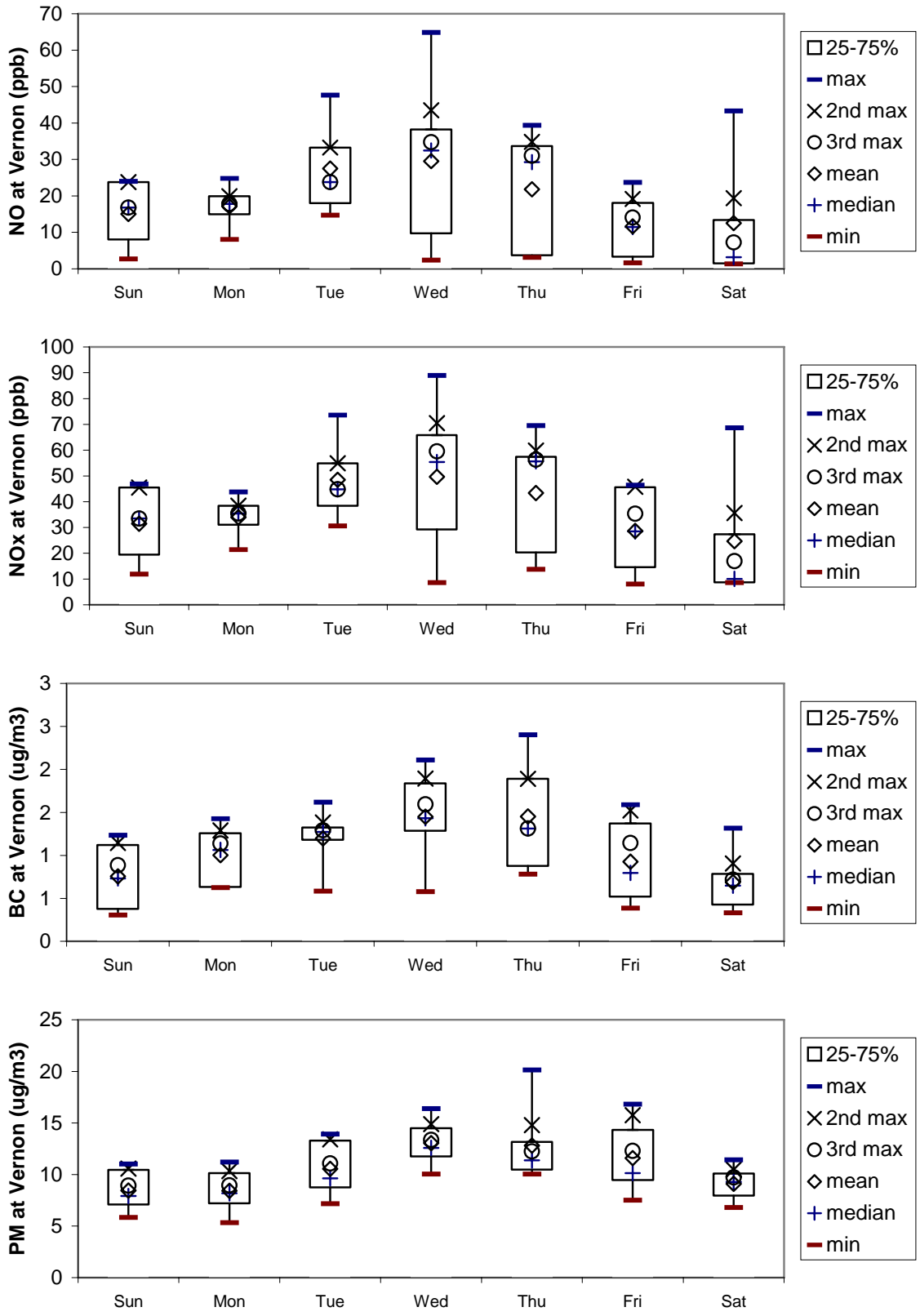


Figure 3–8. Box and whiskers plots showing distribution of data by day-of-week at the Vernon site

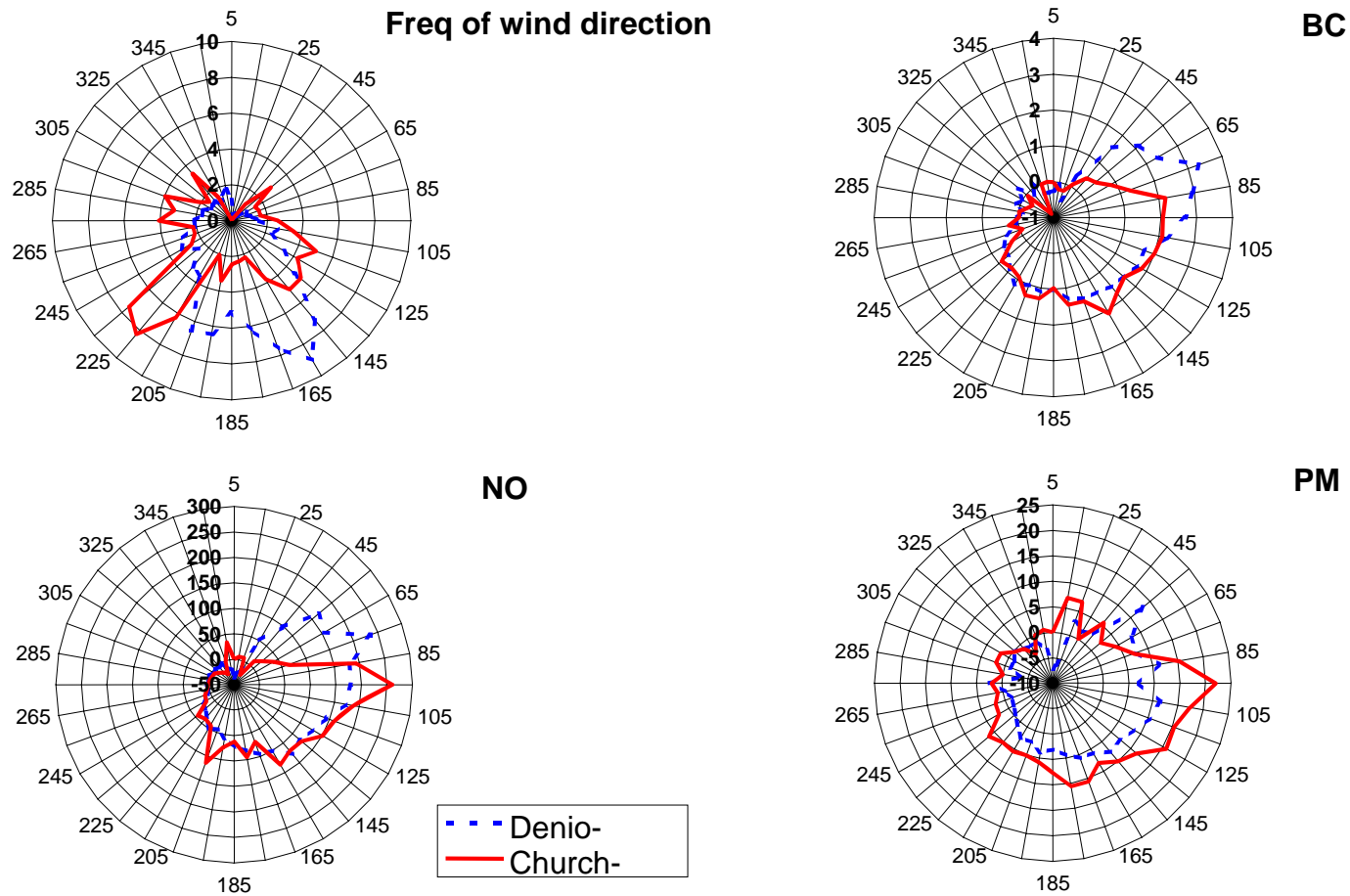


Figure 3–9. Frequency of wind direction (%) and average downwind minus upwind NO, BC and PM_{2.5} concentrations at the downwind sites in 10 degree wind sectors when wind speed > 1 m/s for all hours of the day.

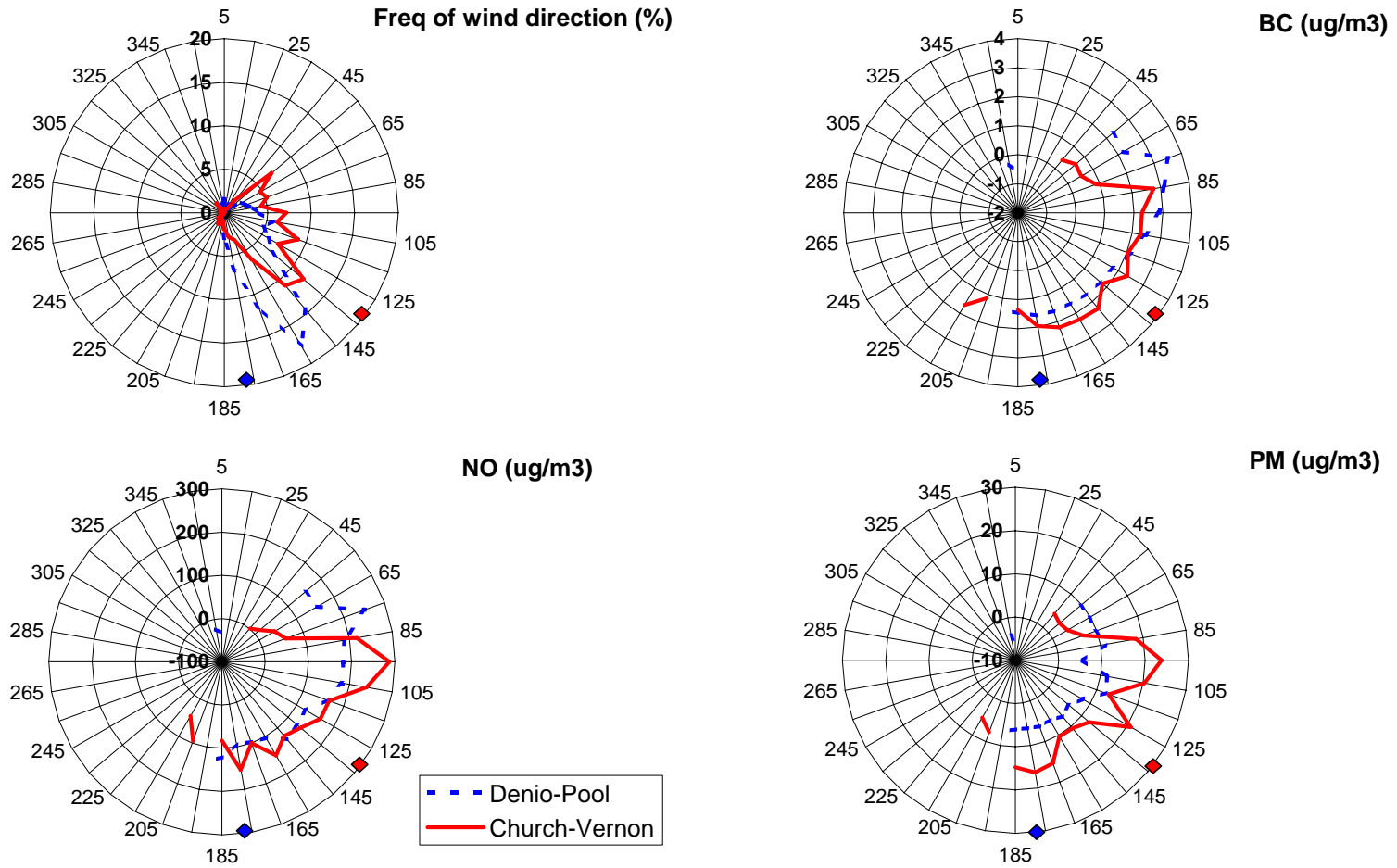


Figure 3–10. Frequency of wind direction (%) and average downwind minus upwind NO, BC and PM_{2.5} concentrations at the downwind sites in 10 degree wind sectors when wind speed > 1 m/s and time period between 10 PM and 5 AM.

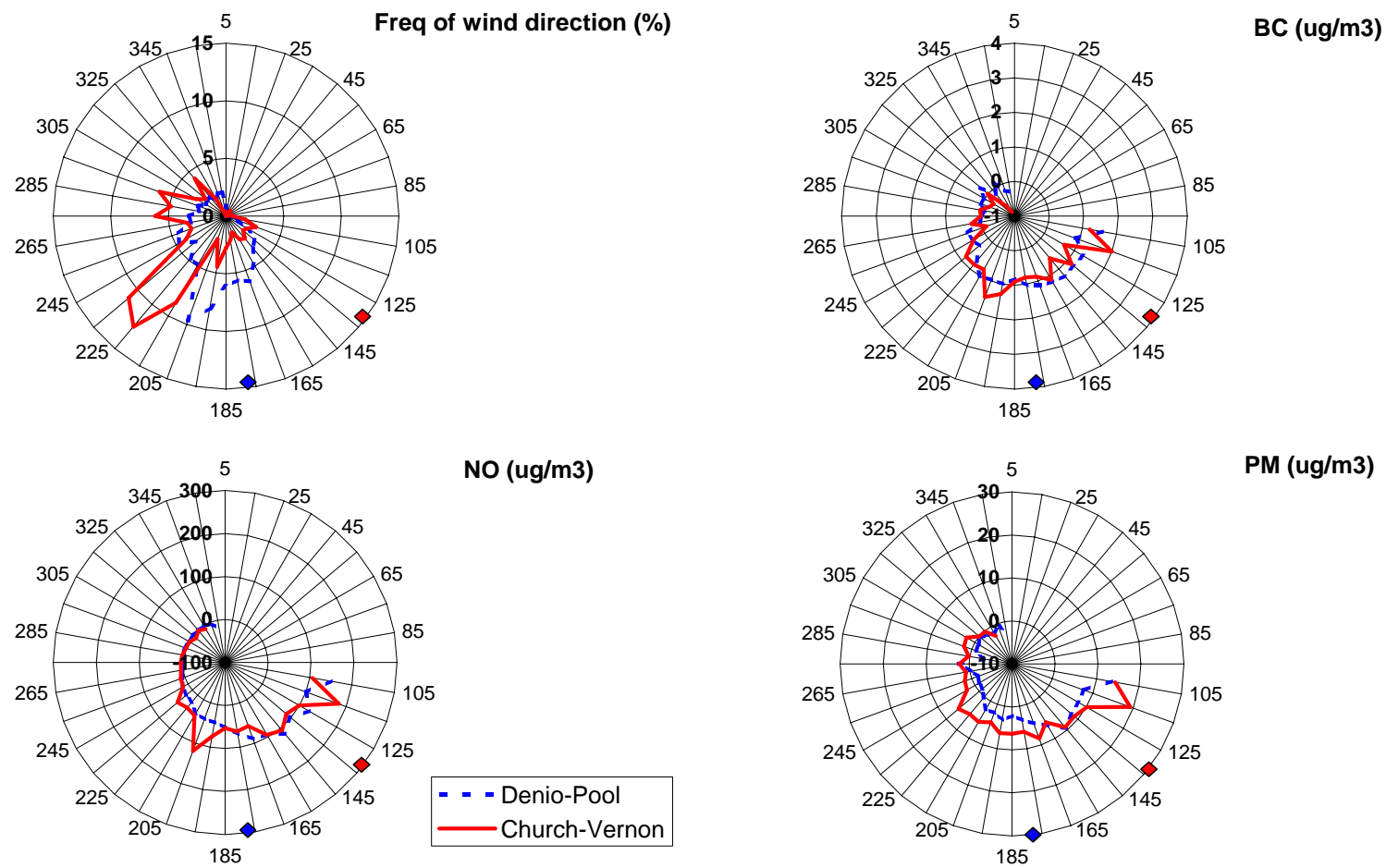


Figure 3–11. Frequency of wind direction (%) and average downwind minus upwind NO, BC and PM_{2.5} concentrations at the downwind sites in 10 degree wind sectors when wind speed > 1 m/s and time period between 6 AM and 9 PM.

Table 3–1. Means and standard deviations for 1-hour and 7-hour mean BC, PM2.5, NO and NOx concentrations from 2200 to 0500 at the four RRAMP sites and standard errors of the means. The differences in mean concentrations between the two pairs of downwind and upwind sites (Denio-Pool and Church-Vernon) and pooled standard error of the differences and root mean squares of the measurement errors are also shown.

Statistics	BC (ug/m ³)				PM2.5 (ug/m ³)				NO (ug/m ³)				NOx (ug/m ³)			
	Denio	Pool	Church	Vernon	Denio	Pool	Church	Vernon	Denio	Pool	Church	Vernon	Denio	Pool	Church	Vernon
Downwind-Upwind																
<u>1-hour averages</u>																
average	2.13	0.43	2.13	0.57	18.51	11.38	22.04	9.51	134.16	2.24	130.52	6.92	186.36	16.58	176.77	18.52
stdev	1.38	0.31	1.14	0.46	10.03	6.52	12.36	5.60	91.67	7.13	114.24	15.39	112.51	15.16	135.21	23.29
n	428	428	126	126	549	549	176	176	475	475	157	157	475	475	157	157
sterr_mean	0.07	0.02	0.10	0.04	0.43	0.28	0.93	0.42	4.21	0.33	9.12	1.23	5.16	0.70	10.79	1.86
avg delta	1.70		1.57		7.13		12.53		131.92		123.59		169.78		158.25	
ster_delta	0.07		0.11		0.51		1.02		4.22		9.20		5.21		10.95	
T-test	0.000		0.000		0.000		0.000		0.000		0.000		0.000		0.000	
<u>2200-0500 averages</u>																
average	2.19	0.42	2.10	0.54	18.64	11.43	21.71	9.56	138.32	2.02	127.91	6.77	191.56	16.52	174.20	18.79
stdev	1.12	0.25	0.75	0.37	6.57	4.56	7.66	4.24	81.24	4.29	85.40	11.06	101.09	11.86	100.37	19.79
n	70	70	20	20	81	81	26	26	70	70	23	23	70	70	23	23
sterr_mean	0.13	0.03	0.17	0.08	0.73	0.51	1.50	0.83	9.71	0.51	17.81	2.31	12.08	1.42	20.93	4.13
avg delta	1.77		1.57		7.21		12.15		136.30		121.14		175.03		155.41	
ster_delta	0.14		0.19		0.89		1.72		9.72		17.96		12.17		21.33	
propag. Error	0.10		0.15		0.44		0.81		1.90		3.60		1.90		3.60	
T-test	0.000		0.000		0.000		0.000		0.000		0.000		0.000		0.000	
<u>2200-0500 averages</u>	Denio	Church	Pool	Vernon	Denio	Church	Pool	Vernon	Denio	Church	Pool	Vernon	Denio	Church	Pool	Vernon
average	2.19	2.10	0.42	0.54	18.64	21.71	11.43	9.56	138.32	127.91	2.02	6.77	191.56	174.20	16.52	18.79
stdev	1.12	0.75	0.25	0.37	6.57	7.66	4.56	4.24	81.24	85.40	4.29	11.06	101.09	100.37	11.86	19.79
n	70	20	70	20	81	26	81	26	70	23	70	23	70	23	70	23
sterr_mean	0.13	0.17	0.03	0.08	0.73	1.50	0.51	0.83	9.71	17.81	0.51	2.31	12.08	20.93	1.42	4.13
avg delta	0.09		-0.12		-3.07		1.87		10.40		-4.76		17.36		-2.27	
ster_delta	0.16		0.05		1.12		0.69		14.09		1.42		17.03		2.76	
T-test	0.347		0.095		0.037		0.031		0.306		0.028		0.238		0.304	

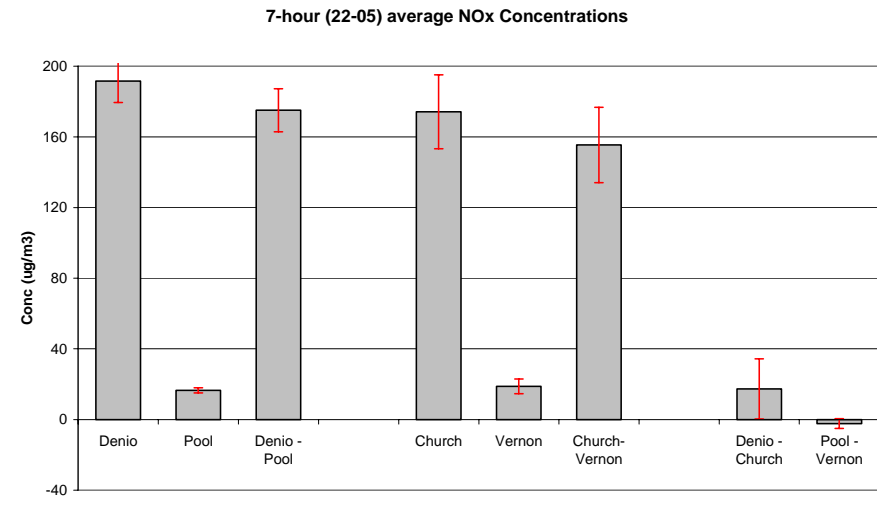
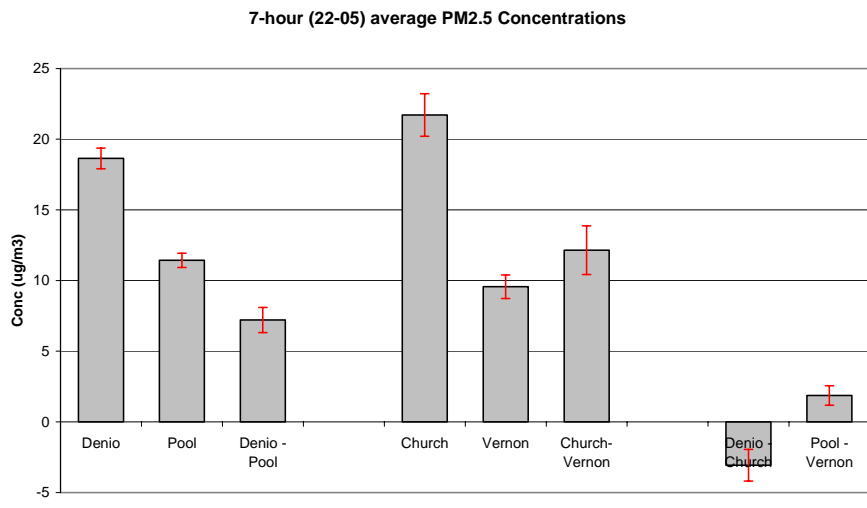
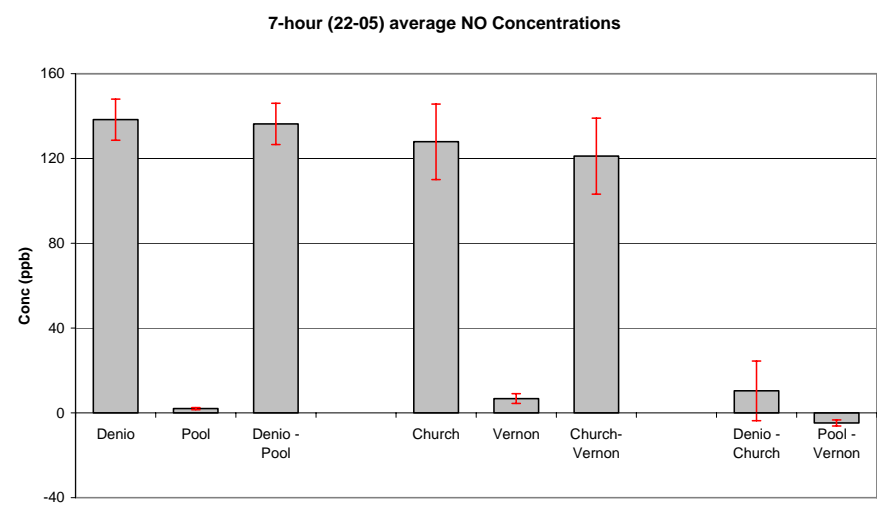
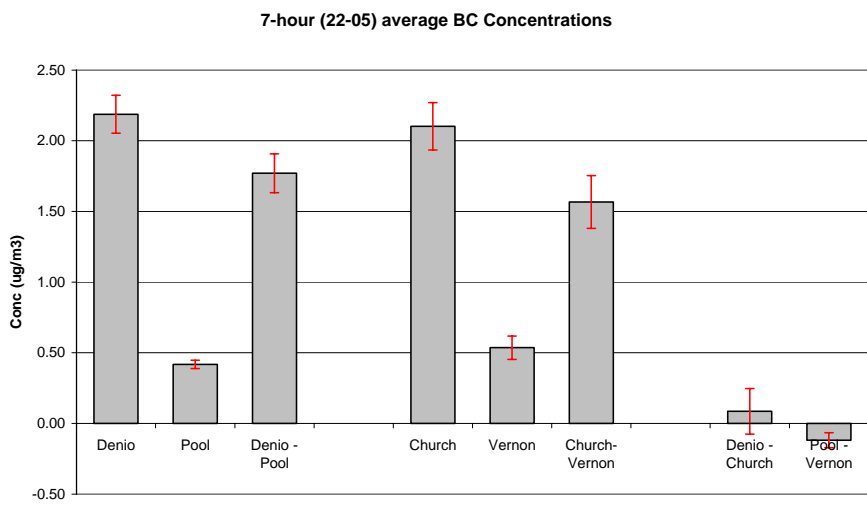


Figure 3–12. Means BC, PM_{2.5}, NO and NO_x concentrations at the four RRAMP monitoring sites and standard errors of the means. Differences of the two pairs of downwind and upwind sites (Denio-Pool and Church-Vernon) are also shown. Differences between the two downwind and two upwind sites are also shown for comparison.

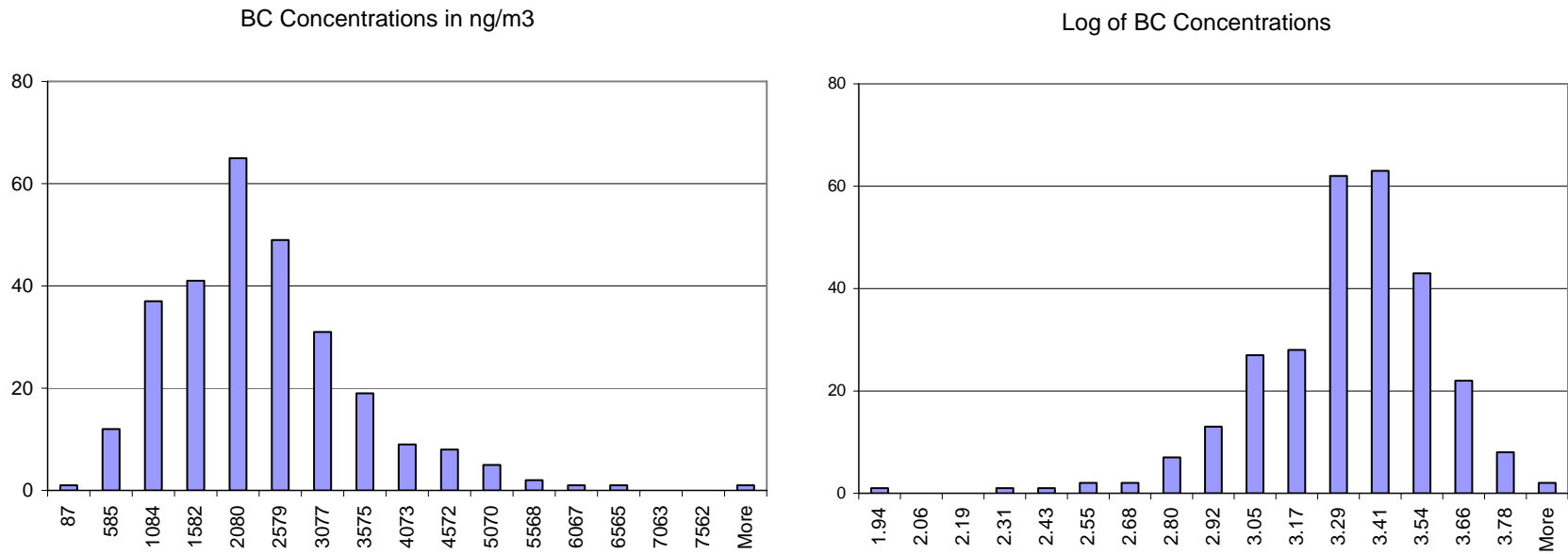


Figure 3–13. Distributions of hourly average BC concentrations (ug/m3) at Denio and the log transform of the data between 2200 and 0500 that meet selection criteria. Note that distribution of concentrations is approximately normal because measurements occurred during comparable atmospheric conditions.

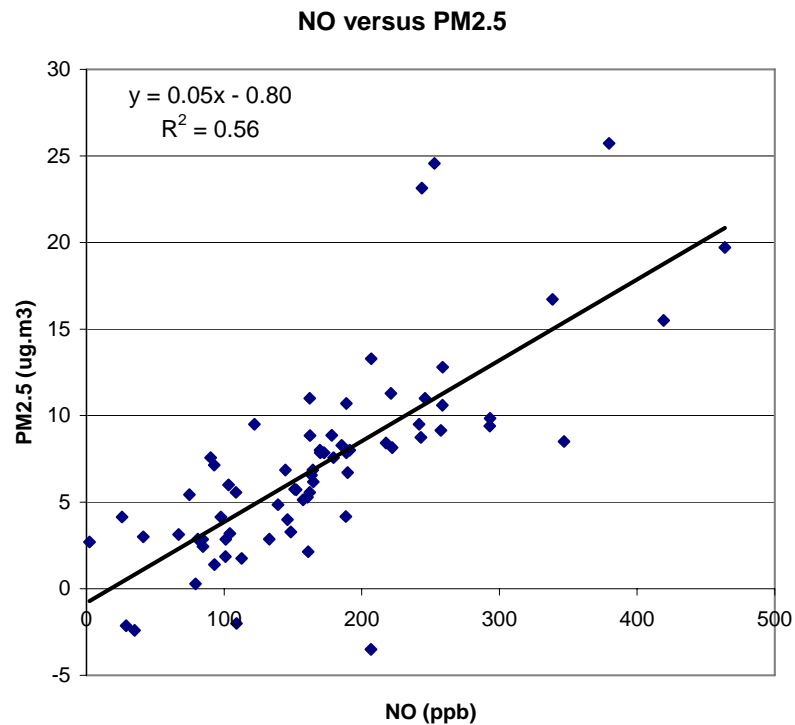
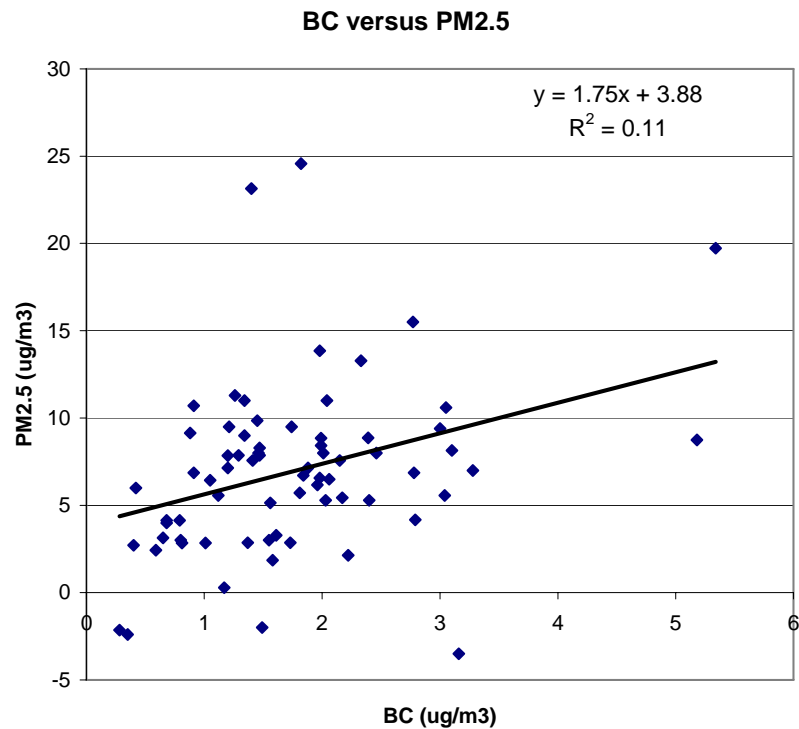


Figure 3–14. Correlations of BC and NO with PM_{2.5}. Values are the difference in daily 7-hour (2200 to 0500) means between the downwind Denio site and the corresponding upwind values at Pool.

4. CONCLUSIONS AND RECCOMENDATIONS

This section summarizes the findings and conclusions from the evaluation and validation of the RRAMP data and analysis of the data. Several modifications to the field measurement protocol is suggested for consideration by the RRAMP Technical Advisory Committee.

4.1 Data Evaluation and Validation

- Collocated aethalometers showed generally good agreement with no significant bias between instruments, but substantial variation (30-40%) on an hourly basis. Causes of the variation appear to be a combination of random electronic noise and irregularly spaced data gaps due to automatic filter tape advances. Correlation of the paired instruments is greatly improved by time-averaging the data over periods of 6 hours or more.

Recommendation - We recommend synchronizing the filter tape advances to regular intervals in future monitoring.

- Instances of heightened electronic noise, resulting in very large positive and negative spikes occurred several times.

Recommendation - We recommend that the raw data be screened for such occurrences carefully, and such periods removed before any time-averaging.

- The random error in 1-hour PM_{2.5} BAM data was too large (± 10 ug/m³) to make comparisons of the hourly data feasible at the measured concentrations. BAM data contained frequent negative values indicating baseline drift. However, collocated BAMs showed good agreement in measured PM_{2.5} concentrations after averaging over periods of 6-hours or more.

Recommendation - We recommend limiting upwind/downwind data analyses to periods of at least 4 hours.

- Wind data indicated similar patterns at all four sites, with lower peak wind speeds at the upwind sites but comparable diurnal variations. Winds tend to blow from the upwind to downwind sites primarily at night. Daytime wind speeds are generally low.
- NO/NO_x data contained some negative values that were removed. Numerous instances of slightly negative NO data were retained to avoid biasing the averages. Recommend removing data where both NO and NO_x are negative by an amount greater than the measurement precision (estimated as ± 10 ppb).
- BC/PM_{2.5} and NO/NO_x ratios are consistently higher at the downwind sites, which is consistent with presence of fresh emissions.
- 24-hour averaged PM_{2.5} data from the BAMs is well correlated with the corresponding filter gravimetric mass data, and shows no bias.

- 24-hour averaged BC data from the aethalometers is well correlated with the corresponding EC from filter samples. The BC/EC ratio is 0.74.
- The averaged BC from both aethalometer channels is similarly correlated with EC, indicating that light attenuation by PAHs is not a significant contributor.

4.2 Data Analysis

- Upwind sites tend to show higher concentrations due to increased traffic during morning and afternoon commutes, especially for NO and NO_x. Similar, but smaller, increases are evident for BC. PM_{2.5} show minimal diurnal variation at the upwind sites.
- Downwind sites show higher concentrations of NO/NO_x, BC and PM_{2.5} throughout the nighttime hours with no increase in concentrations during the morning commute period.
- Pollutant concentrations are generally lower on weekend at the two upwind sites. The Church site show slightly lower pollutant concentrations during weekends and the Denio site shows no variations in pollutant concentrations by day of week. These results are consistent with impact of pollutant emissions from the rail yard at the downwind sites.
- The differences in mean concentrations between the two pairs of downwind and upwind sites (Denio-Pool and Church-Vernon) are all significant at above the 99% confidence level.
- Ratios of pollutant concentrations at the upwind relative to downwind sites are lowest for NO and are larger in increasing order for NO₂, BC and PM. The increasing ratios from NO to PM are consistent with larger contributions of urban background to the measured PM and BC concentrations.

5. REFERENCES

- Arnott, W. P., H. Moosmüller, et al. (1999). "Photoacoustic spectrometer for measuring light absorption by aerosols: Instrument description." *Atmospheric Environment* 33: 2845-2852.
- Arnott, W. P., K. Hamasha, H. Moosmüller, P.J. Sheridan and J.A. Ogren (2005). "Towards Aerosol Light Absorption Measurements with a 7-Wavelength Aethalometer: Evaluation with a Photoacoustic Instrument and 3-Wavelength Nephelometer." *Aerosol Sci. and Technol.* 39:17-29.
- Campbell, D.E. and E.M. Fujita (2005). Deployment of DRI Mobile Van in Support of the Roseville Rail Yard Air Monitoring Project. Final report submitted to Placer County Air Pollution Control District, Auburn, CA, May 6, 2005.

APPENDIX A

Manufacturer's Notes for the Aethalometer

Interpretation of Optical Attenuation in the Ultra-Violet: Definition of 'UVPM'

The discussion presented above relates the mass of a defined species ("black carbon") to the optical absorbance in the visible portion of the spectrum. At these wavelengths, no other species has as strong an absorption, and the optical attenuation measurement can be reasonably interpreted in terms of a mass of this material.

As the illumination wavelength becomes shorter, the absorption cross-section of the six-member graphitic carbon rings increases as the photon frequency increases. Thus, the 'specific attenuation' at blue-violet wavelengths of 440 nm is expected to be twice that for illumination in the near-infra-red at 880 nm, as used for the standard 'BC' measurement of the Aethalometer. However, as the wavelengths become shorter, other molecular absorption processes become active. In particular, these involve spectrally-specific absorbance (i.e. absorption in lines or bands) rather than the broad-spectrum, all-photon absorption that is characteristic of 'black' carbon. (Indeed, if the absorption by elemental carbon were spectrally-specific rather than spectrally broad, it would appear 'colored' rather than 'black'.) At wavelengths shorter than about 400 nm, certain classes of organic compounds (such as polycyclic aromatic hydrocarbons, and also certain compounds present in tobacco smoke and fresh diesel exhaust) start to show strong UV absorbance. Some of these compounds are photo-ionizable, others of them exhibit fluorescence at these higher energies of photon excitation. As a descriptive (though incorrect) term, we sometimes refer to these compounds as 'blue' carbon - suggesting the spectral specificity and also the spectral region.

It is essential to note, though, that the absorption cross-section of these compounds is **highly variable**. The absorption efficiency per molecule may vary by *orders of magnitude*. In UV spectrophotometry, the absorbance per mole must be calibrated for each species of interest. If a sample containing a mixture of these species is illuminated with UV light, the UV-specific absorption can be detected but *cannot* be quantitatively interpreted as an exact amount of a specific compound. A few picograms of one PAH species may absorb as much UV as some tens of nanograms of another PAH compound.

An aerosol sample containing 'black' carbon particles onto which organic compounds have been adsorbed will therefore provide two means of absorbing for incident UV photons. The six-member 'black' carbon rings will absorb photons with the $1/\lambda$ efficiency described above. The 'blue' (i.e. UV-absorbing) organic species will add to this absorption with their own spectrally-specific and compound-specific behavior. The overall absorption in the UV will be greater than that attributable to 'black' carbon alone, due to the addition of 'blue' carbon. This is represented by the addition of a second term to the absorbance equation [4]:

$$A(\lambda') = k(1/\lambda') * [BC] + \text{Sum} \{ P(\lambda') * C(P) \} \quad [7]$$

where $P(\lambda')$ is the UV absorbance (at the short wavelength λ') of the quantity C of compound P, and this UV activity must be summed over all participating compounds, each of which will have a different absorption efficiency P at each different wavelength λ' .

If the aerosol contains a large concentration of a particular organic compound that has a *strong* UV absorption cross-section, then the overall absorbance in the near-UV may be considerably larger than would be predicted by scaling the visible absorption by a $1/\lambda$ factor.

This enhancement is due to the presence of the UV-active material, i.e. the “blue” carbon species. These species are colorless in the visible and may therefore be added or removed *without* affecting the ‘black carbon’ determination based on absorption in the visible or near-infrared: their effect is only seen in results measured by ultraviolet light.

The AE-2 series Aethalometers include light sources illuminating at 370 nm, in addition to the ‘standard’ illumination at 880 nm to detect absorption due to ‘black’ carbon. The 880 nm measurement yields an absorbance of

$$A(\lambda) = k(1/\lambda) * [BC] \quad [8]$$

while the 370 nm measurement yields an absorbance of

$$A(\lambda') = k(1/\lambda') * [BC] + \text{Sum} \{ P(\lambda') * C(P) \} \quad [9]$$

which is enhanced by the UV-specific absorption of the mix of organic compounds P. In the absence of chemical speciation of the mixture P, we *cannot* interpret the enhancement in terms of a mass of any exactly-given compound: we *cannot* assert that the added UV absorption indicates the presence of an exact number of nanograms of PAH’s, for example.

What is done in practice is to *define* an equivalent material based on the optical absorption measurement. We *define* “**UVPM**” (UV-absorbing **P**articulate **M**aterial) as if it were a “blue” material that absorbed UV photons with the same efficiency as Black Carbon does, at the UV wavelength in question. From equation [9], the defined ‘mass’ of UVPM is

$$[UVPM] = \text{Sum} \{ P(\lambda') * C(P) \} / k(1/\lambda') \quad [10]$$

where $\text{Sum}\{P(\lambda')*C(P)\}$ is the *actual* UV absorption due to the mix of organic compounds, and $k(1/\lambda')$ is the absorption cross-section of ‘Black’ carbon *at this same wavelength*. This fictional material ‘UVPM’ is expressed in units of ‘BC Equivalent’.

Equations [8] and [9] can then be re-expressed as the following comparison: the 880 nm ‘black carbon’ measurement yields an absorbance of

$$A(\lambda) = k(1/\lambda) * [BC] \quad [11]$$

while the 370 nm ‘black carbon + blue carbon’ measurement yields an absorbance of

$$A(\lambda') = k(1/\lambda') * [BC + UVPM] \quad [12]$$

In the absence of UV-specific organic compounds, - i.e. if the sample consisted purely of ‘elemental’ carbon - the absorbance measurement made at 370 nm would simply be 880/370 times as large as the absorbance measurement made at 880 nm. If we used the appropriately-scaled values of ‘sigma’ for these two measurements, the absorbances when divided by differing efficiencies would yield *identical masses* of BC or BC-equivalent material. In this situation, ‘UVPM’ is zero.

However, if we now *add* UV-specific absorbing “blue” compounds to the mixture, then the UV absorption will be enhanced. The absorbance at 370 nm will be *greater* than 880/370 times the absorbance at 880 nm which was due to the ‘black carbon’ component. This enhancement can be displayed by the algorithm as if it were due to the presence of an equivalent

material called ‘UVPM’, expressed in nanograms or micrograms of a substance that has the same absorption efficiency as the ‘black carbon’ structure. The added absorption is represented by a non-zero value of [UVPM] in equation [12].

Very Important Note!

‘UVPM’ is NOT a real physical or chemical material!

The above definition is for convenience ONLY. If the display of an AE-2 series instrument reports a concentration of 1.5 $\mu\text{g}/\text{m}^3$ of BC and 2.0 $\mu\text{g}/\text{m}^3$ in the ‘BC + UVPM’ data, this does *not* mean that there is 0.5 micrograms of *any* organic species present. What it means is that the UV measurement data shows an additional optical absorption that is of the same magnitude as if it were produced by the presence of 0.5 $\mu\text{g}/\text{m}^3$ of black carbon. This additional absorption might *actually* be produced by just a few picograms of one particular strongly-absorbing compound: some PAH found in tobacco smoke, for example.

The screen display of an AE-2 series instrument shows two quantities on the lowest line: on the left-hand side, the ‘BC’ result from the 880 nm measurement. This result is always identical to the result from an AE-16 series instrument, since it is obtained in an identical manner using the same light source wavelength. On the right-hand side of the AE-2 display, there is a second result shown as ‘UV’. This represents the *total* UV-data signal, i.e. the entirety [BC + UVPM] of equation 12. If sampling a ‘normal’ aerosol, this ‘UV’ result will be closely equal to the ‘BC’ result. If sampling an aerosol that has a strong “blue” component (e.g. fresh diesel exhaust or tobacco smoke), then this ‘UV’ result will be substantially larger than the ‘BC’ result. The UV data is increased by an amount expressed in nanograms or micrograms *as if* it were BC causing this additional absorbance, but with the clear understanding detailed above that this is an equivalence definition only.

The Aethalometer TM

2005.07

A.D.A. Hansen

Magee Scientific Company

Berkeley, California, USA

Interpretation of Aethalometer Data

Ideally, the data output from any measuring instrument would consist of a smoothly-varying analog voltage (or digital representation thereof) that instantaneously represented the value of the parameter being measured, without any corruption due to noise or other interference. In practice, realistic instruments present their measurements with some reductions from this ideal. The actual Aethalometer™ data output is affected to some degree by its mode of operation, inherent physical and electronic limitations, and the nature of the algorithm used to calculate the result.

The Aethalometer is set to operate on a certain timebase period, and calculates its data from the quantity of aerosol black carbon determined to have been collected on the filter during this period. Thus, the measurement is not presented until the *end* of the measurement period, and represents an arithmetic mean of the actual concentration during that period. The algorithm identifies the data with a date and time stamp that are displayed and recorded: the time shown is the time at the *start* of the measurement period. It is necessary either to know the length of the timebase period, or to examine the time value for the following data entry, in order to determine the *end* time for that period.

It is important to note that the analog voltage presented on the rear panel terminals represents the BC value from the **previous** timebase period. This value will be held until the end of the **next** timebase period. The analog output voltage is therefore always one period “behind” the current measurement.

In addition to the BC calculation, the system also records diagnostic signals to disk in case there is a need to examine the raw measurements from which the BC concentration was calculated. These additional data entries on the record line include: Sensing Beam signal with the lamp ON and OFF, Reference Beam signal with the lamp ON and OFF, the mean air flow rate, and the calculated optical attenuation. All of these quantities are measurements made at the *end* of the measurement timebase period, with the exception of the air flow rate which is the arithmetic mean of measurements taken continuously during the entire period. The BC number shown is the mean BC concentration for the period *starting* at the time and date shown.

The Aethalometer needs to measure extremely small changes in optical transmission in order to calculate BC concentrations with speed and accuracy. The optical transmission through a blank filter will change when vacuum is first applied to it, producing a pressure drop that compacts the filter fibers. This initial change would be interpreted by the algorithm as a large artifact ‘BC’ concentration, and so the software automatically provides a settling period before the first measurement on a fresh filter spot. Valid data are not produced until after at least *one* timebase. While the tape is advancing or the instrument is subsequently initializing and equilibrating, the green ‘Run’ light will *flash* to signify that the instrument is functioning normally but there is no valid data. When the instrument is functioning normally, and valid data are being calculated, the green ‘Run’ light will be *steady*.

The major source of noise in the data is due to small, random fluctuations of digitized signals. These fluctuations have the effect of causing the calculated value of attenuation (ATN) to deviate from a smooth, monotonic increase with time: instead, individual values of ATN may be artificially higher or lower than would be predicted from the rate of accumulation of BC from the air stream. These isolated events give rise to a characteristic signature in the derivative

calculation that yields the BC result. An error in one of the four fundamental signals will usually not be repeated the following measurement cycle, and the calculated ATN will revert to its 'correct' value: but with an intervening false number.

If the error condition produced an artificially high value of ATN for one measurement, the algorithm will interpret that large increase as a large value of the BC concentration for that period. This calculated value may be much larger than the preceding and following data, and the event will be obvious. However, this large value of ATN is used as the starting value for the calculation of the increment in the following cycle. The increase from this value to the 'correct' value at the end of the next period will be much smaller than it should be, resulting in a reduced value for the BC calculation. The result of the single error value of ATN in this case is an artificially large value of BC, followed by an artificially small value. The 'true' value is recovered by replacing the value for each of the periods with the arithmetic mean of the two distorted values. This is equivalent to simply ignoring the one bad signal measurement; determining the increase in ATN between the periods before and after the bad measurement; and calculating the increment in ATN and hence the mean BC concentration over a time interval of two periods rather than one.

In extreme cases, the error in voltage measurement may generate a value of ATN that deviates from the expected smooth progression by a large amount. The algorithm will process these deviations in the same manner: however, if the apparent value of ATN during the 'error' measurement exceeds the subsequent 'correct' value of ATN, the program is presented an optical attenuation value that is smaller than its predecessor. The mathematics will produce a negative apparent value of BC for this situation. This negative value will be adjacent to a slightly larger positive value: the arithmetic mean of the two numbers will still allow a recovery of the correct mean BC concentration for the double period. The derivative nature of the algorithm is such that a single error value in recorded signals produces a symmetrical plus-minus derivative event in the calculated BC result.

If the sign of the superimposed noise event were inverted, the signature in the final data would be reversed in order: a negative or reduced value will be followed by an enlarged positive value, and the BC data would show a characteristic minus-plus excursion.

Excluding data corruption events as described above, it is still clear that some noise of similar appearance will be present when attempting to measure extremely low concentrations of BC. At a very low level, small deviations in measured voltages will occur during each measurement cycle. If the actual increase in ATN is smaller than these fluctuations, due to actual very low levels of BC in the sampled atmosphere, the algorithm may produce positive and negative fluctuations in the same manner. Indeed, one of the tests that each Aethalometer is put through prior to release is to operate it sampling filtered air for 12 to 24 hours. The expected value of detected BC should be zero: in practice, small positive and negative fluctuations are observed. The negative values arise directly from the nature of the algorithm, as discussed above. The cumulative mean of these data values is usually observed to be close to zero: the parameter of interest is the standard deviation of the small fluctuations, as this will determine the effective noise level on the measurement of BC and the minimum detectable amount.

This effective noise level of BC is fundamentally a product of the ability of the detectors and electronics to resolve a very small increase in the amount of BC in the aerosol deposit on the filter. When translated to a BC concentration in the sampled air stream, factors of the air flow

rate and sampling time are introduced. The ‘usual’ performance of an Aethalometer is to be able to resolve an increment of less than 1 nanogram of BC on the filter. If the instrument is operating at a flow rate of 4 liters per minute, this implies that the minimum resolvable concentration would be approximately 50 ng/m³ operating on a 5-minute timebase (i.e. 1 ng noise per 20 liters air flow), or approximately 5 ng/m³ if the timebase period were 1 hour. See the example shown in the previous section 9.2. In practice, we prefer to use more conservative figures for the instrument performance, and normally quote a limit of quantity as 5 nanograms on the filter. The translation of this performance to a concentration figure will then depend on the sampling timebase period and the air flow rate. The greater either of these parameters, the lower the minimum detectable concentration of BC in the sampled air stream.

Note, however, that the appearance of ‘negative’ numbers for the deduced BC concentration is a natural consequence of the algorithm if either (i) there are occasional corrupting events on the voltages being recorded, or (ii) the instrument is being used to study extremely small concentrations of BC. These negative numbers do **not** imply malfunction of the instrument: they are the consequence of differentiating a quantity (ATN) whose increase with time is not perfectly smooth and monotonic. In subsequent data reduction, one must average the BC numbers appropriately until the negative numbers disappear: i.e., effectively increase the averaging time until the increment of BC collected on the filter easily exceeds the minimum amount detectable by the electronics.

Considerations of the nature of the algorithm also lead to a suggested strategy for situations in which post-sampling data analysis is readily available: namely, to perform measurements with a timebase period that is considerably shorter than the final desired time resolution, and then to subsequently average and post-process the data. The reasons for this strategy are two-fold: firstly, to minimize the duration of the effect of any data ‘glitches’ (i.e. voltage measurement errors); and secondly, to allow the instrument to respond rapidly to ‘real’ events in the local atmosphere, while retaining the possibility of averaging the data into longer timebase periods during quiescent periods.

The first of these considerations attempts to minimize the ‘damage’ to the database due to one bad voltage reading. As discussed above, the effects of one bad voltage measurement will affect the measurements in the two contiguous periods. If an instrument is operating at a remote station with a timebase of one hour, a single voltage spike will affect two hours of data, although an average can be recovered. If, on the other hand, the instrument was being operated on a timebase of 5 minutes, with subsequent gathering of the data into one-hour averages, this isolated event would only affect 10 minutes of data and would in fact not affect the one-hour data at all. Although the individual 5-minute measurements have less inherent precision, due to the reduced volume of air sampled, their accumulation into one-hour averages is exactly equivalent to operating the instrument on a one-hour timebase. Nothing is lost by operating on a shorter timebase and post-processing the data into longer periods, if the laboratory data system can be programmed for these actions on the Aethalometer records.

The second advantage of operating on a shorter timebase is that occasionally, short-duration events of **actual BC concentration excursions** do occur. A vehicle may be operated upwind of the measurement site: a local recirculation pattern may bring emissions from one location into the sampling inlets. These events are identified in the database as those in which a large positive excursion is not followed by a compensating negative number.

For these reasons, Aethalometers are shipped from the factory with the timebase set to 5 minutes. We recommend keeping this value unless considerations absolutely suggest otherwise: e.g., shorter timebases (1 or 3 minutes) for local-impact studies in areas of high concentration; very rapid timebases for source studies; or timebases of 10 or 15 minutes (maximum) for remote studies.

Precise Timing

The computer algorithm performs the optical measurement sequence once every timebase period, or at least once every 5 minutes, as described above. The concentration of BC that is calculated and displayed, represents the average over the time interval between this measurement point and the previous. The result is recorded just before the 'zero seconds' rollover of the timebase minute and is flagged as if originating from [Minute Previous, Zero Seconds] to [Minute Present, Zero Seconds]. However, the *actual* optical measurements are made some seconds *prior* to the rollover of the minute, to allow time for calculation, recording to diskette, updating the screen display etc. In cases of very rapid fluctuations of concentration, or precise time synchronization with other instruments, this offset may be noticeable.

The time offset amount depends on the number of wavelengths in use and the timebase setting. At longer timebases, repeated analog/digital conversions and data acquisitions are performed, to improve accuracy and reduce electronic noise. Generally, for single-wavelength instruments, the time offset is about 20 seconds at a 5-minute or longer timebase, reducing at shorter timebases. For dual-wavelength instruments, the offset on a 5-minute timebase is approximately 90 seconds for the UV data and 60 seconds for the BC data. For 7-wavelength instruments, the offset ranges from approximately 120 seconds for the shortest wavelength to 60 seconds for the longest.

Note that although the time offsets may differ for differing wavelength data, the **interval** between successive measurements is always precisely equal to the timebase period. This value multiplies the measured flow rate to calculate the volume of air from which the particles have been collected, and will be identical for all wavelengths in use.